

SPECTRAL AND MAGNETIC STUDIES
OF METALLOCARBOXYPEPTIDASE A'S

Thesis by
Robert Charles Rosenberg

In Partial Fulfillment of the Requirements
for the Degree of
Doctor of Philosophy

California Institute of Technology
Pasadena, California

1974

(Submitted September 12, 1973)

ii

to susi

ACKNOWLEDGMENT

I would like to thank Professor Harry B. Gray for his contagious enthusiasm, insight and advice. Special thanks are due to Professor Charles A. Root for his invaluable collaboration during the year he spent at Cal Tech, and for teaching me that procrastination does not produce results. I would also like to thank Professor George R. Rossman for allowing me to use his Cary 17 I spectrophotometer, Dr. Paula K. Bernstein for measuring and simulating the EPR spectrum of Cu(II)CPA, Mr. Run-Han Wang and Dr. Massimo Cerdonio for the magnetic measurements on Co(II) and Ni(II)CPA, and my other colleagues for their frequently helpful advice.

I am indebted to the National Science Foundation for a predoctoral fellowship and to the N.I.C.E. Foundation for the summer fellowship that introduced me to the wonders of inorganic chemistry.

I thank my parents, not only for their love and encouragement, but for finally learning not to ask me when I would finish.

I thank Susi for making everything worthwhile, and finally I thank the Sierra Nevada for being there.

ABSTRACT

Spectral and magnetic studies on the cobalt(II), nickel(II), and copper(II) derivatives of the zinc containing metalloenzyme carboxypeptidase A (CPA) are reported and discussed.

The absorption spectrum and magnetic moment of Co(II)-CPA are shown to be consistent with a five coordinate metal structure by comparison to the spectra and magnetic moments of a large number of pseudo-tetrahedral and five coordinate cobalt(II) complexes. The usefulness of magnetic susceptibility data in assigning coordination number for high-spin cobalt(II) metalloenzyme systems is demonstrated.

The absorption spectrum and magnetic moment of Ni(II)-CPA are consistent only with an octahedral ground state geometry. The effect of substrate and inhibitor on the spectrum of Ni(II)-CPA was studied.

The absorption and EPR spectra of Cu(II)-CPA were also investigated. A significant pseudo-tetrahedral distortion from planar coordination geometry is indicated for this derivative. The interaction of Cu(II)-CPA and the inhibitor sodium β -phenylpropionate was also studied.

The results of these studies and especially those of Ni(II)-CPA do not agree with the predictions of the entatic state hypothesis.

ABBREVIATIONS

CPA	-	carboxypeptidase A
CA	-	carbonic anhydrase
Na β PP	-	sodium β -phenylpropionate
gly-tyr	-	glycyl-L-tyrosine
BGP	-	benzoyl-glycyl-L-phenylalanine
PGM	-	phosphoglucomutase
TIP	-	temperature independent paramagnetism
B. M.	-	Bohr Magneton
ϵ_m	-	molar extinction coefficient
Tris	-	tris(hydroxymethyl)aminomethane

TABLE OF CONTENTS

	Abbreviations	v
CHAPTER I		1
	Introduction	1
	General Experimental Procedure	11
	References	28
CHAPTER II	COBALT(II)CARBOSYPEPTIDASE A	31
	References	61
CHAPTER III	NICKEL(II)CARBOXYPEPTIDASE A	63
	References	99
CHAPTER IV	COPPER(II)CARBOSYPEPTIDASE A	103
	References	160
CHAPTER V	CONCLUSIONS	164
	References	169
PROPOSITIONS		170

CHAPTER I

Introduction

Carboxypeptidase A (CPA) is a zinc metalloenzyme. One strongly bound zinc(II) ion per molecule is required for full activity.^{1,2} As its name implies, carboxypeptidase A mediates the hydrolysis of the c-terminal amino acid of a polypeptide chain. It is specific for c-terminal amino acid residues that have a free carboxyl group and are in the L-configuration. It also shows specificity towards c-terminal residues that have aromatic or branched aliphatic side chains. Esterase-activity subject to the preceding criteria has also been observed.³

The enzyme, which is usually prepared from bovine pancreas, has a molecular weight of approximately 34,600. Three active chemical forms of CPA are known.^{4,5,6} They differ in their amino-terminal sequences and arise from differing points of enzymatic cleavage of procarboxypeptidase A during the isolation procedure. The relationship of the three forms is shown in Figure (I-I). These three forms have slightly different properties. The α and β forms are more soluble than the γ form. Loss of enzymatic activity on removal of zinc is readily reversible for the α and β forms, whereas the γ form can only be partially regenerated.

The three preparative procedures for CPA in the literature^{7,8,9} yield varying proportions of the α , β , and γ forms.⁶ CPA prepared by



Figure I-1: N-terminal sequence of the α , β , and γ forms of CPA.

the Cox procedure was chosen for this work because CPA(Cox) is predominantly CPA α (~75%) and contains none of the undesirable CPA γ form.

The complete amino acid sequence¹⁰ as well as a 2.0Å resolution X-ray crystallographic study of CPA α and its complex with a model substrate, glycyl-L-tyrosine^{11,12,13} are available. These studies have shown that the ligands of the zinc are the N(I)'s of His 69 and His 196, an oxygen of Glu 72, and one water molecule. These ligands form a very distorted tetrahedral array about the zinc ion.^{14,15} In the enzyme-"substrate" complex, the water is replaced by the carbonyl-oxygen of the first peptide bond, i.e., the peptide bond to be hydrolyzed.

The enzyme was found to be roughly ellipsoidal ($50 \times 42 \times 38$ Å) with a surface groove leading to the active site region where the zinc and its ligands and a hydrophobic pocket are located. The groove is thought to accommodate longer polypeptide substrates, and the pocket binds the aromatic side chain of the C-terminal amino acid of the substrates thus explaining the enzyme's specificity. Based on the high resolution study of the gly-L-tyr-CPA complex, the following model of substrate binding and peptide bond cleavage has been proposed by Lipscomb and co-workers (see Figures I-II and I-III). The pocket, the zinc, Arg 145, and Tyr 248 are the principal binding groups. The large conformational change of Tyr 248 on substrate binding closes off the active site groove from the solvent. This change, however, can only occur after the smaller conformational

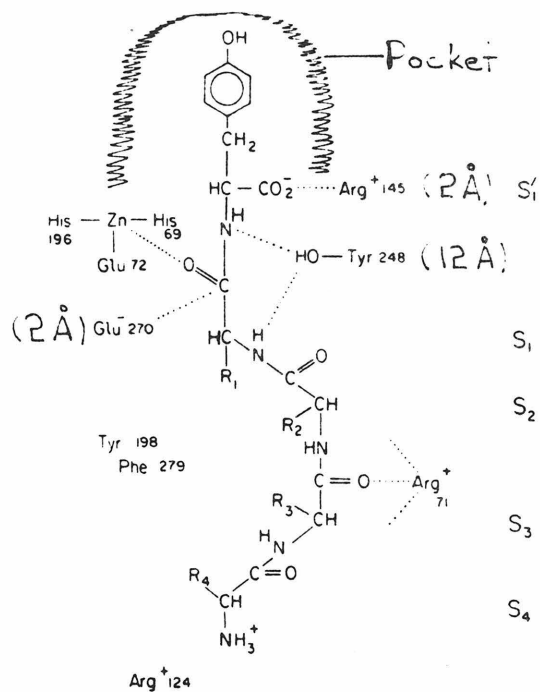


Figure I-II. Lipscomb's model of substrate binding to CPA. The numbers in parenthesis indicate the magnitude of the conformational changes that occur on substrate binding. (from reference 15)

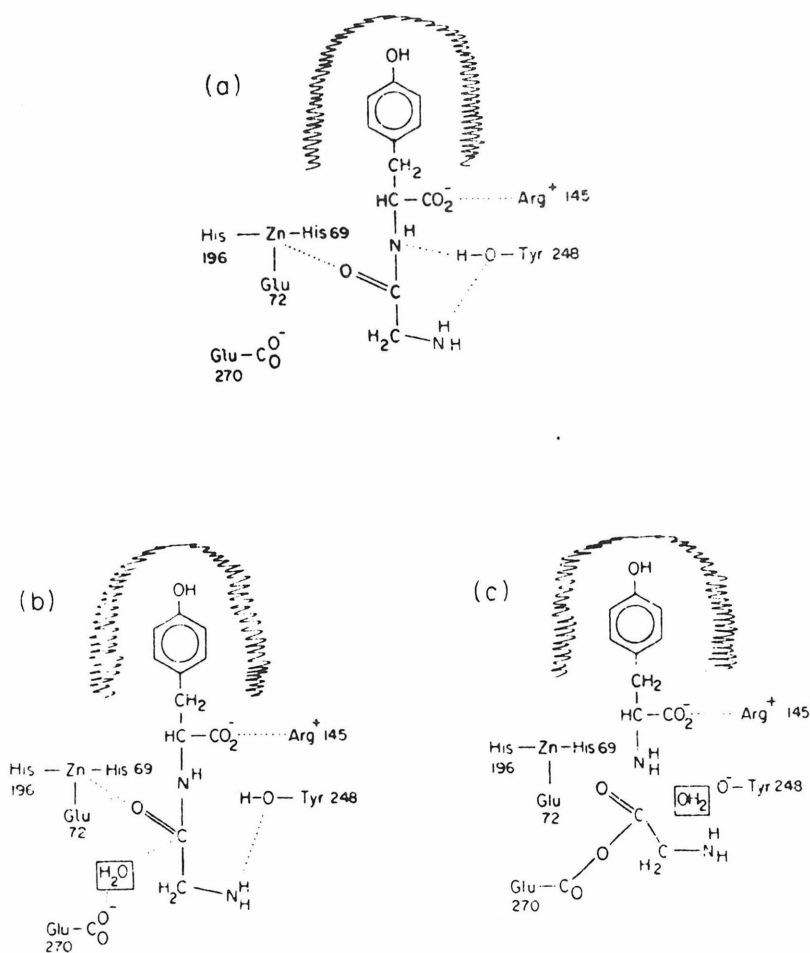


Figure I-III. Lipscomb's proposed mechanisms for substrate hydrolysis. (a) Productive substrate binding. (b) General base attack by water on the carbonyl carbon of the substrate, promoted by Glu 270. (c) Nucleophilic attack by Glu 270 on the carbonyl carbon of the substrate, anhydride formation. (from reference 15)

change associated with Arg 145 has taken place. Their proposed mechanisms of substrate hydrolysis are shown in Figure (I-3). In these mechanisms the zinc functions not only as a binding site but also to polarize the carbonyl bond, making the carbonyl carbon more electrophilic and thus more susceptible to nucleophilic attack, possibly by Glu 270 itself or by water promoted by Glu 270. Tyr 248 serves as a proton donor to the peptide amide nitrogen.

The kinetics of CPA catalyzed reactions are quite complicated. Effects like substrate activation and inhibition as well as product activation and inhibition are common for many of the model dipeptide and diester substrates of CPA.^{16,17} These complications are somewhat reduced when longer, model tripeptides are used.¹⁸

In situations where the kinetics are not complicated by the above effects, bell shaped curves are obtained for the overall reaction rate as a function of pH. The high pH ionization (\sim pH 9) has been interpreted as that of a tyrosine residue.¹⁹⁻²² The origin of the low pH ionization (\sim pH 6), on the other hand, has not been resolved. It has been attributed to a glutamic acid residue, a histidine group coordinated to the metal, and to coordinated water.

Chemical modification studies also support the catalytic or binding functions of tyrosine and arginine residues.¹⁷ One of the striking results of the chemical modification studies, however, is that while peptidase activity can be severely inhibited, esterase activity is often not proportionately effected, suggesting that the peptidase and esterase function may involve different mechanisms.

The zinc ion in native CPA can be removed by dialyzing the enzyme against a buffer solution containing chelating agents such as 1, 10-phenanthroline. This procedure yields an inactive apoenzyme to which activity can be restored by addition of one zinc ion per molecule.²³ It has been shown that the apoenzyme will bind normal model substrates and that bound substrates prevent zinc reconstitution.²⁴ The inhibitor β -phenylpropionate, on the other hand, does not bind to the apoenzyme, suggesting that it is coordinated to the metal.²⁵

ApoCPA can be reconstituted with other divalent metal ions.² The stability constants and relative peptidase and esterase activities of the CPA derivatives that have been examined thus far are summarized in Table (I-1). The order of peptidase activities, $\text{Co}^{+2} > \text{Zn}^{+2} \sim \text{Ni}^{+2} > \text{Mn}^{+2} > \text{VO}^{+2} \gg \text{Cd}^{+2} = \text{Hg}^{+2} = \text{Cu}^{+2} = \text{Co}^{+3} = \text{O}$, is quite different from the order found for esterase activities, $\text{Cd}^{+2} > \text{Mn}^{+2} \sim \text{Co}^{+3} > \text{Co}^{+2} > \text{Zn}^{+2} \sim \text{Ni}^{+2} > \text{VO}^{+2} > \text{Hg}^{+2} > \text{Cu}^{+2} = \text{O}$. The large differences in the order of activities of the various metal derivatives again suggests that different mechanisms are involved in peptidase and esterase function. Unfortunately, no explanation of these relative activities has been advanced.

The physical properties such as absorption spectra, magnetic moments, and EPR spectra of Co(II), Ni(II), and Cu(II) complexes have been extensively studied and used to assign structure in these systems. Only Co(II)-CPA has been studied in any detail. On the basis of its absorption, circular dichroism, magneto circular dichroism, and EPR spectra, Vallee and co-workers have concluded

Table I-1

<u>Derivative</u>	<u>log K^a</u>	<u>Peptidase^b</u>	<u>Esterase^c</u>
Zn(II)-CPA ^d	10.5	5.6	28.6
Cd(II)-CPA ^d	10.8	0	61.5
Hg(II)-CPA ^d	21.0	0	>0
Cu(II)-CPA ^d	10.6	0	0
Ni(II)-CPA ^d	8.2	5.6	27.6
Co(II)-CPA ^d	7.0	7.4	37.7
Co(III)-CPA ^e	--	0	~ 58
Mn(II)-CPA ^d	5.6	2.3	56.8
VO ⁺² CPA ^f	--	1.3	~ 16.0

^a Stability constant corrected for competition by 1M Cl⁻ and 0.05 M Tris buffer pH 8.

^b Data for BGP as substrate ($k_{\text{cat}} \times 10^{-3}$) \times (min)⁻¹.

^c Data for HPLA (Hippuryl-dl- β -phenyllactate) as substrate $k_{\text{cat}} \times 10^{-3} \times$ (min)⁻¹.

^d References 26, 27, 18, 17.

^e Reference 28.

^f Reference 29.

that the cobalt ion is in a very distorted tetrahedral environment in Co(II)-CPA.³⁰⁻³² The magnetic moments of high spin Co(II) complexes have long been used to establish structure in such model systems. The availability at Caltech of an extremely sensitive magnetometer made such an experiment feasible. The wavelength of maximum absorption of Cu(II)-CPA is also briefly mentioned in the literature.³³ Thus a detailed spectral study of the nickel(II) and copper(II) derivatives of CPA and their interactions with substrates and inhibitors seemed potentially rewarding.

Establishing coordination numbers and perhaps coordination geometries for these metallo CPA's might also permit an evaluation of the entatic state hypothesis of Williams and Vallee,^{34, 35} as it applies to metalloenzymes that are so-called "acid-base catalysts." This theory attempts to explain the role or catalytic activity of the metal ion in terms of the metal-protein interaction. The theory postulates that the resting enzyme by virtue of the nature of the metal-protein interaction, has some built-in activation energy with respect to small molecule catalysts. This activation energy can be with respect to substrate binding, i.e., a low coordination number and a geometry favorable to substrate coordination, or in the form of increased substrate attacking power again by virtue of the nature of the metal coordination. As a consequence of the special structural nature of the metal site, this theory predicts that the physical and electronic properties of the metal should be grossly unusual.

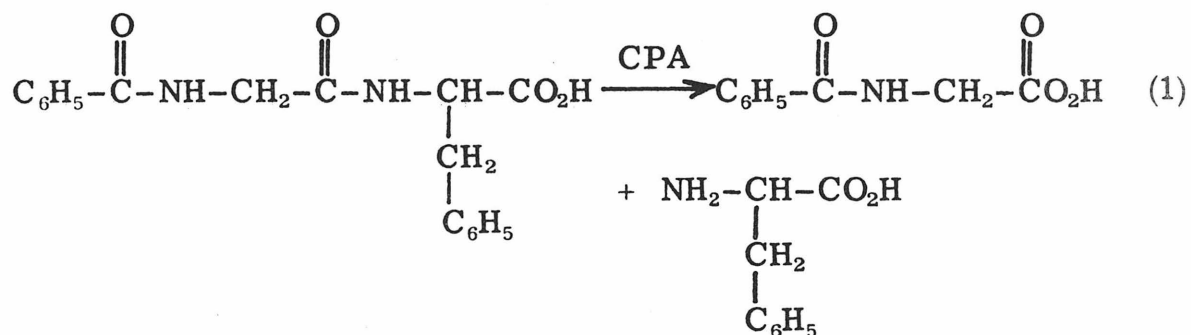
The position, low coordination number, irregular coordination geometry and openness of the zinc in CPA have been cited in support of this theory as has the "unusual" absorption spectrum of Co(II)-CPA.³⁵ Thus it would be particularly interesting to see whether Co(II)-CPA can be further characterized, and to see whether the spectral properties of Ni(II)-CPA, which is fully active, are as grossly unusual as this theory predicts.

General Materials and Methods

In the section that follows, experimental procedures that were used with all of the metallo CPA derivatives are described. Techniques or procedures peculiar to individual derivatives are described in the relevant Chapter.

Assay Procedure

Hippuryl-L-phenylalanine (benzoyl-glycyl-L-phenylalanine, BGP) obtained from Schwarz/Mann Biochem was used as the substrate in all assays of carboxypeptidase A activity. The assay reaction is as follows:



The hydrolysis of BGP can be followed spectrophotometrically since the products absorb uv light more strongly than the substrate. The rate of substrate consumption or product production is simply related to the slope of a plot of absorbance versus time for the reaction mixture.

Let H equal the molar extinction coefficient of a one-to-one solution of Hippuric Acid (BG) and L-phenylalanine at some wavelength. Let S equal the molar extinction coefficient of BGP at the same wavelength. If C_0 is the initial concentration of BGP in both the sample and reference cells and C is the concentration of BG and P at some time t after a small aliquot of Carboxypeptidase A is added to the sample cell, then at time t

$$[\text{BGP}] = C_0 - C \quad (2)$$

and the observed Absorbance, $A_{\text{obs}}(t)$ is given by:

$$\begin{aligned} A_{\text{obs}}(t) = A_{\text{sam}}(t) - A_{\text{ref}}(t) &= C \times H \times \ell + (C_0 - C) \times S \times \ell \\ &\quad - C_0 \times S \times \ell \end{aligned} \quad (3)$$

$$= (H - S) \times C \times \ell = \Delta\epsilon_{\text{PS}} \times C \times \ell \quad (4)$$

where ℓ is the path length of the cell. $\Delta\epsilon_{\text{PS}}$ is the difference in molar absorbance of products and substrate. Thus

$$C = \frac{A_{\text{obs}}(t)}{\Delta\epsilon_{\text{PS}} \ell} \quad (5)$$

and

$$\frac{dC}{dt} = \frac{1}{\Delta\epsilon_{\text{PS}} \times \ell} \times \frac{dA_{\text{obs}}(t)}{dt} = \frac{\text{Slope } (A_{\text{obs}}(t))}{\Delta\epsilon_{\text{PS}} \times \ell} \quad (6)$$

Since the units of C are moles per liter, the number of moles of substrate hydrolyzed per unit time is just dC/dt times the volume of the solution in the cell, V_s . This gives

$$\text{Units of Activity} = \frac{\text{Slope}}{\Delta\epsilon_{PS} \times \ell} \times V_s \quad (7)$$

Specific activity or the number of moles of substrate hydrolyzed per unit time per mg of enzyme was calculated from the activity and the concentration of the enzyme used. Enzyme concentrations were determined spectrophotometrically at 278 nm. At this wavelength, CPA-Cox has a molar extinction coefficient $\epsilon_m = 6.49 \times 10^4 \text{ M}^{-1} \text{ cm}^{-1}$.³⁶ It should be noted that any dilution of the substrate concentration upon addition of enzyme to the sample cell has been neglected. This is reasonable since the cell volume was 2.8 ml while the volume of enzyme solution added was 5 or 10 microliters.

$\Delta\epsilon_{PS}$, the difference in molar extinction coefficients between the hydrolysis products (BG + P) and the substrate (BGP) was determined. A plot of the difference spectrum (BG + P) - (BGP) is shown in Figure (I-IV). All species were at $0.924 \times 10^{-3} \text{ M}$ in 0.5M NaCl, 0.025M Tris buffer pH 7.5, the conditions used in all assays. 256 nm was chosen for following substrate hydrolysis. $\Delta\epsilon_{PS}$ at 256 nm was calculated to be $341 \text{ M}^{-1} \text{ cm}^{-1}$.

Let us now consider the behavior of the appearance of products as a function of time. For a mechanism of the type

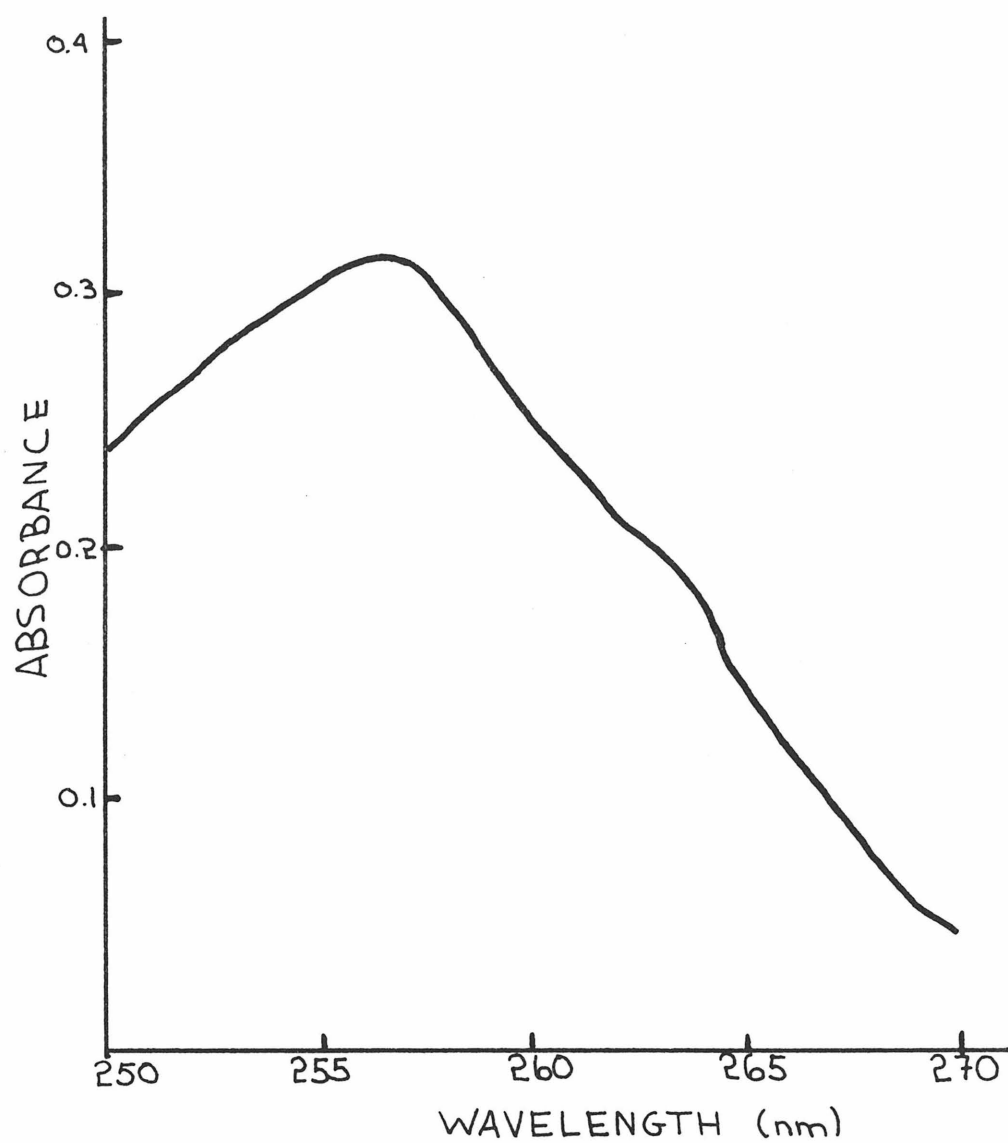
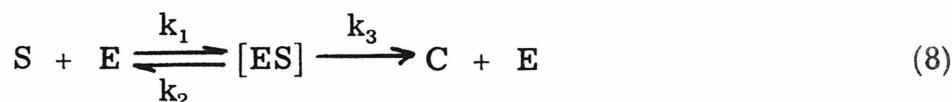


Figure I-IV. Difference spectrum of [products (BG + P) - substrate (BGP)].



it has been shown that³⁷

$$\nu = \frac{dC}{dt} = \frac{k_3 E [S]}{\frac{k_2 + k_3}{k_1} + [S]} \quad (9)$$

The initial velocity, ν_o , is given by

$$\nu_o = \frac{k_3 E S_o}{\frac{k_2 + k_3}{k_1} + S_o} = kE \quad (10)$$

Thus the initial rate of appearance of products should be constant and A_{obs} should increase linearly with time for the first part of the reaction. Equation (10) was found to apply at least for enzyme concentrations below $3.5 \times 10^{-8} M$ (See Figure I-V). An initial substrate concentration of $\sim 1 \times 10^{-3}$ was used in all assays. Under these conditions roughly the first ten to twenty percent of substrate hydrolysis was found to be linear with time.

In actual practice 5λ ($5 \times 10^{-3} ml$) of a stock enzyme solution was added to 2.8 ml of substrate solution in a 1 cm path length cell. So the concentration of enzyme in the stock solutions used was kept below $2.00 \times 10^{-5} M$. In fact, enzyme concentrations of the order of $2-5 \times 10^{-9} M$ gave hydrolysis rates that were slow enough to permit rapid hand mixing of the sample before placing it in the sample compartment of the Cary 17. Generally, the first third of the hydrolysis was followed on a time scale of 10-20 minutes.

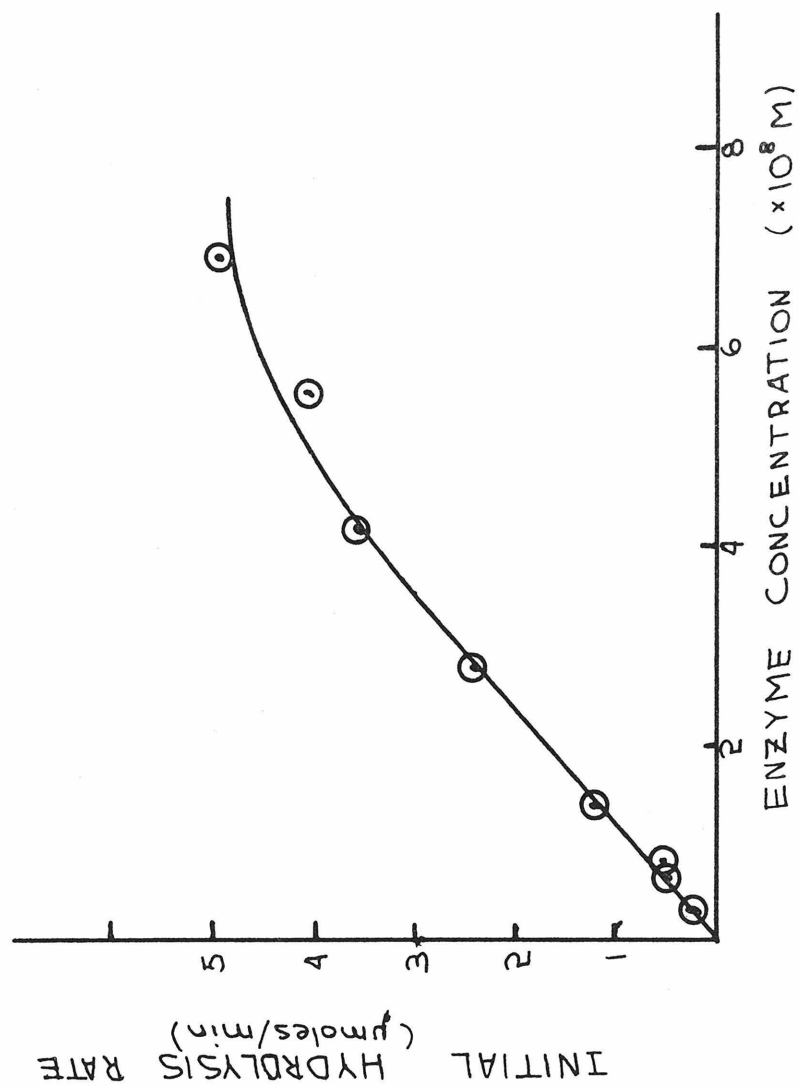


Figure I-V. Plot of initial hydrolysis rate vs. CPA concentration.

Sample Preparation and Handling

Extreme care was taken to prevent contamination of CPA by adventitious metal ions.³⁸ Plastic lab ware and pipets were used, and all buffers were repeatedly extracted with dithiazone in CCl_4 prior to use. A Tris · HCl buffer system was used in all experiments. Reagent grade Trizma Base and Trisma HCl obtained from Sigma Chemical Company were used. Reagent grade NaCl or KF obtained from J. T. Baker Company were also used in the buffer without further purification other than the extraction procedure described above. 1,10-phenanthroline monohydrate (Matheson, Coleman, and Bell) was used without further purification. Dialysis tubing was prepared according to the procedure of Hughes and Klotz.³⁹

Metalloderivatives were prepared by the procedure of Coleman and Vallee.⁴⁰ Crystalline Carboxypeptidase A, isolated by the Cox procedure,⁹ was obtained from Sigma Chemical Company as an aqueous suspension with toluene added to suppress bacterial growth. The CPA so obtained was used without further purification. Samples were checked for activity before use. The aqueous suspension of CPA crystals was placed in a 12 ml nalgene centrifuge tube. The crystals were then centrifuged at 6000 g for 10 minutes and the supernatant discarded. The crystals were then resuspended in a few ml of triple distilled water. After one or two such washings, the CPA crystals were resuspended in 4-12 ml 1M NaCl, 0.05M Tris pH 7.5 buffer and allowed to stand overnight in order for complete

solution to occur. In the morning, the solution was centrifuged at $\sim 8000g$ for one-half hour. The supernatant was then separated from a small yellow-brownish pellet and placed in a small dialysis bag. The enzyme was dialized for 12 hours each against four 500 ml portions of $2 \times 10^{-3}M$ 1,10-phenanthroline in 1M NaCl 0.05M Tris pH 7.5 buffer. This was followed by four changes of plain buffer. At this stage the enzyme was considered to be in the apo form. If apoCPA was desired, the enzyme was dialized against two 500 ml portions of 0.005M Tris pH 7.5 which induced crystallization. The dialysis bag was then carefully opened and the crystals collected by centrifugation at 6000g for 10-15 minutes. When a particular metalloderivative was desired, the apoCPA was further dialized against four changes of a $1 \times 10^{-3}M$ solution of the metal ion in the 1M NaCl 0.05M Tris pH 7.5 buffer, followed by two changes of a $1 \times 10^{-4}M$ solution of the metal ion in the same buffer. The metalloCPA was precipitated and collected as described immediately above. Crystalline apo or metallo-CPA was then resuspended on a vortexer in an appropriate amount of 1M NaCl 0.05M Tris pH 7.5 buffer and allowed to stand overnight to insure maximal dissolution. Just prior to use, the solution was centrifuged at 15000g for 1 hour to remove any particulate matter.

Metal solutions were made up from 0.1M metal ion stock solutions. These stock solutions were made by dissolving the pure metal in metal-free HCl. Minimum 99.8% pure metal powders, obtained from Alfa Inorganic, Inc. were used.

Metal Analysis

All metal analyses were done by atomic absorption spectroscopy.⁴¹ A Varian Techtron model AA-5 atomic absorption spectrometer equipped with a Jarrell-Ash model 82-000 monochromator was used. Varian-Techtron hollow cathode element specific lamps were also used. Lamp currents and slit widths recommended by the manufacturer were employed. An air-acetylene flame was used. The following absorption lines were used: Co, 240.73 nm; Ni, 232.00 nm; Cu, 324.75 nm; Zn, 213.86 nm. Solutions to be analyzed were made up to be approximately 1 to 5 ppm in the metal except for zinc where 0.2 to 1.0 ppm solutions were used. A calibration curve was run before each individual analysis on standard solutions that covered the concentration range of interest. These standard solutions had the metal ion in the same buffer solution used for the enzyme samples. They were made up from 1000 ppm standard solutions purchased from Varian Techtron.

Occasional clogging of the nebulizer was encountered, perhaps because of the relatively high concentration of NaCl in the buffer. This problem was alleviated by thorough rinsing of the nebulizer by aspiration of distilled water after each standard or sample was measured. Reproducibility of better than 5% was common on sample volumes of 0.2 ml or less per measurement.

Near Infrared and Visible Spectra

Near infrared and visible absorption spectra of the metallo CPA's, apoCPA, and buffer controls were measured on a Cary 17I recording spectrometer. This machine, which had been extensively modified, was kindly made available by Dr. George R. Rossman. In the normal Cary 17I, a constant energy input or photon flux is maintained on the reference detector by varying the slit width, as the lamp output is strongly dependent on wavelength. On the 0.0-0.1 absorbance slidewire, considerable variation in the baseline is observed in regions where the slit width is changing rapidly with wavelength. On the modified machine, constant reference photon flux is maintained by a feedback loop that modulates the lamp voltage and thus the lamp intensity. The slit width is held constant, and the baseline observed is considerably flatter especially in the regions of solvent absorption.

The main problem in doing near infrared absorption spectroscopy on dilute solutions (1×10^{-3} M or less) of weakly absorbing species ($\epsilon_m \leq 100$) is that long pathlengths (5 cm) are required in order to get any measurable absorption, even on the 0.0-0.1 absorbance range slide wire. Almost all solvents have weak but significant vibrational overtones in the near infrared. Water is particularly bad, as is shown in Figure (I-VI). The practical long wavelength cut-off for H₂O is 900 nm for 5 cm pathlength matched cells on the 0.0-0.1 absorbance range. The situation in D₂O is somewhat better, as the figure also illustrates. D₂O is completely

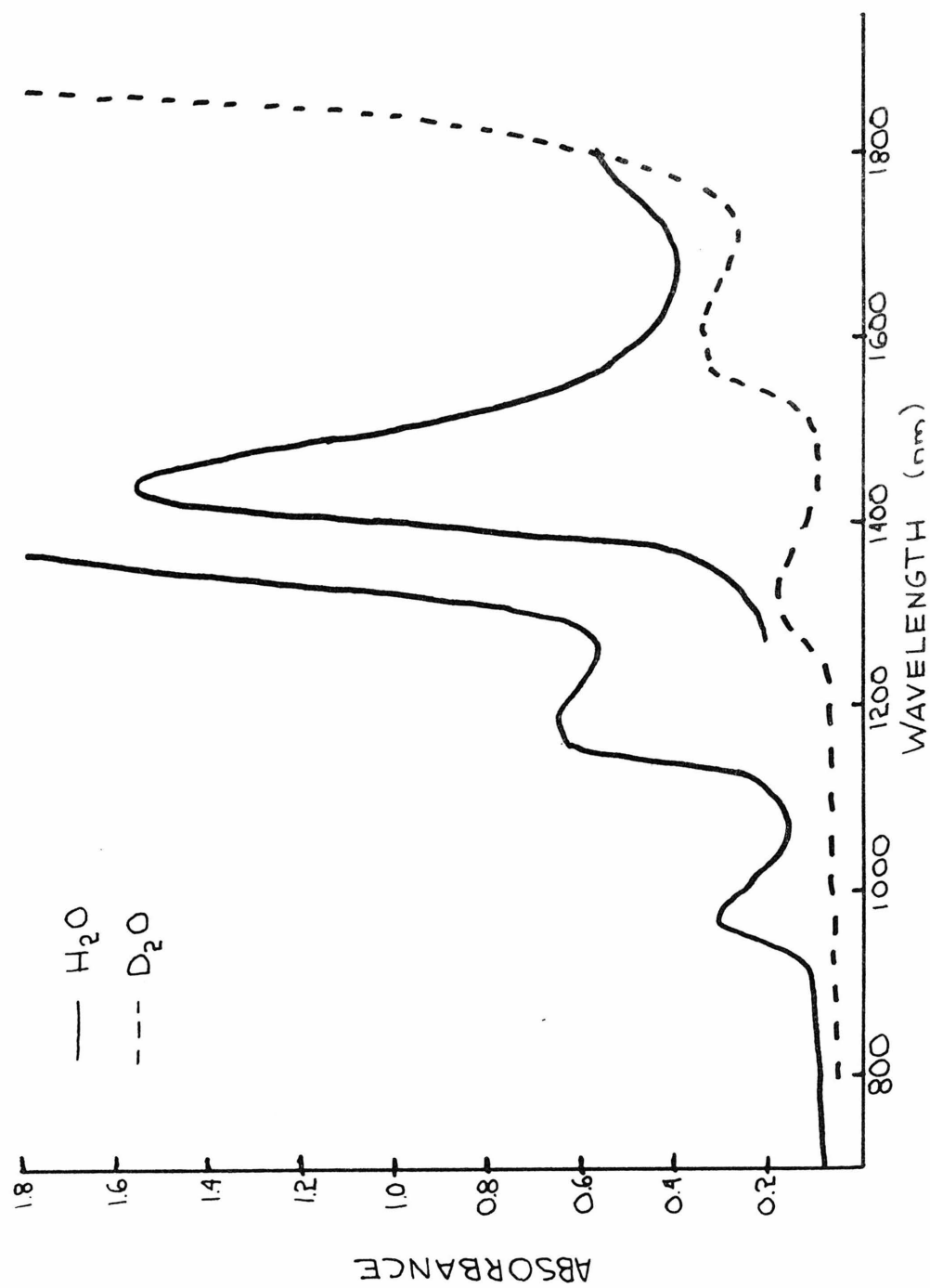


Figure I-VI. Near infrared absorption spectra of H_2O and D_2O .

clear out to approximately 1225 nm. In practice, under the above conditions, data can be taken out to 1500 nm, as the highest energy overtone in D₂O is considerably less intense than the corresponding one for H₂O. However, extreme care must be taken in evaluating any absorption peaks around 1320 nm since this is where the D₂O absorbs.

Frequently, a peak around 1420 nm is observed in D₂O solution. This absorption, especially if it is sharp, is undoubtedly due to residual H₂O in the D₂O. Absorptions at or around 972 nm and 1190 nm are to be similarly suspect.

The absorption spectra of the metallo CPA's were measured by a difference technique. A baseline consisting of the absorption spectrum of apoCPA versus apoCPA was subtracted from the absorption spectrum obtained when a small volume of metal ion in buffer was added to the sample cell. An equivalent volume of metal free buffer was added to the reference cell in order to keep the concentrations of protein equal. A similar procedure was followed when inhibitor or substrate were added. The matched cells, obtained from Hellma Cell, Inc. had a pathlength of 50 mm and held 1.95 ml of solution. Disposable micro-sampling pipets (Corning Glass, Inc.) were used to introduce solutions of additional species. In a typical spectral experiment, a total of 50 λ (50×10^{-3} ml) of metal ion solution was added to the apoCPA. An additional 300 λ of either inhibitor or substrate was then introduced in several aliquots. All treatment of the spectral data beyond the plots of absorbance vs. wavelength includes corrections for enzyme dilution. This method

shall hereafter be referred to as the apo difference method. Another method was also used at the start of this work. It too is a difference method. The spectrum of buffer vs. buffer is subtracted from the spectrum of metalloenzyme vs. buffer. This method will subsequently be referred to as the buffer difference method. These difference techniques are necessary because no matter how well adjusted the spectrometer, significant baseline variations as a function of wavelength are observed on the 0.0-0.1 absorbance range.

During the spectral runs, both the sample and reference compartments were maintained at 6-12 °C in order to inhibit protein denaturation. Nitrogen gas was passed through a liquid nitrogen heat exchanger and then admitted to the sample and reference compartments. The temperature was controlled by adjusting the flow rate. The temperature was monitored by a thermocouple attached to the outside of the sample cell. Tris has a non-negligible temperature coefficient. Based on data supplied by the manufacturer, the actual pH of the buffer at these temperatures is about 8.0. This means that the spectrum of Ni(II)-CPA, for example, was measured at the pH of maximum activity.⁴⁰

Preparation of Deuterated Buffer and Deuterated apoCPA

3.172 gms Trizma HCl and 0.590 gm of dried Trisma Base were placed into a 500 ml polyethylene bottle. These amounts would give a 0.05 M Tris pH 7.5 solution when dissolved in 500 ml of water. 10 ml of 99.5 % D₂O, obtained from Columbia Organic Chemical Co. was added and the solution was evaporated to dryness under vacuum.

This procedure was repeated three times at which point according to a simple dilution calculation the exchangeable proton (H^+) concentration was well below the level from H_2O in the D_2O . 24.22 gms of NaCl that had been extracted with dithiazone in CCl_4 and then dried was then added. D_2O was then added to bring the solution volume to 500 ml.

A 28 cm \times 1 cm diameter Chelex 100 column was prepared from resin that had been put through one regeneration cycle according to the manufacturer's directions and then equilibrated with extracted 1M NaCl, 0.05M Tris pH 7.5 buffer. The D_2O buffer was run through the Chelex column at a flow rate of approximately 2 ml/min. The first 100 ml of column effluent was discarded (this allowed over four bedvolumes for deuteration of the column). The absorption spectrum of the 50-100 ml fraction in the near infrared was identical to that of D_2O . The subsequent column effluent was collected and stored tightly sealed until needed.

ApoCPA, prepared as previously described, was dissolved in approximately 10 ml of the deuterated buffer overnight and then centrifuged in order to remove any undissolved matter. The solution was placed in a small dialysis bag, dialyzed against 6 changes of deuterated buffer in a sealed 50 ml nalgene graduated cylinder in the cold, removed from the dialysis bag and centrifuged.

Binding Constant of the Inhibitor Na β PP to CPA

The binding constant K_I for the reaction



was determined spectrophotometrically using the analytical procedure of Furman and Garner.⁴² The spectra of the M(II)-CPA were measured before and after the successive addition of several equivalents of Na β PP. The only species that contribute to the observed absorbance are the M(II)-CPA and the M(II)-CPA \cdot β PP complex. According to this procedure, the data are treated as follows.

Let

$$\begin{aligned} E &= [MCPA]_{\text{total}} \\ I &= [\beta PP^-]_{\text{total}} \\ C &= [MCPA \cdot \beta PP] \end{aligned}$$

At some wavelength λ the absorbance will be given by

$$A_\lambda = p(E - C) \epsilon_{MCPA} + pC \epsilon_{MCPA \cdot I} \quad (12)$$

where p is the pathlength of the cell used in the experiment and ϵ is the molar extinction coefficient.

Now

$$K_I = \frac{C}{(E - C)(I - C)} \quad (13)$$

or

$$C^2 - (E + I + \frac{1}{K_I})C = -E \times I \quad (14)$$

expanding in terms of a series we get

$$C = \frac{EI}{E + I + \frac{I}{K_I}} + \frac{(EI)^2}{(E + I + \frac{I}{K_I})^3} + \frac{2(EI)^3}{(E + I + \frac{I}{K_I})^5} + \dots \quad (15)$$

taking only the first term since $EI \ll (E + I)$ and substituting in equation (12) we get

$$A_\lambda = p(E - \frac{EI}{E + I + \frac{I}{K_I}})\epsilon_{MCPA} + (\frac{EI}{E + I + \frac{I}{K_I}})p\epsilon_{MCPA \cdot I} \quad (16)$$

expanding and rearranging terms gives

$$\frac{A_\lambda - pE\epsilon_{MCPA}}{EI} = \frac{p(\epsilon_{MCPA \cdot I} - \epsilon_{MCPA})}{E + I + \frac{I}{K_I}} \quad (17)$$

taking the reciprocal of both sides and expanding gives finally

$$\frac{EI}{A_\lambda - pE\epsilon_{MCPA}} = \frac{E + I}{p(\epsilon_{MCPA \cdot I} - \epsilon_{MCPA})} + \frac{1}{K_I} \quad (18)$$

Because of the form of equation 18 a plot of

$$\frac{EI}{A_\lambda - pE\epsilon_{MCPA}} \quad \text{vs. } (E + I) \quad \text{should be a straight line with}$$

$$\text{Slope} = [(\epsilon_{MCPA \cdot I} - \epsilon_{MCPA})p]^{-1} \quad (19)$$

$$\text{Intercept} = [K_I(\epsilon_{\text{MCPA} \cdot \text{I}} - \epsilon_{\text{MCPA}})p]^{-1} \quad (20)$$

Thus

$$\frac{\text{Slope}}{\text{Intercept}} = K_I \quad (21)$$

The nice feature of this procedure is that it permits calculation of K_I even when $\epsilon_{\text{MCPA} \cdot \text{I}}$ is not known. Rather it can be calculated from the slope. Thus

$$\epsilon_{\text{MCPA} \cdot \text{I}} = \epsilon_{\text{MCPA}} + (\text{Slope} \times p)^{-1} \quad (22)$$

It is important to note that the validity of this procedure depends on the assumption made in truncating the series expansion of C , equation (15), after the first term. In the studies to be described below, $E \sim 5 \times 10^{-4}M$, $I \simeq 5 \times 10^{-3}M$ so $EI \ll E + I$, and so taking only the first term is reasonable.

There is one other point worth making about the values of K_I calculated by this procedure. At or near an isobestic point, where $\epsilon_{\text{MCPA} \cdot \text{I}} = \epsilon_{\text{MCPA}}$, there will be a discontinuity in the calculated value of K_I . The discontinuity will occur since both the slope (equation 19) and the intercept (equation 20) will equal zero at this particular wavelength.

References

1. B. L. Vallee and H. Neurath, J. Amer. Chem. Soc., 76, 5006 (1954).
2. B. L. Vallee, J. A. Rupley, T. A. Coombs, and H. Neurath, J. Amer. Chem. Soc., 80, 4750 (1958).
3. J. E. Snoke, G. W. Schwert, and H. Neurath, J. Biol. Chem., 175, 7 (1948).
4. P. H. Pétra and H. Neurath, Biochem., 8, 2466 (1969).
5. P. H. Pétra and H. Neurath, Biochem., 8, 5029 (1969).
6. P. H. Pétra, M. A. Herwodson, K. A. Walsh, and H. Neurath, Biochem., 10, 4023 (1971).
7. M. L. Anson, J. Gen Physiol. 20, 777 (1937).
8. B. A. Allen, P. J. Keller, and H. Neurath, Biochem., 3, 40 (1964).
9. D. J. Cox, F. C. Bovard, J. -P. Bargetzi, K. A. Walsh, and H. Neurath, Biochem., 3, 44 (1964).
10. R. A. Bradshaw, L. H. Ericsson, K. A. Walsh, and H. Neurath, Proc. Nat. Acad. Sci. U.S., 63, 1389 (1969).
11. T. A. Steitz, M. L. Ludwig, F. A. Quiocho, and W. N. Lipscomb, J. Biol. Chem., 242, 4662 (1967).
12. W. N. Lipscomb, J. A. Hartsuck, G. N. Reeke, Jr., F. A. Quiocho, P. H. Bethge, T. A. Steitz, H. Muirhead, and J. C. Coppola, Brookhaven Symp. Biol., 21, 24 (1968).
13. W. N. Lipscomb, G. N. Reeke, Jr., J. A. Hartsuck, F. A. Quiocho, and P. H. Bethge, Phil. Trans. Roy. Soc. London, B257, 177 (1970).

14. W. N. Lipscomb, *Accounts Chem. Res.*, 3, 81 (1970).
15. F. A. Quioco and W. N. Lipscomb, *Adv. in Protein Chem.*, 25, 1 (1971).
16. J. A. Hartsuck and W. N. Lipscomb in *The Enzymes*, P. D. Boyer ed., Vol. III, 3rd ed., Academic Press, New York, 1971, p. 1.
17. M. L. Ludwig and W. N. Lipscomb in *Inorganic Biochemistry*, G. Eichhorn, ed., Elsevier, Amsterdam, in press, Chap. 15.
18. D. S. Auld and B. L. Vallee, *Biochem.*, 9, 602 (1970).
19. D. S. Auld and B. L. Vallee, *Biochem.*, 9, 4352 (1970).
20. D. S. Auld and B. L. Vallee, *Biochem.*, 10, 2892 (1971).
21. F. W. Carson and E. T. Kaiser, *J. Amer. Chem. Soc.*, 88, 1212 (1966).
22. E. T. Kaiser and B. L. Kaiser, *Accounts Chem. Res.*, 5, 219 (1972).
23. B. L. Vallee, J. A. Rupley, T. A. Coombs, and H. Neurath, *J. Biol. Chem.*, 235, 64 (1960).
24. J. E. Coleman and B. L. Vallee, *Biochem.*, 1, 1083 (1962).
25. J. E. Coleman and B. L. Vallee, *Biochem.*, 3, 1874 (1964).
26. J. E. Coleman and B. L. Vallee, *J. Biol. Chem.*, 236, 2244 (1961)
27. R. C. Davies, J. F. Riordan, D. S. Auld, and B. L. Vallee, *Biochem.*, 7, 1090 (1968).
28. E. P. Kang and C. B. Storum, *Biochem. Biophys. Res. Comm.*, 49, 62 (1972).

29. N. D. Chasteen, private communication.
30. S. A. Latt and B. L. Vallee, *Biochem.*, 10, 4263 (1971).
31. T. A. Kaden, B. Holmquist, and B. L. Vallee, *Biochem. Biophys. Res. Comm.*, 46, 1654 (1972).
32. F. S. Kennedy, H. A. O. Hill, T. A. Kaden, and B. L. Vallee, *Biochem. Biophys. Res. Comm.*, 48, 1533 (1972).
33. B. L. Vallee and W. E. C. Wacker, The Proteins, Vol. V, Metalloproteins, H. Neurath, ed., Academic Press, New York, 1970, p. 99.
34. B. L. Vallee and R. J. P. Williams, *Proc. Nat. Acad. Sci. U.S.*, 59, 498 (1968).
35. R. J. P. Williams, *Inorg. Chim. Acta Revs.*, 5, 137 (1971).
36. P. H. Pétra, *Methods in Enzymology*, 19, 460 (1970).
37. H. R. Mahler and E. H. Cordes, Biological Chemistry, Harper and Row, New York, 1966, p. 228-229.
38. R. E. Thiers in Methods of Biochemical Analysis, D. Glick, ed., Vol. V, p. 273, Interscience, New York, 1957.
39. T. R. Hughes and I. M. Klotz in Methods of Biochemical Analysis, D. Glick, ed., Vol. III, p. 280, Interscience, New York, 1956.
40. J. E. Coleman and B. L. Vallee, *J. Biol. Chem.*, 235, 390 (1960).
41. K. Fawa, P. Pulido, R. McKay, and B. L. Vallee, *Anal. Chem.*, 36, 2407 (1964).
42. S. C. Furman and C. S. Garner, *J. Amer. Chem. Soc.*, 73, 4528 (1951).

CHAPTER II

COBALT(II)CARBOXYPEPTIDASE A

Cobalt(II)-CPA is the most active of the "synthetic" CPA's towards model peptide substrates.^{1,2,3} Considerable effort has been devoted to elucidating the coordination geometry of the metal center in Co(II)-CPA by various spectroscopic techniques. The absorption, circular dichroic, and magneto-circular dichroic spectra of Co(II)-CPA,⁴ as well as other cobalt(II) analogues of zinc metalloenzymes,⁵ have been studied. The low temperature EPR spectra of these systems have also been reported.⁶ Except for the absorption spectra, extensive model system data are simply not available. Based on the very limited model system work that accompanied their results on the cobalt(II) metalloenzymes, Vallee and co-workers have concluded that the spectral properties of Co(II)-CPA are consistent with a distorted tetrahedral geometry about the metal center.

The magnetic moments and the intensities of the visible absorption bands attributable to electronic transitions from the ground state to the ligand field levels derived from the free ion $^4P(\text{Co}^{+2})$ excited state are well established indicators of coordination geometry for high-spin Co(II) complexes. Thus, an accurate determination of the magnetic susceptibility of Co(II)-CPA along with a detailed comparison of the value obtained with those of relevant model complexes seemed potentially rewarding, especially if it was coupled with a thorough review of the available absorption spectral data.

Sample Preparation

Crystalline Co(II)-CPA was prepared by the dialysis procedure previously described. A small sample of the crystalline Co(II)-CPA was then redissolved in buffer for activity and metal analyses. Only samples containing less than one cobalt(II) ion per enzyme molecule were used in the susceptibility determination. In order to obtain a suitable sample, the suspension of crystalline Co(II)-CPA was spread on a glass slide and allowed to dry. Some early samples of the protein were contaminated by ferromagnetic impurities. In order to eliminate this problem, subsequent samples were handled in a scrupulously dust free enclosure. For the susceptibility measurement, the sample was placed in a quartz tube. After the measurement, a total metal analysis was performed by digesting the protein in a 1:1 HNO_3 - H_2SO_4 mixture, diluting it to a known volume, and then determining the metal concentration by atomic absorption spectroscopy, as previously described.

Air dried crystalline Co(II)-CPA retains its red-purple color. In order to verify that the drying procedure did not significantly disrupt the metal-protein interaction, the spectrum of a pellet of the air dried Co(II)-CPA was measured. The visible spectrum of Co(II)-CPA in solution as well as that of a pellet of air dried crystalline Co(II)-CPA are shown in Figure (Co-I). In overall shape and position of the bands the two spectra are virtually identical. The minor variation in the shoulder at 515-525 nm can be attributed to differences in the relative amount of light scattered by each sample.

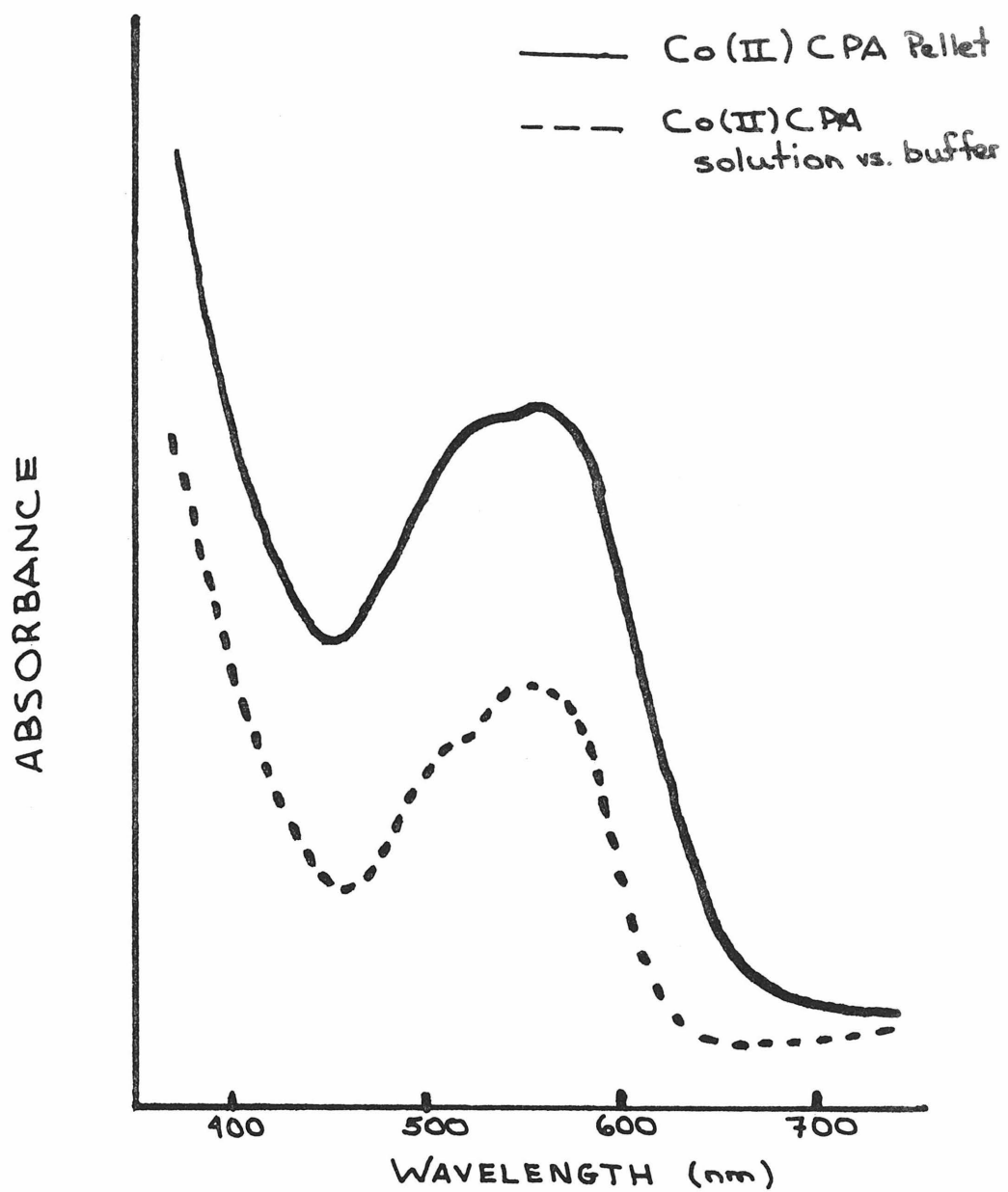


Figure Co-I. Visible spectra of Co(II)CPA samples.

The preparation and purification of the model complexes we investigated will be described later.

Magnetic Susceptibility Measurements and Results

All measurements on protein samples were made on a superconducting, quantum mechanical magnetometer of ultrahigh sensitivity. Complete details of the operation of the system will be described in detail elsewhere.⁷ In simple terms, a superconducting sensor inductively coupled to an rf tank circuit induces a current due to a change of magnetic flux in the sample, arising from either movement of the sample or change in sample temperature. This induced current is used to drive a feed-back loop so that the compensation current, which depends linearly on the sample-related flux, can be accurately converted into magnetic flux. Two types of magnetic susceptibility measurements can be made. In the first type, the total magnetic susceptibility in an axial field is determined by moving the sample from one pickup coil into another wound in the opposite direction so as to compensate for the effect of the sample holder, which extends through both primary coils of the dc superconducting flux transformer. In the second mode of operation, the relative change of susceptibility is measured as a function of temperature up to 120°K. This change is independent of the large diamagnetic background arising from the host protein. A total susceptibility measurement was performed on a 24.4 mg sample of Co(II)-CPA over a temperature range of 30-130°K in fields between 31 and 47 gauss. The sample was subsequently

shown to contain 29.7 μg of Co^{+2} by the procedure previously described. The sample data were corrected for the temperature-independent susceptibility contribution and the magnetic moment was calculated from the slope of the χ vs. $1/T$ plot.

The magnetic susceptibilities of the model Co(II) complexes were measured on a Princeton Applied Research Associates vibrating sample magnetometer, Model FM-1, equipped with an Andronian Associates liquid He dewar for variable temperature measurements. HgCo(CNS)_4 was used as calibrant. Magnetic moments excluding the effect of temperature were calculated from the slopes of $1/\chi$ versus T plots (Curie-Weiss plots).

For some of the tetrahedral Co(II) complexes cited below only room temperature effective magnetic moments are available in the literature. The reported moments of these complexes were corrected for the small but significant temperature independent susceptibility contribution. The calculation of this correction is outlined below.

When the ground state is the only thermally populated state, Van Vleck has shown⁸ that the magnetic susceptibility can be represented as:

$$\chi = \frac{N}{j_m} \left[\sum_m \frac{(\langle \psi_{om} | \hat{\mu} | \psi_{om} \rangle)^2}{kT} - 2 \sum_m \frac{|\langle \psi_{om} | \hat{\mu} | \psi_{nm} \rangle|^2}{E_o - E_n} \right] \quad (1)$$

where the subscripts o and n refer respectively to the ground and excited states and $\hat{\mu} = -\beta(\hat{\mathbf{L}}_Z + 2\hat{\mathbf{S}}_Z)$. The first term in equation (1) represents the first order Zeeman effect, while the second term is the second order Zeeman effect or high frequency term. It should be

noted that while the first order Zeeman effect explicitly has a $1/T$ dependence in it, the second order term is independent of temperature. Hence, it is often called the temperature independent susceptibility or paramagnetism (TIP). The deviations of the observed magnetic susceptibility from the spin only value, which we will be using in an empirical way, arise in the first-order Zeeman effect and are explained in terms of a mixing in of excited state wavefunctions into the ground state wavefunction by spin-orbit coupling. In evaluating the magnitude of the second order Zeeman effect only the first excited state is usually considered, since for higher excited states the denominator $E_o - E_n$ becomes very large. For tetrahedral Co(II), which has a d^7 configuration with a 4A_2 ground state and a 4T_2 first excited state, it has been shown⁹ that:

$$\chi_{\text{TIP}} = \frac{8N\beta^2}{10Dq} = \frac{2.09}{10Dq} \quad (2)$$

in c.g.s. units. The parameter Dq can be evaluated from the absorption spectra of the complex. The energy levels of a tetrahedral d^7 complex are shown in Figure (Co-II) and Table (Co-I) along with the transition energies for the three spin allowed bands. Since only ν_2 and ν_3 are usually observed, some simple algebraic manipulation gives:

$$Dq = \frac{9(\nu_2 + \nu_3) \pm [81(\nu_2 + \nu_3)^2 - 340\nu_2\nu_3]^{\frac{1}{2}}}{340} \quad (3)$$

$$B = \frac{\nu_2 + \nu_3}{15} - 2Dq \quad (4)$$

Figure Co-II. Tanabe-Sugano diagram for a d^n ion in a tetrahedral field ($C/B = 4.5$).

Table Co-I
 Energy Levels of Quartet States and
 Spin Allowed Transitions for
 a d^7 Ion in a Tetrahedral Ligand Field

<u>State</u>		<u>Energy</u>
4A_2		$-12 Dq$
4T_2		$- 2 Dq$
$^4T_1(F)$		$7.5 B + 3 Dq - \frac{1}{2} (225 B^2 + 100 Dq^2 - 180 Dq B)^{\frac{1}{2}}$
$^4T_1(P)$		$7.5 B + 3 Dq + \frac{1}{2} (225 B^2 + 100 Dq^2 - 180 Dq B)^{\frac{1}{2}}$

<u>Transition</u>		<u>Energy</u>
ν_1	$^4A_2 \rightarrow ^4T_2$	$10 Dq$
ν_2	$^4A_2 \rightarrow ^4T_1(F)$	$7.5 B + 15 Dq - \frac{1}{2} (225 B^2 + 100 Dq^2 - 180 B Dq)^{\frac{1}{2}}$
ν_3	$^4A_2 \rightarrow ^4T_1(P)$	$7.5 B + 15 Dq + \frac{1}{2} (225 B^2 + 100 Dq^2 - 180 B Dq)^{\frac{1}{2}}$

For our purposes ν_2 and ν_3 are assumed to correspond to the centers of gravity of the band multiplets that are usually observed. The absorption spectrum of bis(5,5-diethylbarbiturato)-bis-imidazoleCo(II) shown in Figure (Co-III) is typical of the spectra of distorted tetrahedral Co(II) complexes. Two groups of bands can be discerned. The weak bands out in the near infrared can be assigned to components of the ${}^4A_2 \rightarrow {}^4T_1(F)$ transition for idealized tetrahedral geometry. The splitting most probably arises from the presence of lower symmetry components in the ligand field. The intense bands centered at approximately $18,000\text{ cm}^{-1}$ can be assigned to components of the ${}^4A_2 \rightarrow {}^4T_1(P)$ transition.

The absorption spectra of the tetrahedral models listed in Table (Co-II) were assigned in this manner. The magnetic moments μ_{eff} , corrected for TIP, were calculated as outlined above. The correction for TIP lowers the effective magnetic moments by about 0.1 B.M. from their room temperature values.

The temperature dependence of the magnetic susceptibility of one tetrahedral and several five-coordinate Co(II) model complexes is shown in Figures (Co-IV to Co-IX). The magnetic moments determined from the Curie-Weiss plots as well as the room temperature moments are summarized in Table Co-III. For the five coordinate complexes there is essentially no difference in the moments calculated from the variable temperature susceptibility data and the room temperature moments. Thus, for comparative purposes we can use the room temperature moments of the complexes for which no variable

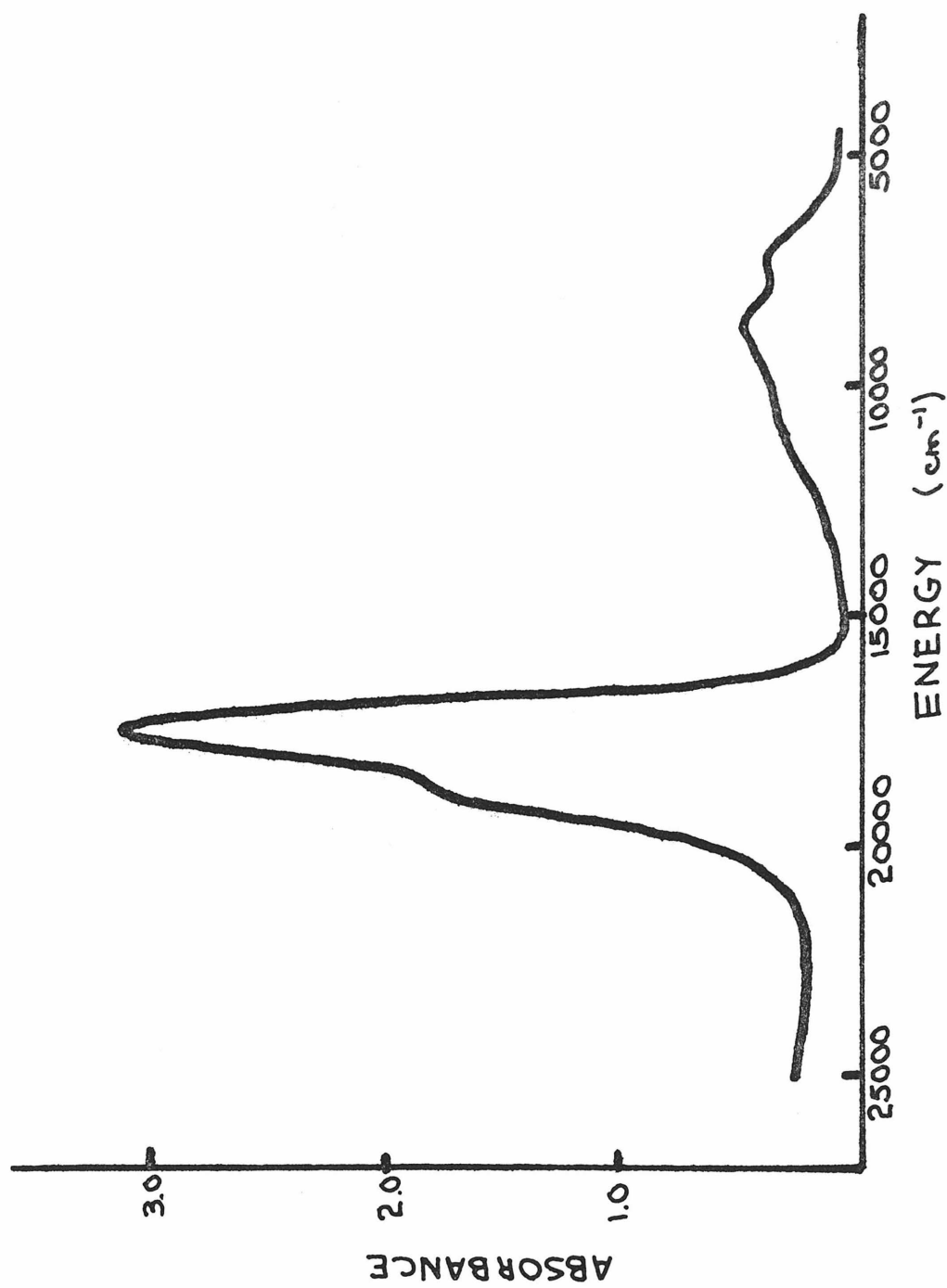


Figure Co-III. Absorption spectrum of $\text{Co}(\text{Barb})_2(\text{Im})_2$ KBr pellet.

Table Co-II
TIP Corrected Magnetic Moments of
Four Coordinate Co(II) Complexes

Complex	$\bar{\nu}_2$ (cm ⁻¹)	$\bar{\nu}_3$ (cm ⁻¹)	Dq (cm ⁻¹) × 10 ⁶	χ_{TIP}	μ_{eff} (RT)	μ_{eff} (TIP Corr)
Co(EDM)Cl ₂	7688 ^a	15587 ^a	451	463	4.48 ^a	4.36
Co(Me ₄ en)Cl ₂	8336 ^b	16837 ^b	490	427	4.65 ^b	4.54
Co(MOBenNEt)Cl ₂	7531 ^c	16108 ^c	439	476	4.50 ^c	4.37
Co(PA) ₂	9117 ^d	19775 ^d	531	394	4.67 ^d	4.56
Co(MBrPM) ₂	10107 ^e	16700 ^e	625	334	4.53 ^e	4.44
Co(barb) ₂ Im ₂ ^f	8897	17938	523	400	4.53	4.43

^a Reference 10, EDM = ethylenedimorpholine.

^b Reference 11, Me₄en = N,N,N',N' -tetramethylethylenediamine.

^c Refernce 12, MOBENNEt₂ = N,N-diethyl-N' (o-methoxybenzylidene)-ethylenediamine.

^d Reference 13, PA = N,t-butyl-pyrolle-2-alimine.

^e Reference 14, MBrPM = 5' -Bromo-3,4',5-trimethyl dipyrromethene-3',4-dicarboxylate. Note: The position of ν_3 is uncertain in this complex.

^f Barb = 5,5' -diethylbarbituric acid, Im = imidazole.

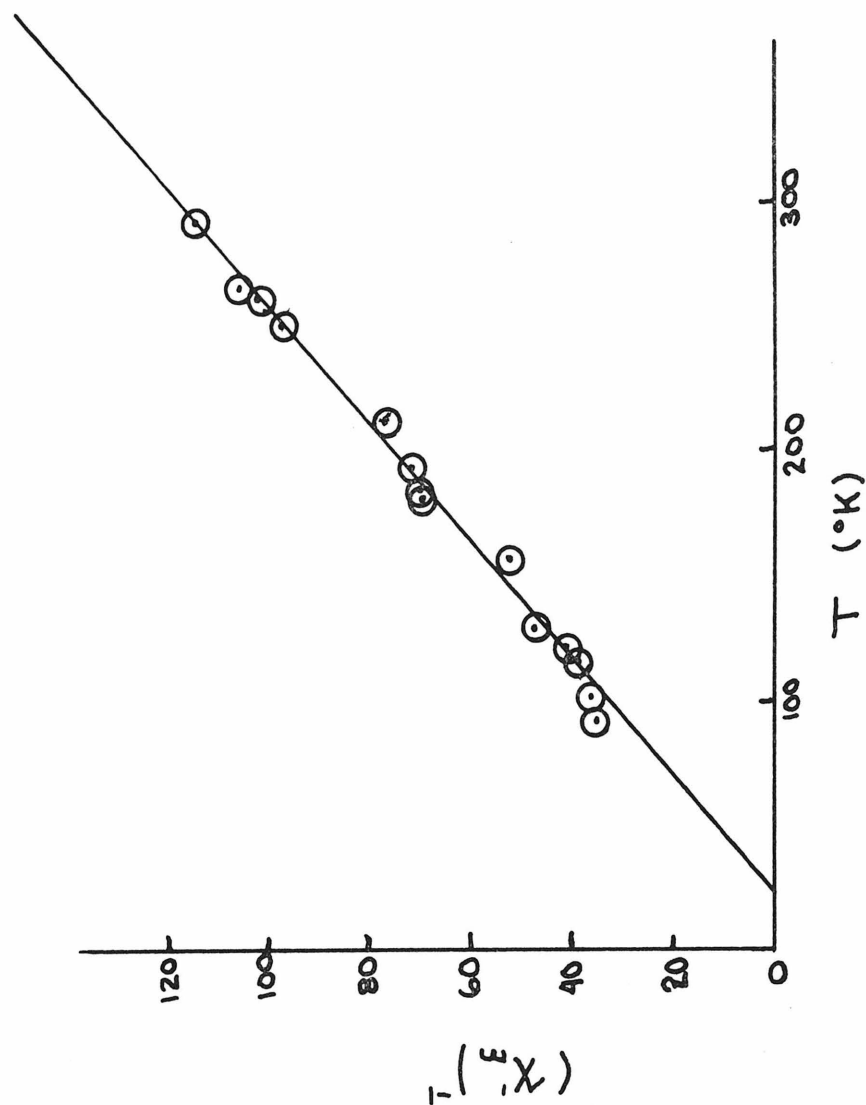


Figure Co-IV. Plot of $(\chi'_m)^{-1}$ vs. T for $\text{Co}(\text{Barb})_2(\text{Im})_2$. $\mu_{\text{eff}} = 4.33$ B. M., $\theta = -22.6^\circ \text{K}$.

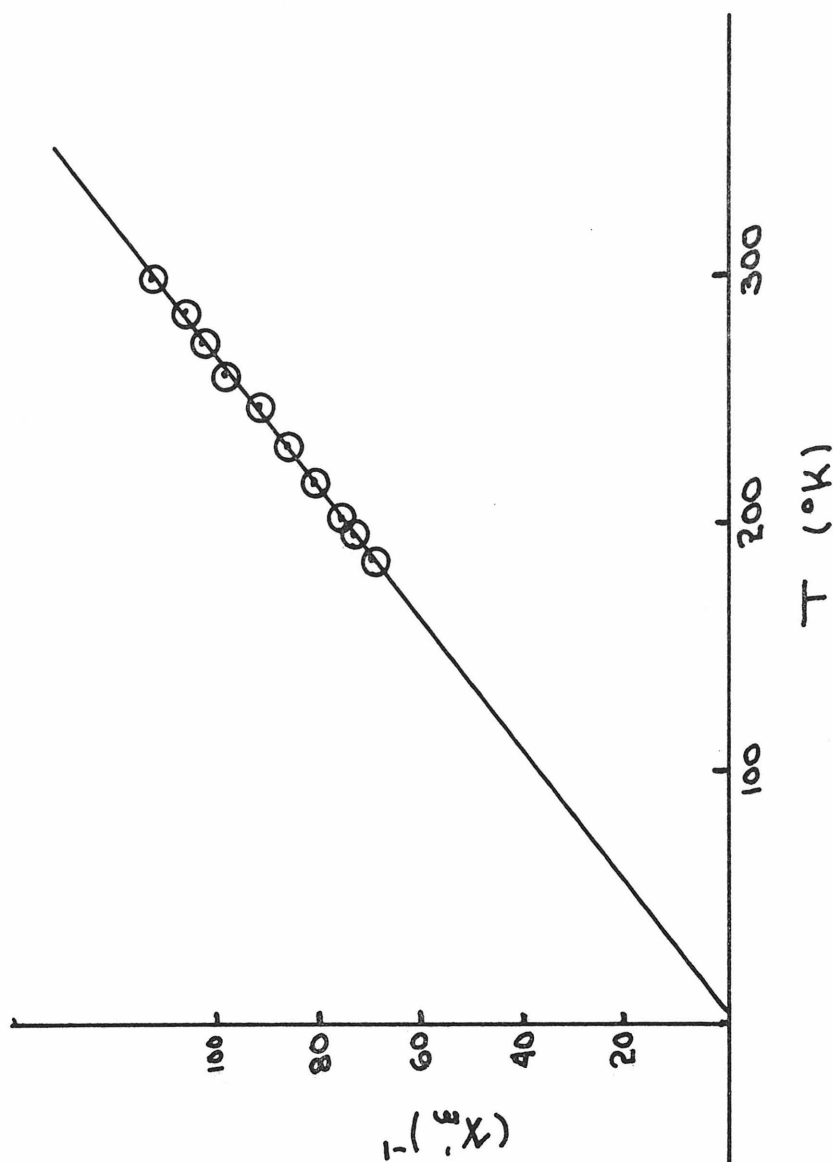


Figure Co-V. Plot of $(\chi'_m)^{-1}$ vs. T for $\text{Co}(\text{Et}_4\text{dien})\text{Cl}_2$.
 $\mu_{\text{eff}} = 4.59 \text{ B.M.}$, $\theta = -3^\circ\text{K}$.

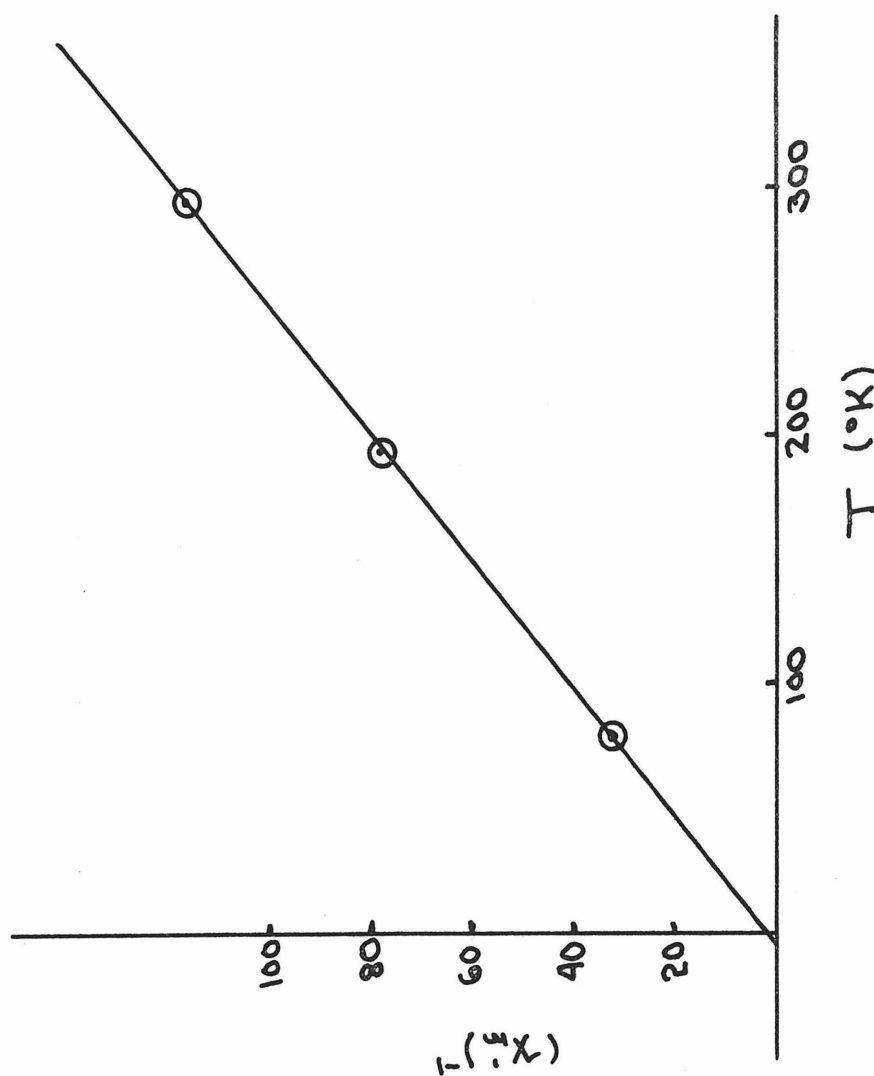


Figure Co-VI. Plot of $(\chi'_m)^{-1}$ vs. T for $[\text{Co}(\text{Me}_5\text{tren})\text{Cl}]\text{Cl}$. $\mu_{\text{eff}} = 4.51$ B.M., $\theta = +4^\circ\text{K}$. Data from reference 15.

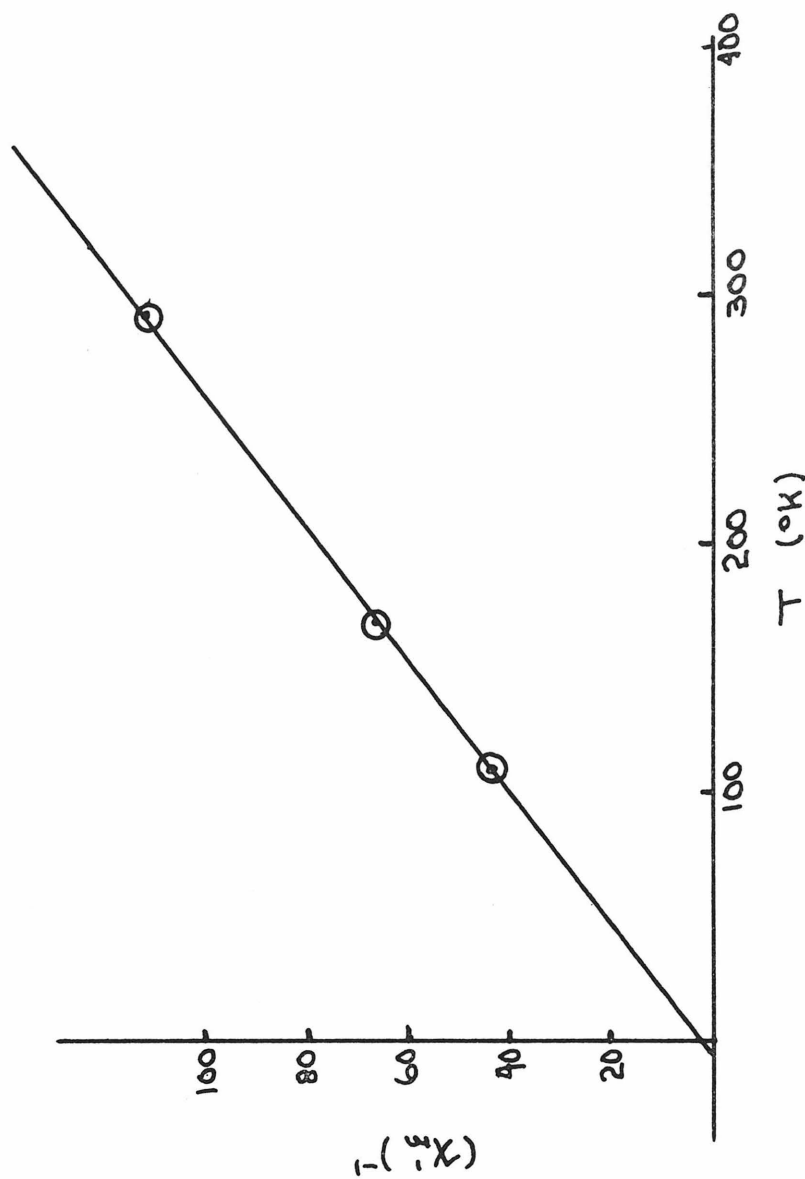


Figure Co-VII. Plot of $(\chi'_m)^{-1}$ vs. T for $\text{Co}(\text{Me}_5\text{dien})\text{Cl}_2$. $\mu_{\text{eff}} = 4.61$ B. M., $\theta = 6^{\circ}\text{K}$. Data from reference 16.

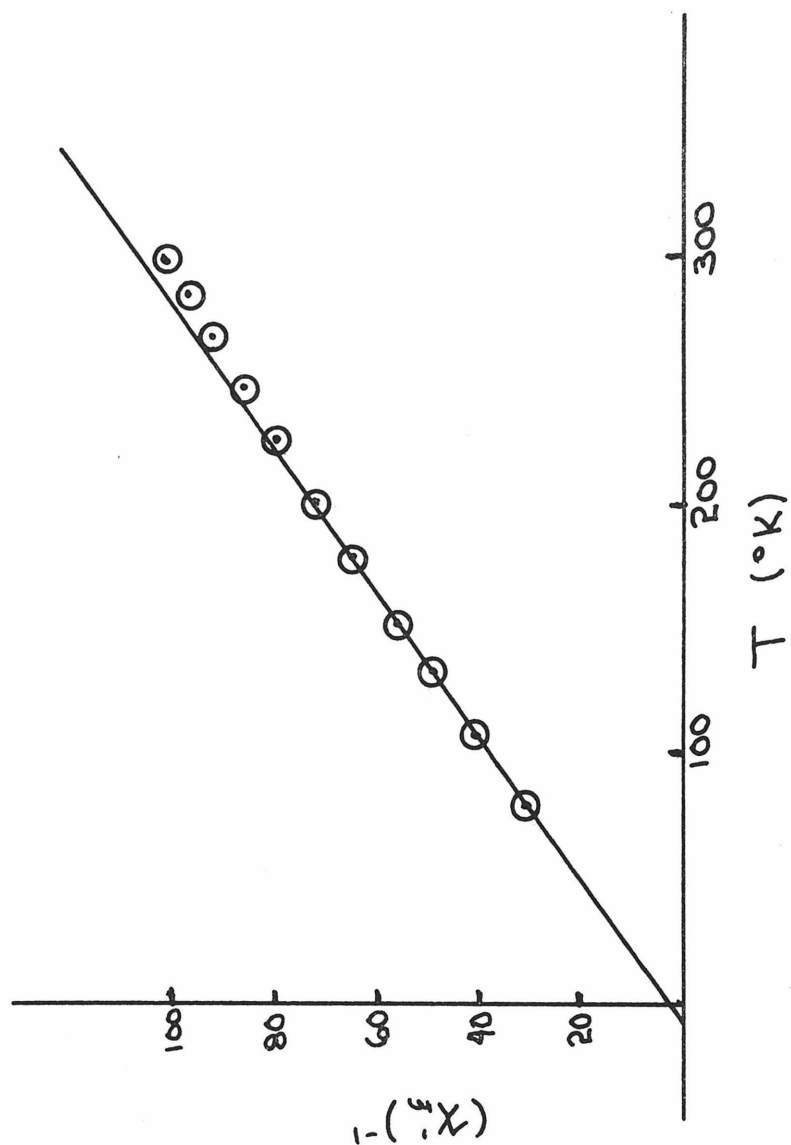


Figure Co-VIII. Plot of $(\chi'_m)^{-1}$ vs. T for β -Co(Paphy)Cl₂. $\mu_{\text{eff}} = 4.79$ B. M., $\theta = +9^\circ\text{K}$. Data from reference 17.

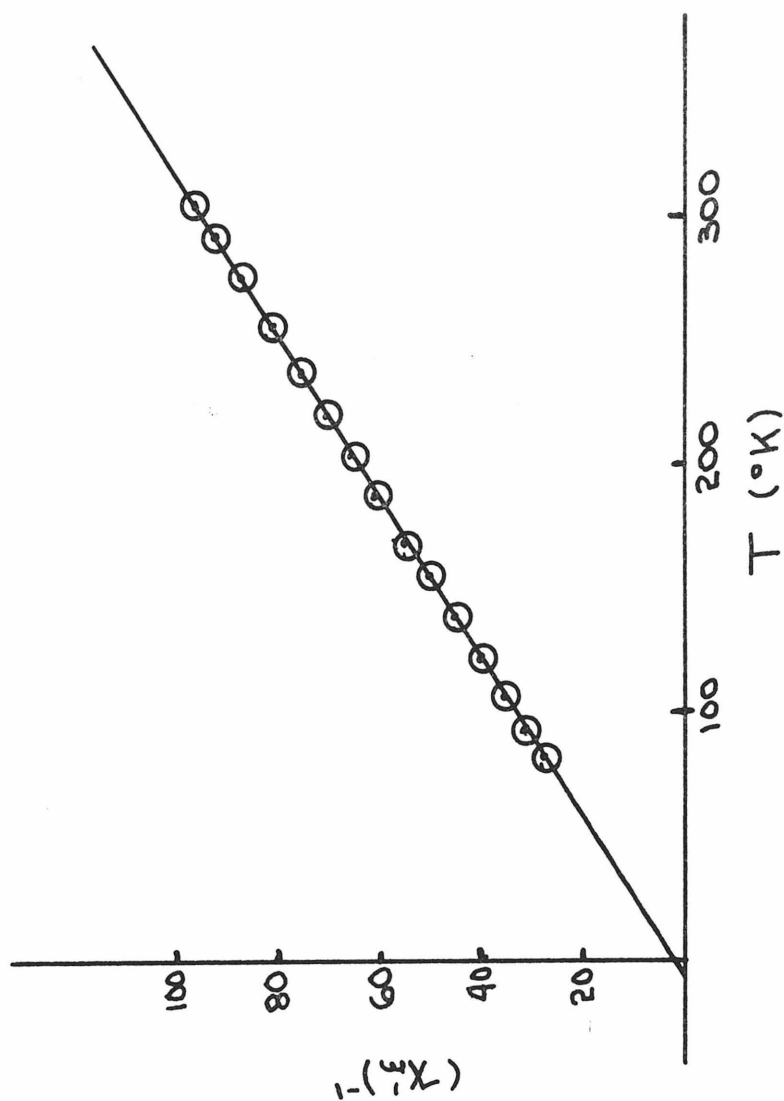


Figure Co-IX. Plot of $(\chi'_m)^{-1}$ vs. T for $\text{Co}(\text{Terpy})\text{Cl}_2$.
 $\mu_{\text{eff}} = 5.08$ B.M., $\theta = +6^\circ\text{K}$. Data from reference 17.

Table Co-III
Temperature Independent Magnetic Moments of
Four and Five Coordinate Co(II) Complexes

<u>Complex</u>	<u>$\mu_{\text{eff}}(\text{RT})$</u>	<u>μ_{eff}</u>
Co(Barb) ₂ Im ₂ ^a	4.53	4.33
Co(Et ₄ dien)Cl ₂ ^b	4.65	4.59
[Co(Me ₆ tren)Cl]Cl	4.49 ^c	4.51
Co(Me ₅ dien)Cl ₂	4.56 ^d	4.61
β -Co(Paphy)Cl ₂	4.84 ^e	4.79
Co(Terpy)Cl ₂	5.03 ^e	5.08
Co(Me ₄ daeo)Cl ₂	4.70 ^f	--
Co(Py(Cy) ₂)Cl ₂	4.85 ^g	--
Co(MABenNEt ₂)Cl ₂	4.82 ^h	--

^a Barb = 5, 5' -diethylbarbituric acid, Im = imidazole

^b Et₄dien = 1, 1, 7, 7-tetraethyldiethylenetriamine.

^c Reference 15, Me₆tren = tris(2-dimethylaminoethyl)amine.

^d Reference 16, Me₅dien = bis(2-dimethylaminoethyl)methylamine.

^e Reference 17, Paphy = pyridine-2-aldehyde-2-pyridylhydrazone,
terpy = terpyridine.

^f Reference 18, Me₄daeo = bis(2-dimethylaminoethyl)oxide.

^g Reference 19, Py(cy)₂ = N, N' -dicyclohexyl, 2, 6-diacetylpyridine-
bisimine.

^h Reference 20, MABenNEt₂ = N, N-diethyl-N' (o-methylamino-
benzylidene)ethylenediamine.

temperature data are available. As expected, the moment of the distorted tetrahedral complex, $\text{Co}(\text{Barb})_2\text{Im}_2$ is significantly lower than the room temperature value. The value determined from the Curie-Weiss plot agrees well with the room temperature value corrected for TIP.

The temperature dependence of the magnetic susceptibility of $\text{Co}(\text{II})$ -CPA is shown in Figure (Co-X). It follows the Curie law over the temperature range investigated. A value of 4.77 ± 0.15 B.M. for the magnetic moment of $\text{Co}(\text{II})$ -CPA is obtained from the data. This value confirms that the ground state of $\text{Co}(\text{II})$ -CPA arises from a high spin (spin-quartet) electronic configuration.

Discussion

A square planar coordination site in $\text{Co}(\text{II})$ -CPA can be completely ruled out on the basis of the observed ground state. No high spin, square planar $\text{Co}(\text{II})$ complex has ever been observed. Both the positions and the intensities of the visible absorption bands of $\text{Co}(\text{II})$ -CPA eliminate an octahedral metal site geometry as well.⁴ In fact, the positions of the absorption bands of $\text{Co}(\text{II})$ -CPA are remarkably similar to those of model distorted tetrahedral $\text{Co}(\text{II})$ complexes such as the ones discussed earlier. Extremely reasonable values of the parameters Dq and B can be obtained by fitting the spectrum of $\text{Co}(\text{II})$ -CPA with the tetrahedral model.

As indicated previously, it is possible to calculate an upper limit on the first order Zeeman effect if the parameter Dq is known.

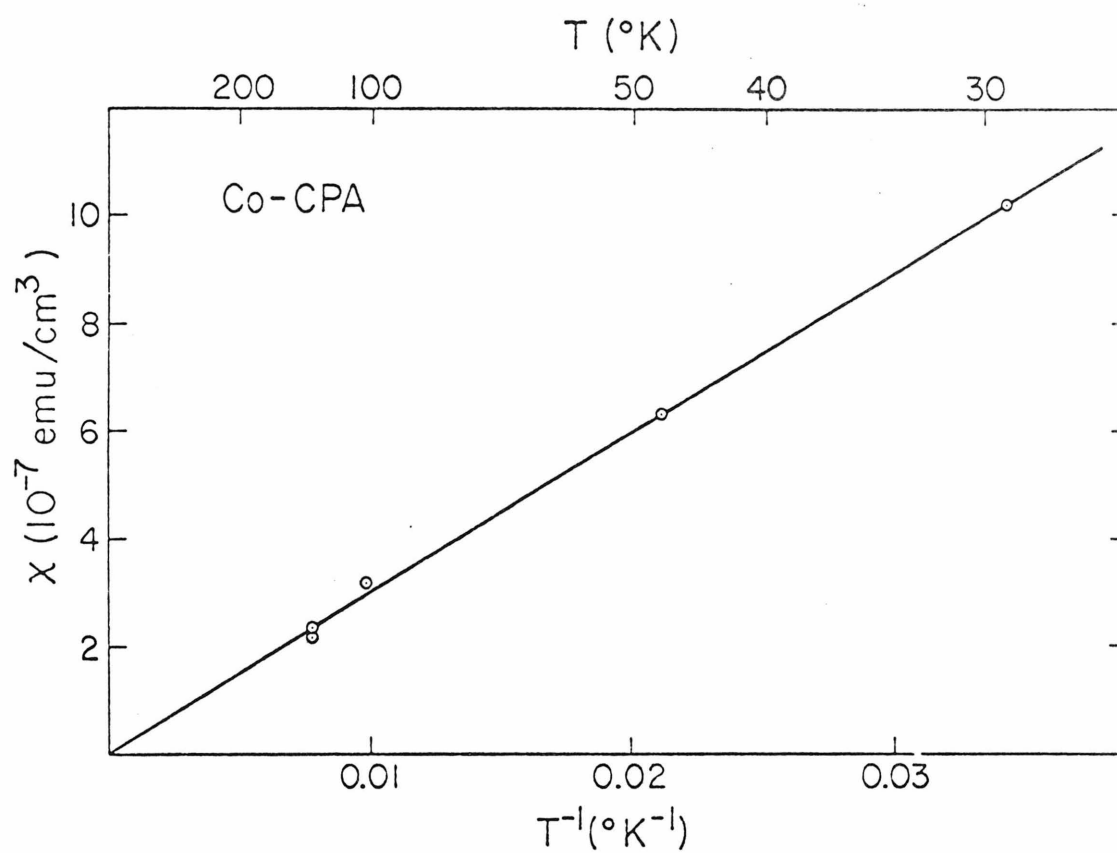


Figure Co-X. Temperature dependence of the magnetic susceptibility (χ) of Co(II)CPA in the range 30 - 130 $^{\circ}\text{K}$.

Because the spin orbit coupling operator mixes a small amount of one component of the excited 4T_2 state into the ground state 4A_2 wave function, the orbital angular momentum is not completely quenched. It is well known that in the case of Co(II) in a tetrahedral environment:

$$\mu_{\text{eff}} = \mu_{\text{so}} \left(1 - \frac{4k^2\lambda}{10Dq} \right) \quad (5)$$

where μ_{so} is the spin only magnetic moment of 3.87 B.M. for three unpaired electrons, λ is the free ion spin orbit coupling constant, and k is the orbital reduction factor. We note that since λ is negative for a d^7 ion, the calculated moment will be higher than the spin only value, consistent with the results previously reported. The orbital reduction factor which has a value between 0 and 1, accounts for the observation that λ is reduced below its free ion value in metal complexes. The spectral parameters as well as the calculated and observed magnetic moments for the model tetrahedral complexes, Co(II)-CPA, and some model five coordinate complexes are shown in Table (Co-IV). We emphasize again that we are using a tetrahedral model even for the five coordinate complexes. Maximum values of the magnetic moments were calculated by letting $k = 1$ in equation (5). A value for λ of -180 cm^{-1} was assumed.

The band positions and the calculated ligand field parameters for both the four and five coordinate models are very similar. Only the large discrepancy between the observed and calculated effective magnetic moments of the five coordinate complexes indicates that the tetrahedral model is not applicable to them. Thus, on the basis of

Table Co-IV

Ligand Field Parameters and Maximum Magnetic Moments Calculated for

a Tetrahedral Model

<u>Complex</u>	$\bar{\nu}_2$ (cm^{-1})	$\bar{\nu}_3$ (cm^{-1})	<u>Dq</u> (cm^{-1})	B (cm^{-1})	$\mu_{\text{eff}}(\text{calc})$ (B.M.)	$\mu_{\text{eff}}(\text{obs})$ (B.M.)
Distorted Tetrahedral						
Co(EDM)Cl ₂	7688	15587	451	649	4.49	4.36
Co(Me ₄ en)Cl ₂	8336	16837	490	699	4.44	4.54
Co(MOBen·NEt ₂)Cl ₂	7531	16108	439	697	4.50	4.37
Co(PA) ₂	9117	19775	531	864	4.39	4.56
Co(Barb) ₂ (Im) ₂	8897	17938	523	743	4.40	4.33
Co(BenzIm) ₄ (ClO ₄) ₂	9009	17700	531	718	4.39	4.28
Five Coordinate						
β -Co(Paphy)Cl ₂	7680	15850	450	669	4.49	4.79
Co(Me ₆ tren)Cl ₂	9090	18333	534	760	4.39	4.51
Co(Me ₅ dien)Cl ₂	9762	17487	586	644	4.35	4.61
Co(Me ₄ daeo)Cl ₂	8519	16923	501	693	4.43	4.70

Table Co-IV (Continued)

Complex	$\bar{\nu}_2$ (cm^{-1})	$\bar{\nu}_3$ (cm^{-1})	Dq (cm^{-1})	B (cm^{-1})	$\mu_{\text{eff}}(\text{calc})$ (B.M.)	$\mu_{\text{eff}}(\text{obs})$ (B.M.)
Co(Py(Cyl ₂)Cl ₂)	7741	17168	450	761	4.49	4.85
Co(MABenNEt ₂)Cl ₂	8965	16600	534	635	4.39	4.82
<u>Co(II) Enzymes</u>						
Co(II)-CPA	8616	17750	504	748	4.42	4.77
Co(II)-CA	8962	17490	529	705	4.40	4.23

band positions alone it is easy to see how distorted tetrahedral and five coordinate environments can be confused. Co(II)-CPA is an excellent example. The values of Dq and B obtained from fitting its spectrum with the tetrahedral model fit nicely in terms of both the spectrochemical and nephelauxetic series, falling between the four nitrogen and the two nitrogen two chloride donor sets. However, the maximum magnetic moment calculated by this model, 4.42 B.M., is significantly less than the observed moment of 4.77 B.M. The failure to predict a large enough magnetic moment indicates that distorted tetrahedral coordination is not a good structural model for Co(II)-CPA.

The intensities of the visible absorption bands attributable to the electronic transitions from the ground state to the ligand field levels derived from the free ion 4P (Co^{+2}) excited state are also widely used as indicators of the coordination geometry for Co(II) complexes. The visible absorption spectral maxima, molar extinction coefficients, and magnetic moments of selected distorted tetrahedral and five coordinate model Co(II) complexes are shown in Table (Co-V). Data for the Co(II)-CPA and Co(II)-CA are also included. An attempt was made to choose only model complexes with donor atoms similar to those available from the protein. Unfortunately, the range of suitable models available in the literature is not very great. So in practice, complexes having at least two nitrogen donor atoms were picked.

Table Co-V

Spectral and Magnetic Properties of Cobalt(II) Complexes

<u>Complex</u>	<u>Donor Set</u>	<u>μ_{eff}(B. M.)</u>	<u>ν_{max} (cm⁻¹) (ϵ_{molar})</u>
<u>Four Coordinate</u>			
Co(EDM)Cl ₂	N ₂ Cl ₂	4.36	14, 600(320), 15, 070(311), 17, 250(232), 18, 200(sh)
Co(Me ₄ en)Cl ₂	N ₂ Cl ₂	4.54	15, 200(447), 17, 300(214)
Co(MOBenN-Et ₂)Cl ₂	N ₂ Cl ₂	4.37	15, 400(410), 15, 750(425), 17, 150(425)
Co(PA) ₂	N ₄	4.56	16, 000(58), 17, 100(129), 19, 610(600), 20, 830(629)
Co(MBrPM) ₂	N ₄	4.44	13, 010(498), 14, 090(383)
Co(Barb) ₂ (Im) ₂	N ₄	4.33	17, 270(~350), 18, 867(sh)
Co(BenzIm) ₄ (ClO ₄) ₂ ^a	N ₄	4.28	17, 400(645), 18, 600(sh)
<u>Five Coordinate</u>			
Co(Et ₄ dien)Cl ₂	N ₃ Cl ₂	4.59	18, 300(60), 19, 200(58)
[Co(Me ₆ tren)Cl]Cl	N ₄ Cl	4.51	15, 600-16, 100(128), 19, 200-19, 800 (112)

Table Co-V (Continued)

<u>Complex</u>	<u>Donor Set</u>	<u>μ_{eff}(B.M.)</u>	<u>ν_{max} (cm⁻¹) (ϵ_{molar})</u>
Co(Me ₅ dien)Cl ₂	N ₃ Cl ₂	4.61	16,100(106), 18,800(112)
β -Co-Co(Paphy)Cl ₂	N ₃ Cl ₂	4.79	15,700, 20,000(sh)
Co(Terpy)Cl ₂	N ₃ Cl ₂	5.08	15,850, 20,000(sh)
Co(Me ₄ daeo)Cl ₂	N ₂ OCl ₂	4.70	16,200(225), 18,500(151)
Co(Py(Cy) ₂)Cl ₂	N ₃ Cl ₂	4.85	16,500(52), 17,900(52)
Co(MABenNET ₂)Cl ₂	N ₃ Cl ₂	4.82	15,800(187), 16,700(sh), 17,800(sh)
<u>Trigonal Prismatic</u>			
[Co(PccBF)[BF ₄]] ^b	N ₆	4.91	8130(3.6), ~22,000(230)
<u>Cobalt Enzymes:</u>			
Co(II)-CPA		4.77	6370(18), 10,640(20), 17,480-18,020(150)
Co(II)-CA ^c		4.23	15,670(250), 16,180(250), 18,180(400), 19,600(240)

^aReference 21, BenzIm = Benzimidazole.^bReference 22, PccBF = Fluoroborotris(2-aldoximo-6-pyridyl)phosphine.^cReference 23.

The distorted tetrahedral complexes have magnetic moments that range from 4.3 to 4.6 B.M. The most intense visible bands in these complexes generally have molar extinction coefficients that exceed 250. The five coordinate models, on the other hand, have magnetic moments of 4.5-5.1 B.M. and an effective ϵ_{\max} range of 80-225.

The spectral and magnetic properties of Co(II)CPA fall nicely into the range observed for the five coordinate models. As we have seen, the magnetic moment of Co(II)-CPA is too high to be explained by a distorted tetrahedral structure. On the basis of the data in Table (Co-V), the molar extinction coefficient of Co(II)-CPA, 150, is really too low to reflect a distorted tetrahedral environment. The properties of Co(II)-CA, on the other hand, fit a distorted tetrahedral model quite well. The observed magnetic moment is low, 4.23 B.M., and the molar extinction coefficient of the most intense visible band is relatively large, 400. Further, the values 520 cm^{-1} and 705 cm^{-1} calculated for Dq and B respectively are quite reasonable (see Table Co-IV). The maximum magnetic moment calculated on the basis of these parameters is 4.40 B.M. which is in good agreement with the observed value of 4.23 B.M. It is interesting to note that the values of B obtained in complexes having imidazole nitrogen donors are much lower than the value obtained with the pyrrole-2-aldimino ligand system. The value of B in Co(II)-CA is consistent with this trend.

Some trigonal prismatic Co(II) complexes also have visible absorption bands with molar extinction coefficients of around 200 and magnetic moments of 4.9 B.M.²² The near infrared spectra of these complexes, however, show only one band that cannot be attributed to Co(I) impurities. The fact that only one band is observed in the near infrared allows us to eliminate trigonal prismatic coordination as a possible model for Co(II)-CPA. In Co(II)-CPA two distinct bands, separated by over 4000 cm^{-1} , are observed in the near infrared.

In summary, the large differences in the observed molar extinction coefficients and magnetic moments of Co(II)-CPA and Co(II)-CA suggest different coordination environments in these systems. A five coordinate structure for Co(II)-CPA gives the best agreement with the data. Co(II)-CA almost certainly has a distorted tetrahedral structure. This conclusion confirms the assignment made by Lindskog and Ehrenberg²³ on the basis of much more limited and less relevant model system data.

Again, we emphasize the importance of the magnetic moment as an aid in assigning structure in high spin Co(II) systems. As the case of Co(II)-CPA indicates, band positions alone are not reliable. Even band intensities can sometimes be ambiguous. For example, the most intense visible band in Co(II) phosphoglucomutase has a molar extinction coefficient in excess of 200,²⁴ which places the ϵ_M of this derivative near the interface of ϵ_M values observed in five coordinate and distorted tetrahedral Co(II) complexes. The

spectrum of this derivative can be interpreted in terms of a tetrahedral model with $Dq = 407 \text{ cm}^{-1}$ and $B = 811 \text{ cm}^{-1}$. Without an experimental value for the magnetic moment of this derivative, however, no reliable structural assignment is possible.

Appendix

Preparation of Model Complexes

$\text{Co}(\text{Barb})_2(\text{Im})_2$: The bis(5, 5-diethylbarbiturate)-bisimidazolecobalt(II) complex was prepared by the procedure of Wang and Craven.²⁵

MP > 240 °C.

Analysis: Found: C, 46.64; H, 5.52; N, 19.22.

Theory: C, 47.06; H, 5.39; N, 19.96.

$\text{Co}(\text{Et}_4\text{dien})\text{Cl}_2$: $\text{Co}(\text{Et}_4\text{dienCl}_2)$ was prepared by the procedure of Dori and Gray.²⁶ MP = 190 °C sharp.

References

1. J. E. Coleman and B. L. Vallee, *J. Biol. Chem.*, 236, 2244 (1961).
2. R. C. Davies, J. F. Riordan, D. S. Auld, and B. L. Vallee, *Biochem.*, 7, 1090 (1968).
3. D. S. Auld and B. L. Vallee, *Biochem.*, 9, 602 (1970).
4. S. A. Latt and B. L. Vallee, *Biochem.*, 10, 4263 (1971).
5. T. A. Kaden, B. Holmquist, and B. L. Vallee, *Biochem. and Biophys. Res. Comm.*, 46, 1654 (1972).
6. F. S. Kennedy, H. A. O. Hill, T. A. Kaden, and B. L. Vallee, *Biochem. and Biophys. Res. Comm.*, 48, 1533 (1972).
7. R. H. Wang, H. E. Hoenig, G. R. Rossman, and J. E. Mercereau, to be published.
8. J. H. VanVleck, Electric and Magnetic Susceptibilities, Oxford University Press, Oxford and New York, 1932.
9. B. N. Figgis, Introduction to Ligand Fields, Interscience, New York, 1966, p. 266.
10. A. L. Lott, III, and P. G. Rasmussen, *J. Inorg. Nucl. Chem.*, 32, 101 (1970).
11. L. Sacconi, I. Bertini, and F. Mani, *Inorg. Chem.*, 6, 262 (1967).
12. L. Sacconi and I. Bertini, *Inorg. Chem.*, 7, 1178 (1968).
13. R. H. Holm, A. Chakravorty, and L. Theriot, *Inorg. Chem.*, 5, 625 (1966).

14. J. E. Fergusson and C. A. Ramsay, J. Chem. Soc. (London), 5222 (1965).
15. M. Ciampolini and N. Nardi, Inorg. Chem., 5, 41 (1966).
16. M. Ciampolini and G. P. Speroni, Inorg. Chem., 5, 45 (1966).
17. S. F. Lions, I. B. Dance, and J. Lewis, J. Chem. Soc. (A), 565 (1967).
18. M. Ciampolini and N. Nardi, Inorg. Chem., 6, 445 (1967).
19. L. Sacconi, R. Morassi, and S. Midolfani, J. Chem. Soc. (A), 1570 (1968).
20. L. Sacconi, I. Bertini, and R. Morassi, Inorg. Chem., 6, 1548 (1967).
21. M. Goodgame and F. A. Cotton, J. Amer. Chem. Soc., 84, 1543 (1962).
22. E. Larsen, G. N. LaMar, B. E. Waegner, J. E. Parks, and R. H. Holm, Inorg. Chem., 11, 2652 (1972).
23. S. Lindskog and A. Ehrenberg, J. Mol. Biol., 24, 133 (1967).
24. W. J. Ray, Jr. and J. S. Multani, Biochem., 11, 2805 (1972).
25. B. C. Wang and B. M. Craven, Chem. Comm., 290 (1971).
26. Z. Dori and H. B. Gray, J. Amer. Chem. Soc., 88, 1394 (1966).

CHAPTER III

NICKEL(II)CARBOXYPEPTIDASE A

Nickel(II) has not been widely used as a spectroscopic probe of the metal sites in metalloenzymes. The nickel(II) derivatives of many zinc metalloenzymes show little or no enzymatic activity. Ni(II)-CA and Ni(II) alkalinephosphatase are totally inactive,^{1,2} while Ni(II)-yeast aldolase has only 11% of the activity of the native enzyme.³ Ni(II)-CPA is apparently unique in that it is fully active.⁴ As such, it has great potential for study by magnetic and spectroscopic techniques.

Some sketchy spectral data on Ni(II)-CA are available. Coleman has found one band in the visible spectrum of Ni(II)-CA centered at about 625 nm with a molar extinction coefficient of approximately 10.⁵ The low value of the molar extinction coefficient led him to conclude that the nickel ion is bound in an octahedral coordination site in carbonic anhydrase. As noted above, Ni(II)-CA is inactive. A similar result in the fully active CPA system would be extremely significant, since it would severely discredit the entatic state hypothesis, at least as it has been applied to lytic metalloenzymes.

Sample Preparation and Spectral Measurements

The sample of Ni(II)-CPA used in the magnetic susceptibility determination was prepared by the dialysis and drying procedure previously described. The sample ultimately used had 0.76 mole Ni^{+2} per mole enzyme, and its specific activity agreed well with the literature values. The actual measurement was made on a 14 mg sample containing 16.8 μg of Ni^{+2} .

Spectroscopic measurements were made by the apo difference method that has been previously described. Unfortunately considerable time and sample were wasted in an attempt to measure the spectrum of Ni(II)-CPA using the buffer reference method. Only the 413 nm absorption band was reproducibly discernible by this method. A dithiazone extracted Tris buffer containing 1 M KF instead of 1 M NaCl was used to study the effects of fluoride ion on Ni(II)-CPA and its complex with the inhibitor β -phenyl-propionate. The apo enzyme was unfortunately not too soluble in the 1 M KF buffer, so the solution was diluted with an equal volume of NaCl buffer. The solution subsequently referred to as KF buffer is really 0.5 M NaCl, 0.5 M KF, 0.05 M Tris, pH 7.5 buffer.

Results and Discussion

Ni(II)-CPA - Spectra

The absorption spectrum of Ni(II)-CPA in D₂O buffer is shown in Figure (Ni-I). For comparison, the spectrum of an equimolar solution of Ni⁺² ion in Tris buffer is shown in Figure (Ni-II). Under these conditions the principal species in solution is probably $[\text{Ni}(\text{tris})_2\text{H}_2\text{O}_4]^{+2}$.⁶ The absorption at and beyond 1400 nm is undoubtedly due to H₂O impurities in the D₂O. Similar features are present in the spectrum of Cu(II)-CPA, which indicate that they have no relation to the features due to transitions associated with either the Ni⁺² or Cu⁺² centers. The large differences in band intensities and positions clearly indicate that the Ni⁺² is bound to the enzyme and not free in solution. The absorption maxima and molar extinction

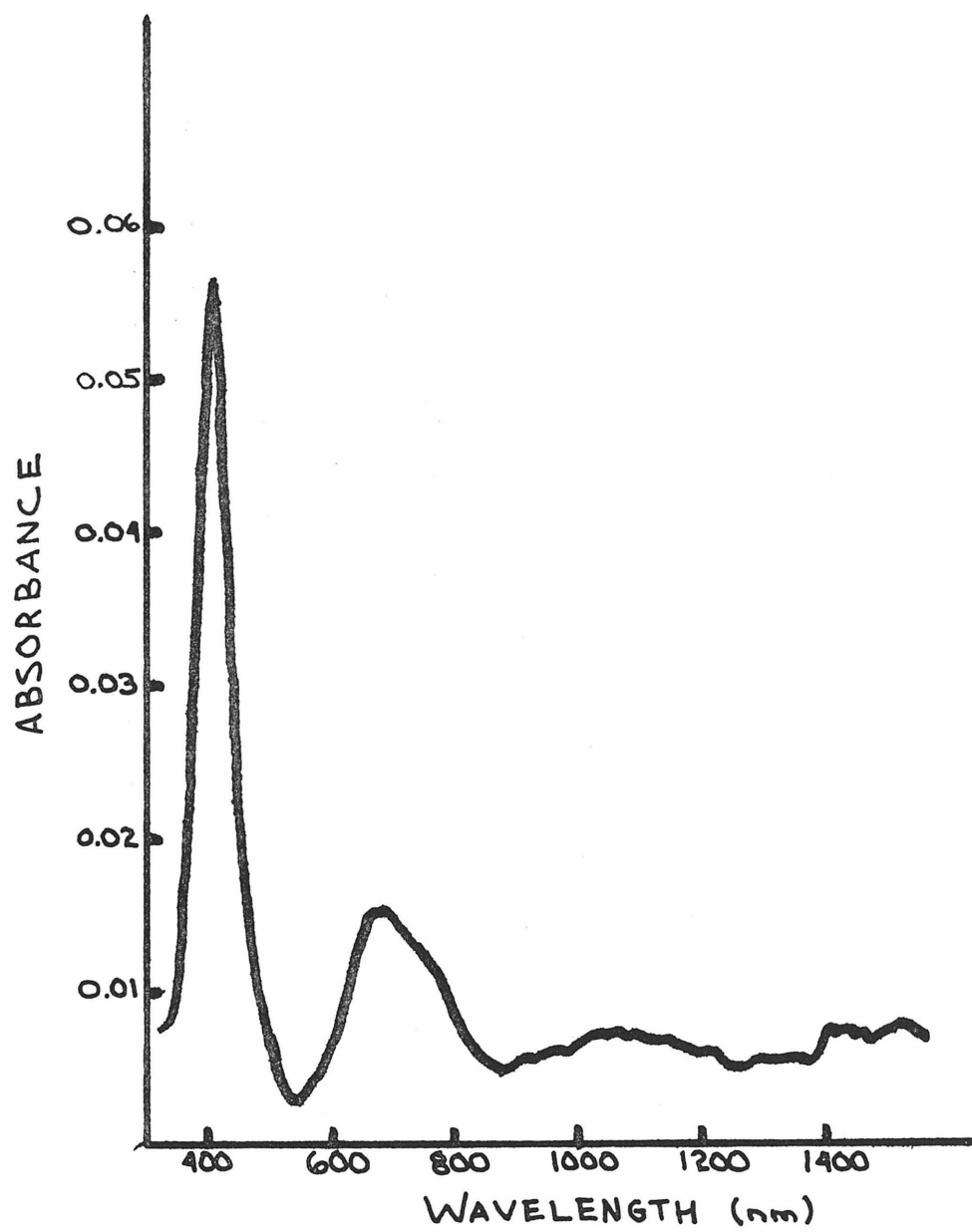


Figure Ni-I. Absorption spectrum of Ni(II)CPA in D₂O buffer.

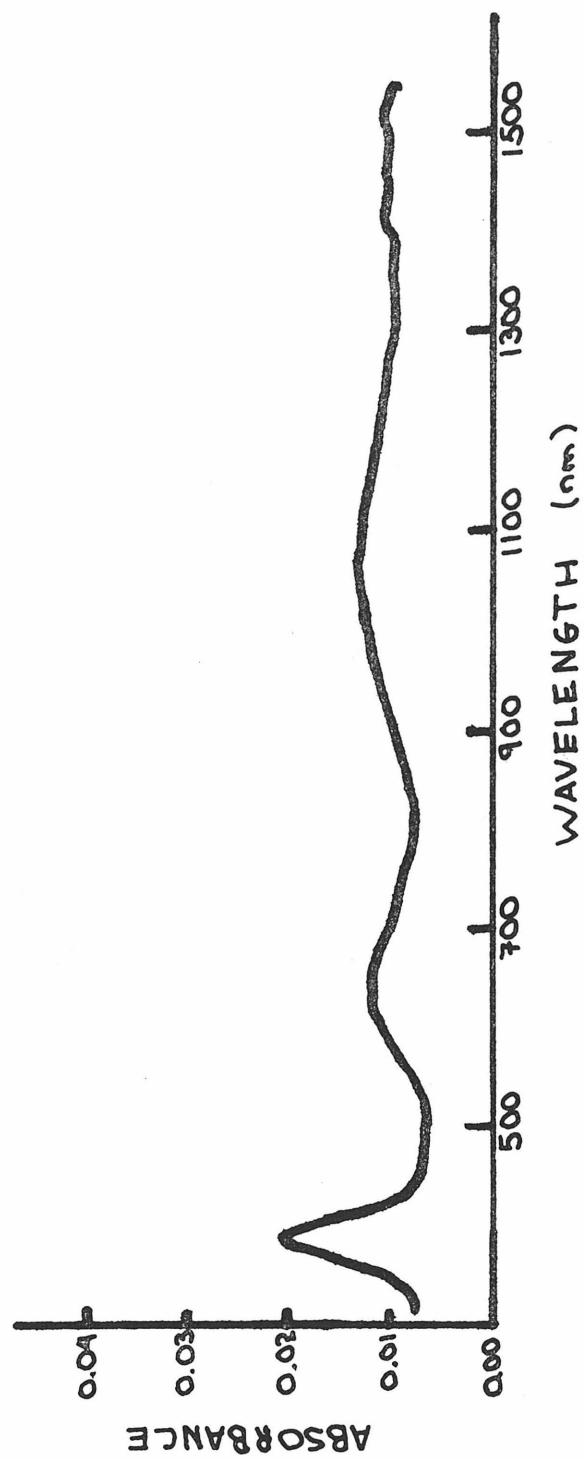


Figure Ni-II. Absorption spectrum of Ni²⁺ ions in Tris buffer.

coefficients of Ni(II)-CPA, Ni(II)-CA, and Ni(II)-PGM are shown in Table (Ni-I). The pattern of three bands with low molar extinction coefficients is extremely characteristic of nickel(II) in an octahedral environment. The observed molar extinction coefficients for the ν_3 band are somewhat higher than the values usually found in model octahedral systems, although values greater than 20 are known (vide infra).

The effect of fluoride ion (F^-) on the spectrum of Ni(II)-CPA is shown in Figure (Ni-III). The band positions and molar extinction coefficients in both chloride and fluoride media are summarized in Table (Ni-II). It should be noted that the enzyme concentrations are similar but not identical for the two curves shown in the figure. Addition of fluoride ion causes the spectrum of Ni(II)-CPA to shift to lower energy. There is also some intensity enhancement particularly of the highest energy transition. The red shift of the spectrum is consistent with one or more fluoride ions replacing coordinated water at an octahedrally coordinated nickel(II) center. It should be noted that the spectrum of free Ni^{+2} ion in the fluoride buffer is identical to that obtained in chloride buffer.

The theory of the spectra of octahedral nickel(II) complexes is relatively simple. Octahedral symmetry (O_h point group) splits the 3F ground state of a d^8 ion into three components: $^3A_{2g}$, $^3T_{2g}$, and $^3T_{1g}$. The first triplet excited state in the free atom is a 3P state. It is not split by an octahedral field and belongs to the $^3T_{1g}$ irreducible representation. A relatively simple perturbation

Table Ni-I

Enzyme	Band Position, nm (ϵ_m)		
	ν_1	ν_2	ν_3
Ni(II)CPA	$\sim 1060(3)$	675(7) 765(sh)	413(24)
Ni(II)CA ^a	--	$\sim 625(10)$	--
Ni(II)PGM ^b	1300(5)	700(6) 760(7)	410(23)

^a Reference 5.

^b Reference 7.

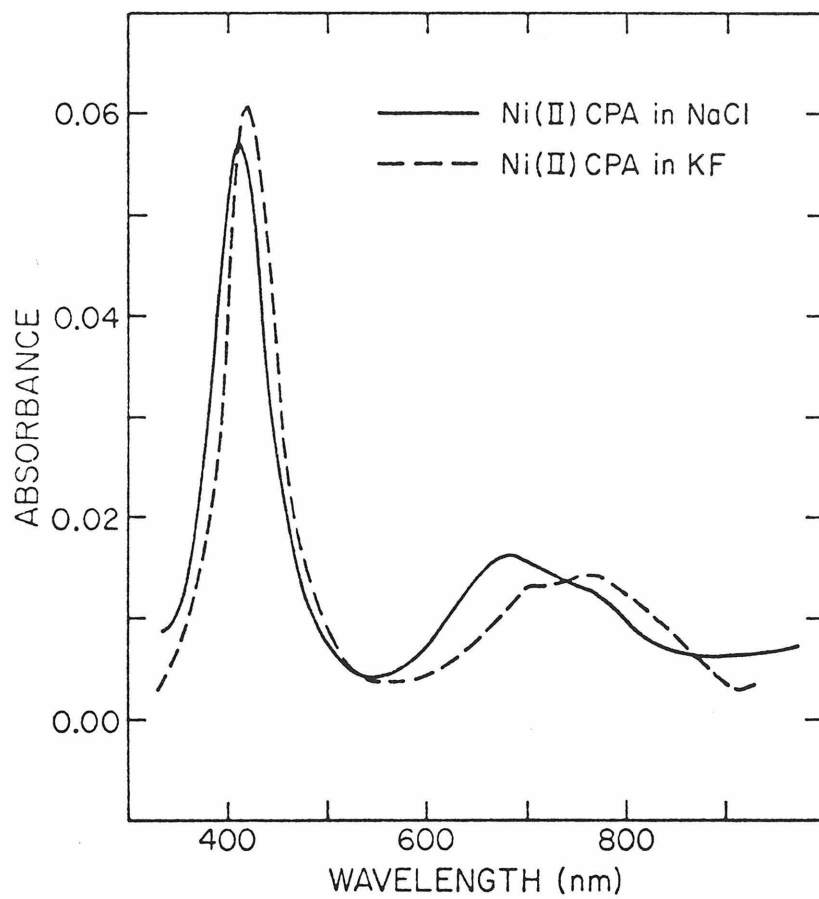


Figure Ni-III. The absorption spectra of Ni(II)CPA in sodium chloride buffer, $[\text{Ni}^{+2}] = 4.71 \times 10^{-4} \text{ M}$ and potassium fluoride buffer, $[\text{Ni}^{+2}] = 3.35 \times 10^{-4} \text{ M}$.

Table Ni-II

Spectra of Ni(II)CPA in Cl^- and F^- Buffers

	Band Position, nm, (ϵ_m)	
	ν_2	ν_3
Ni(II)CPA in Cl^-	685(7), 765(sh)	413(24)
Ni(II)CPA in F^-	760(6), 700(sh)	421(33)

calculation including the interaction of the two ${}^3T_{1g}$ states via the ligand field gives the following energies for the various triplet states:

$$E({}^3A_{2g}) = -12 Dq \quad (1)$$

$$E({}^3T_{2g}) = -2 Dq \quad (2)$$

$$E({}^3T_{1g}) = 7.5 B + 3 Dq - \frac{1}{2}(225 B^2 + 100 Dq^2 - 180 BDq)^{\frac{1}{2}} \quad (3)$$

$$E({}^3T_{1g}) = 7.5 B + 3 Dq + (225 B^2 + 100 Dq^2 - 180 BDq)^{\frac{1}{2}} \quad (4)$$

A complete energy level diagram (Tanabe-Sugano Diagram) for a d^8 ion in an octahedral field is shown in Figure (Ni-IV). The parameter Dq represents the ligand field strength. The parameter B , the inter-electronic repulsion parameter, is related to the separation of the free ion 3F and 3P levels. In fact:

$$E({}^3P) - E({}^3F) = 15 B \quad (5)$$

It is clear from the energy level diagram shown in Figure (Ni-IV) and equations 1-4 that there should be three spin allowed transitions with the following energies:

$$\nu_1 ({}^3A_{1g} \rightarrow {}^3T_{2g}) = 10 Dq \quad (6)$$

$$\nu_2 ({}^3A_{2g} \rightarrow {}^3T_{1g}(F)) = 7.5 B + 15 Dq - \frac{1}{2}(225 B^2 + 100 Dq^2 - 180 B Dq)^{\frac{1}{2}} \quad (7)$$

$$\nu_3 ({}^3A_{2g} \rightarrow {}^3T_{1g}(P)) = 7.5 B + 15 Dq + \frac{1}{2}(225 B^2 + 100 Dq^2 - 180 B Dq)^{\frac{1}{2}} \quad (8)$$

Although these transitions are allowed by the spin selection rule ($\Delta S = 0$), they are Laporte or orbitally forbidden since they all are transitions to and from states with g symmetry. This

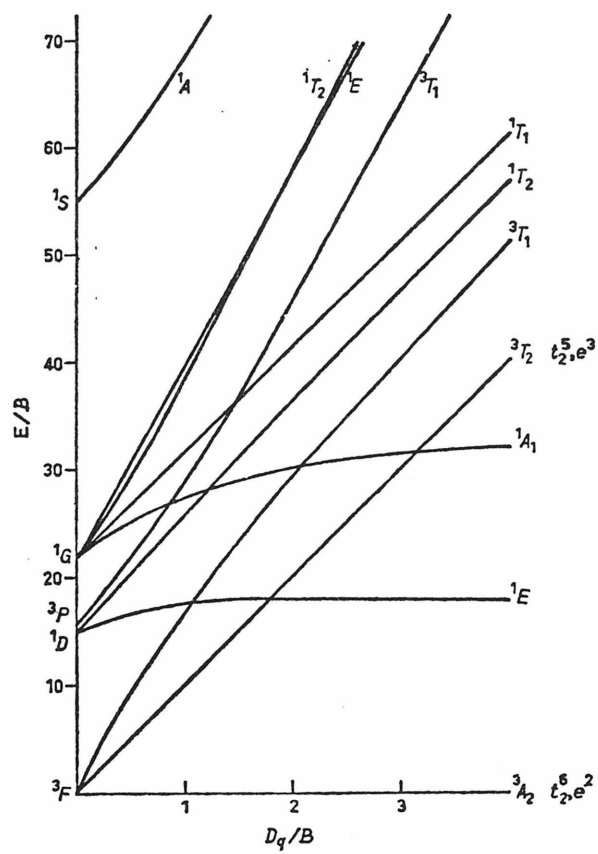


Figure Ni-IV. Energy level diagram (Tanabe-Sugano) for d^8 ions in an octahedral field ($C = 4.7 B$).

selection rule can be partially relaxed by a vibronic coupling mechanism. For example, coupling the ground state with a vibration of u symmetry and the excited state with a vibration of g symmetry or vice versa, will give a net u \rightarrow g or g \rightarrow u transition which is orbitally allowed. Another mechanism that can relax the Laporte forbiddenness of these bands is a reduction of symmetry, such as removal of the center of symmetry by some type of distortion. Indeed one would expect the metal coordinating site in a metallo-enzyme to be quite asymmetric. Perhaps this is a possible explanation for the observed intensities of the ν_3 band in Ni(II)-CPA and Ni(II)-PGM.

The energies of the spin allowed transitions for octahedral nickel(II) depend on only two parameters, Dq and B. Thus, from the position of any two of the three spin allowed bands it is possible to calculate both Dq and B. Using the ν_2 and ν_3 transitions some simple algebraic manipulation yields:

$$Dq = \frac{9(\nu_2 + \nu_3) \pm [81(\nu_2 + \nu_3)^2 - 340 \nu_2 \nu_3]^{\frac{1}{2}}}{340} \quad (9)$$

$$B = \frac{\nu_2 + \nu_3}{15} - 2Dq \quad (10)$$

In order to use equations 9 and 10 to evaluate the ligand field parameters Dq and B, the band positions must be known accurately. The ν_2 band in many nickel(II) complexes is often significantly split. The spectra of Ni(II)-CPA and particularly Ni(II)-PGM illustrate this effect.

It has been observed that this splitting of the ν_2 transition occurs in complexes that have $Dq/B \simeq 1$.⁸

Considerable controversy exists in the literature regarding the theoretical explanation of this effect. Ballhausen has explained it in terms of spin-orbit coupling.⁹ Jørgensen, on the other hand, attributes one component of the doublet to the ${}^3A_{2g} \rightarrow {}^1E_g$ transition which has gained intensity from singlet-triplet mixing mediated by spin-orbit coupling.¹⁰ It should be noted that the cross-over point for the ${}^3T_{1g}(F)$ and 1E_g states, as shown in Figure Ni-IV, occurs at approximately $Dq/B = 1$. Since the magnitude of the enhancement or mixing is dependent on the energy separation between the states involved, the effect should be most pronounced at or near the cross-over point. Recently, Ballhausen¹¹ has proposed that the splitting is due to an interference effect caused by the superposition of a sharp ligand field independent spin forbidden transition (${}^3A_{2g} \rightarrow {}^1E_g$) on the broad, ligand field dependent, spin allowed (${}^3A_{2g} \rightarrow {}^3T_{1g}(F)$) transition. This effect has been observed on the ${}^4A_2 \rightarrow {}^4T_2$ transition of $Cr(en)_3^{+3}$ and on both the ${}^4A_{2g} \rightarrow {}^4T_{2g}$ and ${}^4A_{2g} \rightarrow {}^4T_{1g}$ transitions of vanadium(II) ion doped into $KMgF_3$.^{12,13} According to Fano's theory for this effect the band shape, $\alpha(h\nu)$, is given by the following expression.¹⁴

$$\alpha(h\nu) = \alpha_\beta + \alpha_0 (q^2 + 2q\epsilon - 1)/(1 + \epsilon^2) \quad (11)$$

$$\text{where} \quad \epsilon = \frac{2(h\nu - E_r)}{\Gamma} \quad (12)$$

and α_β is the gaussian spectral envelope, E_r is the position of the spin forbidden state, Γ is the full band width of decay to the spin allowed state, and q is the ratio of the matrix element for the transition directly to the spin forbidden state to the matrix element for the transition directly to the allowed state. q , Γ , and α_0 are treated as adjustable parameters. For values of q less than or only slightly greater than one, the theory predicts that the position of the (${}^3A_{2g} \rightarrow {}^1E_g$) transition will roughly correspond to the dip or minimum in the gaussian envelope. The position of the spin allowed ${}^3A_{2g} \rightarrow {}^3T_{1g}(F)$ transition corresponds to the unperturbed gaussian band maximum. The appropriate band positions are illustrated in Figure (Ni-V).

In cases where the dip in the observed spectrum occurs at or near the maximum of the unperturbed gaussian band there can be considerable difference in the position assigned to the ${}^3A_{2g} \rightarrow {}^3T_{1g}(F)$ transition, depending on which band shape theory is employed. The spectrum of Ni(II)-CPA in KF buffer (Figure Ni-III) is an excellent example. Differences of roughly 50 cm^{-1} in the values calculated for Dq and B by equations 10 and 11 are obtained, depending on which way the assignment is made.

In order to resolve this dilemma, and in order to have some basis for comparison with the enzyme systems, the parameters Dq and B were calculated for a wide variety of model octahedral nickel(II) complexes having predominantly nitrogen and oxygen donor atoms.

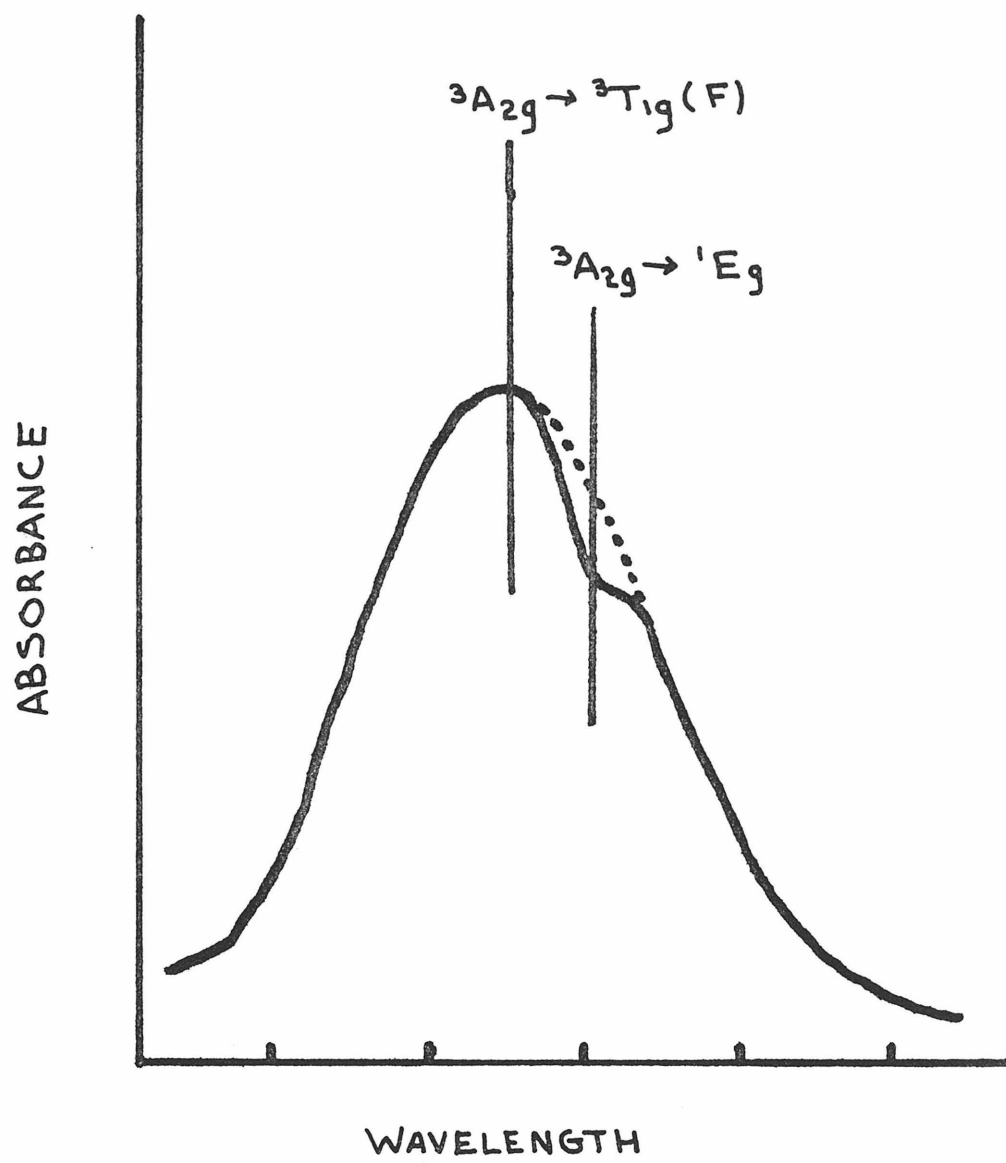


Figure Ni-V.

Two methods based on different sub-sets of the spectral data were used. A computer program written by Dr. Jack Thibeault of this laboratory was used. This program chooses the set of parameters Dq and B which gives the best fit of the observed bands to the calculated transition energies by minimizing the standard deviation. The positions of all three bands were the input. In six out of eight cases where there was a possible ambiguity in the position of the ${}^3A_{2g} \rightarrow {}^3T_{1g}(F)$ transition a better fit of the observed band positions was obtained using assignments based on the singlet-triplet mixing approach. These two approaches gave values of Dq and B that differed from each other by roughly 30 cm^{-1} . It should be emphasized that this limited set of data does not represent a comprehensive test of the competing band shape theories. In what follows, then, the ${}^3A_{2g} \rightarrow {}^3T_{1g}(F)$ transition was assigned according to the singlet-triplet mixing band shape theory.

The calculated values of the ligand field parameters Dq and B for a rather extensive series of model octahedral nickel(II) complexes are set out in Table (Ni-III). The results indicate that in general the calculation based on only ν_2 and ν_3 yields slightly higher values for Dq and slightly lower values for B than does the computer fit of all three observed bands. Yet the relative magnitudes of both Dq and B within each donor set group and between different donor sets are independent of the calculation method as they should be. As expected, Dq gets smaller as the ligands donors change from nitrogen to oxygen while B gets larger. This result is in line with both the

Table Ni-III

Octahedral Ni(II) Complexes and Ni(II) Enzymes

Complex	Donor Set	ν_1	ν_2	ν_3	$\text{Dq}(2, 3)^{\dagger}$	$\text{B}(2, 3)^{\dagger}$	Dq	B	
Ni(en)_3^{+2}	N_6	11,600(7)	18,350(7)	29,000(9)	1177	802	--	--	a
Ni(Im)_6^{+2}	N_6	11,100	18,150	28,700	1163	796	1131	849	b
Ni(tn)_3^{+2}	N_6	10,900(6)	17,800(11)	28,200(15)	1138	790	1110	836	c
$\text{Ni(CH}_3\text{CN)}_6^{+2}$	N_6	10,700	17,400	27,800	1102	808	1085	836	d
$\text{Ni(NH}_3)_6^{+2}$	N_6	10,750(4)	17,500(5)	28,200(6)	1100	846	--	--	a
$\text{Ni(NC}_2\text{H}_5)_6^{+2}$	N_6	10,500(7)	17,100(7)	27,500(12)	1077	819	1063	841	e
$\text{Ni(C}_2\text{H}_5\text{NH}_2)_6^{+2}$	N_6	9,662	16,666	27,027	1043	826	1006	881	f
$\text{Ni(n-C}_3\text{H}_7\text{NH}_2)_6^{+2}$	N_6	9,826(6)	16,502(5)	26,809(14)	1031	824	1006	862	f
$\text{Ni(C}_5\text{H}_5\text{N)}_6^{+2}$	N_6	10,150(4)	16,500(5)	27,000(10)	1027	847	1022	852	c
$\text{Ni(i-C}_3\text{H}_7\text{NH}_2)_6^{+2}$	N_6	9,480	15,267	26,042	931	891	939	881	f
Ni(His)_2	N_4O_2	10,700(7)	18,000(8)	28,000(10)	1200	666	1109	826	g
$\text{Ni(tren)(H}_2\text{O)}_2^{+2}$	N_4O_2	10,500(15)	17,800(9)	27,800(2)	1167	705	1092	834	c
$\text{Ni(C}_5\text{H}_5\text{N)}_4(\text{CF}_3\text{CO}_2^-)_2$	N_4O_2	9,874(5)	15,870(10)	28,080(19)	985	827	988	821	h
Ni(NTA)(en)^{-1}	N_3O_3	9,400(11)	16,900(8)	27,200(13)	1064	812	1004	901	c

Table Ni-III (Continued)

Complex	Donor Set	ν_1	ν_2	ν_3	$\underline{Dq(2,3)}^{\dagger}$	$\underline{B(2,3)}^{\dagger}$	\underline{Dq}	\underline{B}
Ni(gly)_3^-	N_3O_3	10, 100(10)	16, 600(8)	27, 600(14)	1024	899	1018	906 a
Ni(NTA)Glg)^{-2}	N_2O_4	9, 900	17, 100	26, 200	1083	720	1043	772 c
Ni(HEDTA)^{-1}	N_2O_4	10, 100	16, 785	26, 455	1081	721	1038	792
$\text{Ni(asparaginate)}_2$	N_2O_4	9, 810(7)	16, 340(5)	27, 930(13)	996	960	990	967 i
Ni(Gly-Gly)_2	N_2O_4	9, 720(7)	16, 130(5)	27, 030(9)	991	895	983	907 i
$\text{Ni(Gly)}_2(\text{H}_2\text{O})_2$	N_2O_4	9, 720(7)	16, 050(6)	27, 100(9)	983	911	979	917 i
$\text{Ni(tris)}_2(\text{H}_2\text{O})_4$	N_2O_4	9, 540	15, 750	25, 975	976	831	965	846
$\text{Ni(NTA)(H}_2\text{O)}_2^-$	NO_5	9, 500(16)	16, 000(7)	25, 600(13)	1012	749	980	799 c
$\text{Ni(CH}_3\text{OH)}_6^{+6}$	O_6	8, 431(2)	14, 226(4)	25, 000(6)	859	897	853	905 j
$\text{Ni(H}_2\text{O)}_6^{+2}$	O_6	8, 500(2)	13, 800(2)	25, 300(5)	824	958	834	947 k
Ni(DMF)_6^{+2}	O_6	8, 500(6)	13, 600(5)	25, 000(15)	812	949	826	933 l
NiO in MgO	O_6	8, 600	13, 500	24, 600	808	925	827	901 k
$\text{Ni(C}_2\text{H}_5\text{OH)}_6^{+2}$	O_6	8, 180(3)	13, 404(3)	24, 795(7)	799	948	806	941 i
$\text{Ni}^{+2}(\text{CH}_3\text{CO}_2)_6$ in Li^+, Na^+ Acetate Glass	O_6	7, 800	13, 200	24, 200	789	916	786	919 m

Table Ni-III (Continued)

Complex	Donor Set	ν_1	ν_2	ν_3	$\text{Dq}(2, 3)^{\dagger}$	$\text{B}(2, 3)^{\dagger}$	Dq	B	
$\text{Ni}(\text{DMSO})_6^{+2}$	O_6	7, 728(3)	12, 970(3)	24, 038(10)	773	921	773	920	n
$\text{Ni}(\text{DMA})_6^{+2}$	O_6	7, 690	12, 900	23, 920	769	917	769	916	l
$\text{Ni}(\text{SO}_4^{=})$ in K_2^+ , $\text{Zn}^{+2} \text{SO}_4^-$ glass	O_6	7, 300	12, 200(6)	23, 100(21)	724	905	726	903	o
KNiF_3	F_6	7, 250(6)	12, 530(11)	23, 810(23)	743	937	937	943	p
$\text{Ni}(\text{Quinoline})\text{Cl}_2$	N_2Cl_4	6, 400(5)	11, 100(9)	21, 100(12)	658	830	652	837	q
$\text{Ni}(\text{II})\text{CPA}$	$\text{N}_2\text{O}_4?$	9, 430(3)	14, 600(7)	24, 250(24)	900	788	923	755	80
$\text{Ni}(\text{II})\text{CPA} + \text{F}^-$	$\text{N}_2\text{O}_{4-x}\text{F}_x?$	--	13, 158(6)	23, 810(~33)	788	888	--	--	
Ni(II)PGM	$\text{O}_6?$	7, 692(5)	13, 160(6)	24, 390(23)	784	935	779	940	r
$\text{Ni}(\text{II})\text{CA}$	$\text{N}_3\text{O}_3?$	--	16, 000(10)	--	--	--	--	--	s

[†] Calculated from ν_2 and ν_3 only. ^a From Reference 10.^b Data from Reference 15; Im = imidazole.^c Data from Reference 16; tn = trimethylenediamine; tren = triethylenetetraamine; NTA = nitrilotriacetate.^d Data from Reference 17.^e Data from Reference 18.^f Data from Reference 19.

Table Ni-III (Continued)

g	Data from Reference 20.
h	Data from Reference 21.
i	Data from Reference 22.
j	Data from Reference 23.
k	Data from Reference 24.
l	Data from Reference 25; DMF = dimethylformamide; DMA = dimethylacetamide.
m	Data from Reference 26.
n	Data from Reference 27.
o	Data from Reference 28.
p	Data from Reference 29.
q	Data from Reference 30.
r	Data from Reference 7.
s	Data from Reference 5.

spectrochemical and nephelauxetic series. One result that is somewhat surprising is that water appears to be slightly higher in the nephelauxetic series than fluoride ion although the reverse order is generally accepted.

It is interesting to note that imidazole ranks with the strongest sigma donor nitrogen ligands, en and tn. The complex $\text{Ni}(\text{His})_2$ also has a rather high Dq compared to the other N_4O_2 donor sets, but unfortunately the number of such complexes is rather limited. The complexes involving polyacetate type ligands, such as NTA and HEDTA, have rather low values of B , a fact consistent with the position of oxalate in the nephelauxetic series. The only exception is nickel(II) ion in the lithium, sodium acetate glass which has $B = 919 \text{ cm}^{-1}$, a value typical for an oxide or carbonyl oxygen type donor.

Of the two nickel(II) enzymes for which complete spectral data are available, Ni(II)-PGM is the simplest to understand in terms of the model system data. The values $Dq = 779 \text{ cm}^{-1}$, $B = 940 \text{ cm}^{-1}$ are typical of those observed in model systems having six very weak field oxygen donors available from the enzyme. The most likely possibilities are the side chains of aspartic or glutamic acid, the carbonyl oxygen of asparagine or glutamine, tyrosine, serine or possibly threonine, as well as solvent water.

The ligand field parameters of Ni(II)-CPA , $Dq = 923 \text{ cm}^{-1}$, $B = 755 \text{ cm}^{-1}$ are not quite as straightforward. The value of Dq is less than that found for any of the mixed nitrogen oxygen donor

systems, yet it is significantly larger than the values found in the all-oxygen donor systems. The value of B, the interelectronic repulsion parameter, is also quite low, lower than but analogous to the values observed with tri- and tetra-acetate type ligands. In the presence of fluoride ion, Dq decreases while B increases by roughly 100 cm^{-1} . These changes are consistent with fluoride ion(s) replacing water(s) in the coordination sphere of the nickel.

One explanation of the low values of both the ligand field parameters might be that the protein conformation prevents optimal metal ligand interactions or requires some type of distortion from strict octahedral symmetry. It should be emphasized that this proposed distortion is not large. The absorption spectrum of Ni(II)-CPA plotted on an energy scale is shown in Figure (Ni-VI). It shows three relatively symmetric bands. The ${}^3A_{2g} \rightarrow {}^3T_{1g}(P)$ transition is particularly sensitive to both tetragonal and trigonal distortion.^{31, 32} The fact that this transition is symmetrical and not at all split eliminates the possibility of any significant tetragonal or trigonal distortion. Of course, a small deviation from strict octahedral symmetry is expected. Perhaps a small non-axial distortion of some kind increases the metal-ligand overlap and thus causes a reduction in the interelectronic repulsion parameter. Another possible explanation is that the protein conformation places one or both of the imidazole rings in an orientation that increases ligand to metal π -bonding. An interaction of this type would tend to lower both Dq and B.

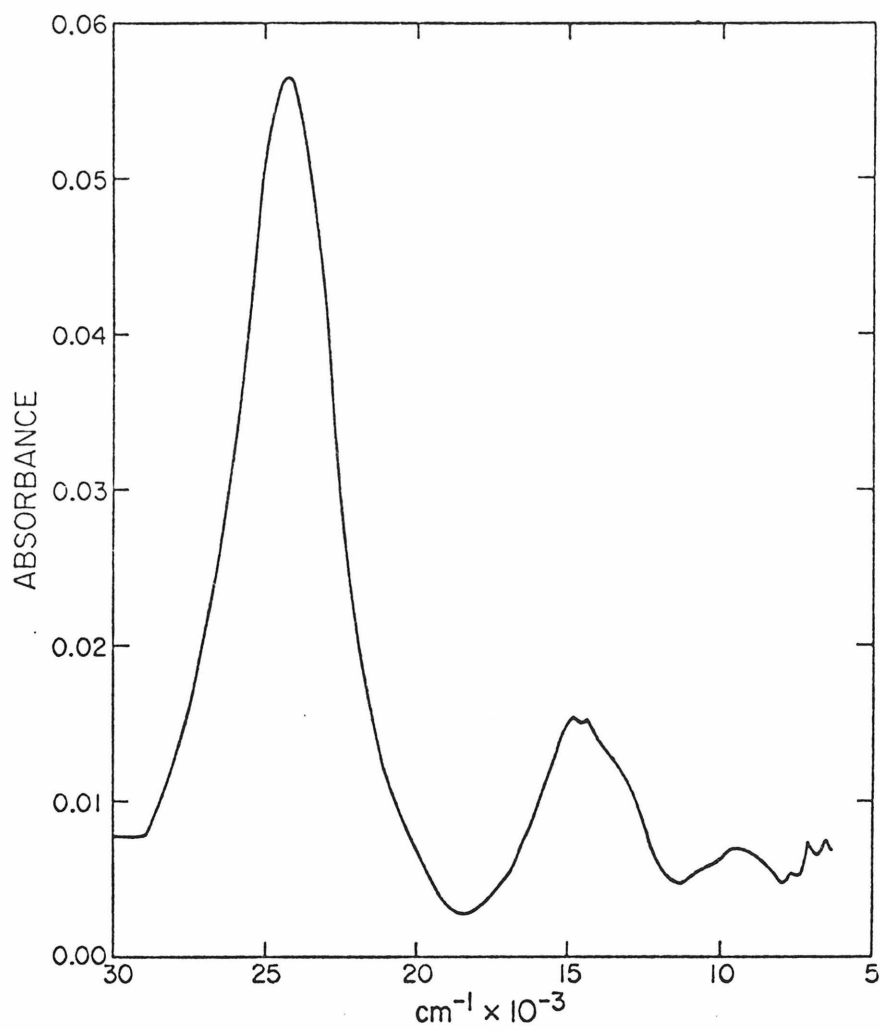


Figure Ni-VI. The absorption spectrum of Ni(II)CPA in D₂O buffer.

Ni(II)-CPA - Magnetic Susceptibility

The magnetic susceptibility of a Ni(II)-CPA was measured by the procedure previously described. A 14 mg sample containing 16.8 μg of Ni^{+2} was measured in a field of 150 gauss from 8 to 75 °K. A plot of χ vs $1/T$ for Ni(II)-CPA is shown in Figure (Ni-VII). The value of $\mu_{\text{eff}} = 2.53 \pm 0.10$ B.M. establishes an orbitally nondegenerate spin-triplet ground state for the Ni(II)-CPA. The observed deviation from Curie Law behavior below 10 °K is attributable to a small zero-field splitting of the spin-triplet ground state.³³

In order to compare the value of the effective magnetic moment for Ni(II)-CPA to those of model complexes a correction for the neglected TIP term must be applied. For an ${}^3\text{A}_{2g}$ ground state it has been shown that³⁴:

$$\chi_{\text{TIP}} = \frac{8N\beta^2}{10Dq} = \frac{2.09}{10Dq} \quad (13)$$

Using the value of $Dq = 920 \text{ cm}^{-1}$ determined from the spectrum, the corrected value of the effective magnetic moment for Ni(II)-CPA is 2.64 ± 0.10 B.M. This value is rather low, lower than the spin only moment for two unpaired electrons which is 2.83 B.M. The low effective magnetic moment of Ni(II)-CPA is consistent with octahedral coordination geometry. The observed high spin ground state does not fit either a five coordinate or pseudo-tetrahedral nickel(II) center since all such complexes have magnetic moments in excess of 3.2 B.M., due to a substantial unquenched orbital contribution.³⁵

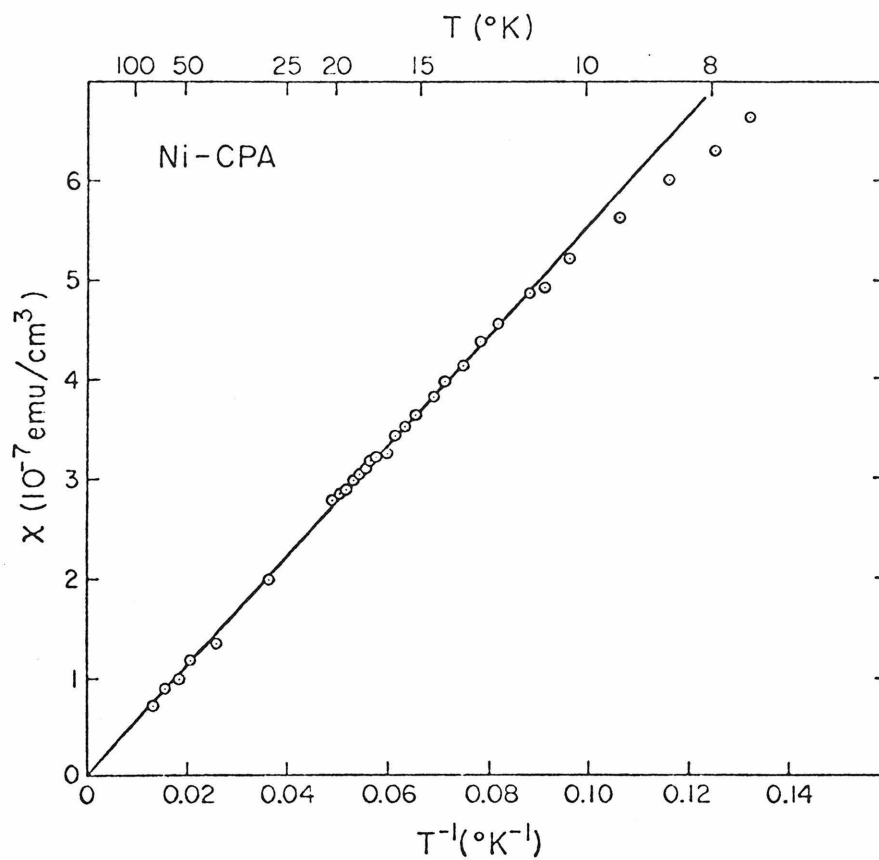


Figure Ni-VII. Temperature dependence of the magnetic susceptibility (χ) of Ni(II)CPA in the range 7 - 75 $^{\circ}\text{K}$.

Ni(II)-CPA and "Substrate"

Information about the metal coordination environment in the enzyme-substrate complex would be extremely important. Unfortunately the normal model peptide substrates of CPA are hydrolyzed extremely rapidly. Turnover numbers on the order of 10^4 moles substrate hydrolyzed per mole enzyme per minute are common, which means that the lifetime of the enzyme-substrate complex is extremely short. In order to examine the properties of the enzyme substrate complex several workers have used glycyl-L-tyrosine as a model "substrate".^{36,37} With the native enzyme this dipeptide acts as a competitive inhibitor of other model substrates.³⁸ It should be emphasized that even though the gly-tyr competes for the same site, its mode of binding may be different from that of rapidly hydrolyzed substrates.

The effect of four equivalents of gly-tyr on the absorption spectrum of Ni(II)-CPA is shown in Figure (Ni-VIII). A substantial decrease in intensity along with a slight broadening or shift to higher energy is observed. At lower ratios of gly-tyr to Ni(II)-CPA only a decrease in intensity is apparent. A similar but less marked decrease in band intensity has been observed when gly-tyr is added to Co(II)-CPA.³⁷

A large excess of gly-tyr was avoided because it is likely to be a good ligand for nickel(II) and might extract the metal from the enzyme to give bis-(glycyl-L-tyrosinate) nickel(II) in solution. Although the binding constants for nickel(II) and gly-tyr are not

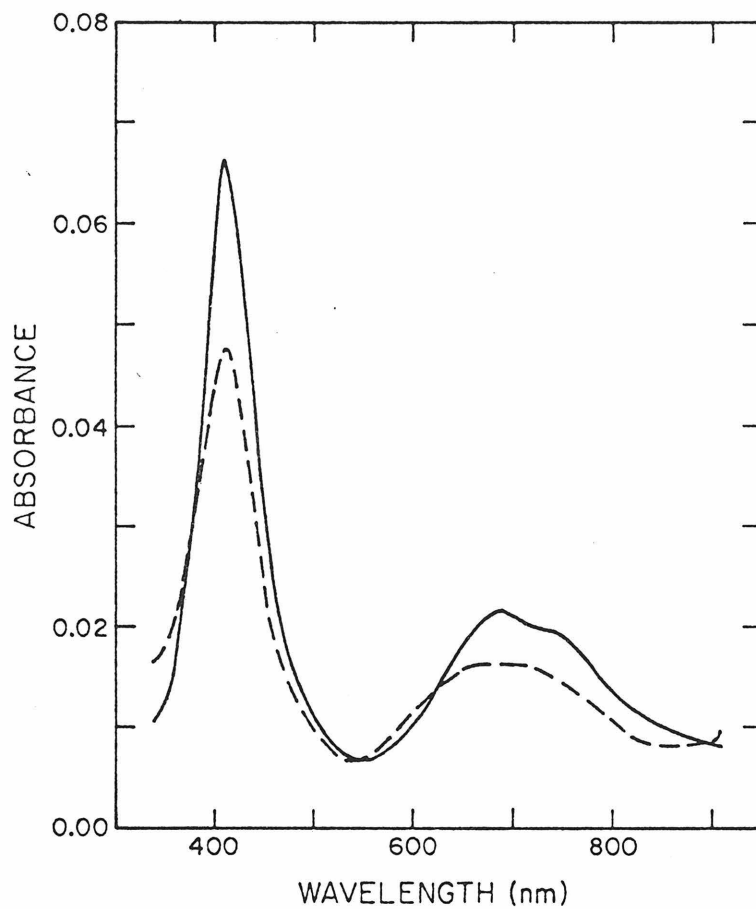


Figure Ni-VIII. Absorption spectra of Ni(II)CPA, $[\text{Ni}^{+2}] = 4.60 \times 10^{-4} \text{ M}$, ———; and Ni(II)CPA + 4 gly-tyr, $[\text{Ni}^{+2}] = 4.38 \times 10^{-4} \text{ M}$, -----.

known, log K for the reaction:



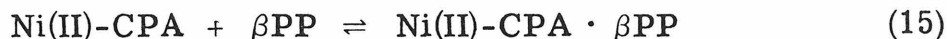
is 7.2.³⁹

The observed changes in the spectra are consistent with formation of some Ni(gly-tyr)_2 in solution. However, it is important to note that addition of gly-tyr to Ni(II)-CPA does not alter the octahedral character of the spectrally detectable species. As we shall now see, however, addition of the inhibitor β -phenylpropionate does produce a large change in the environment of the nickel ion.

Ni(II)CPA + Inhibitor

When the inhibitor β -phenylpropionate is added to Ni(II)-CPA its visible absorption spectrum is dramatically altered, as Figure (Ni-IX) illustrates. The most obvious change is a two to three fold increase in the intensity of the visible absorption bands. Slight, but significant, red shifts in the band maxima are also apparent. As we noted earlier, the absorption above 1400 nm can be attributed to residual H_2O and should therefore be neglected.

By measuring the spectrum at several different inhibitor concentrations it is possible to calculate a binding constant for the reaction



by the procedure of Furman and Garner,⁴⁰ Reasonably linear plots of $(E \times I/A_\lambda - pE\epsilon_{\text{NiCPA}})$ vs $(E + I)$ were obtained only for the region 405 to 460 nm. Plots for a few representative wavelengths in this

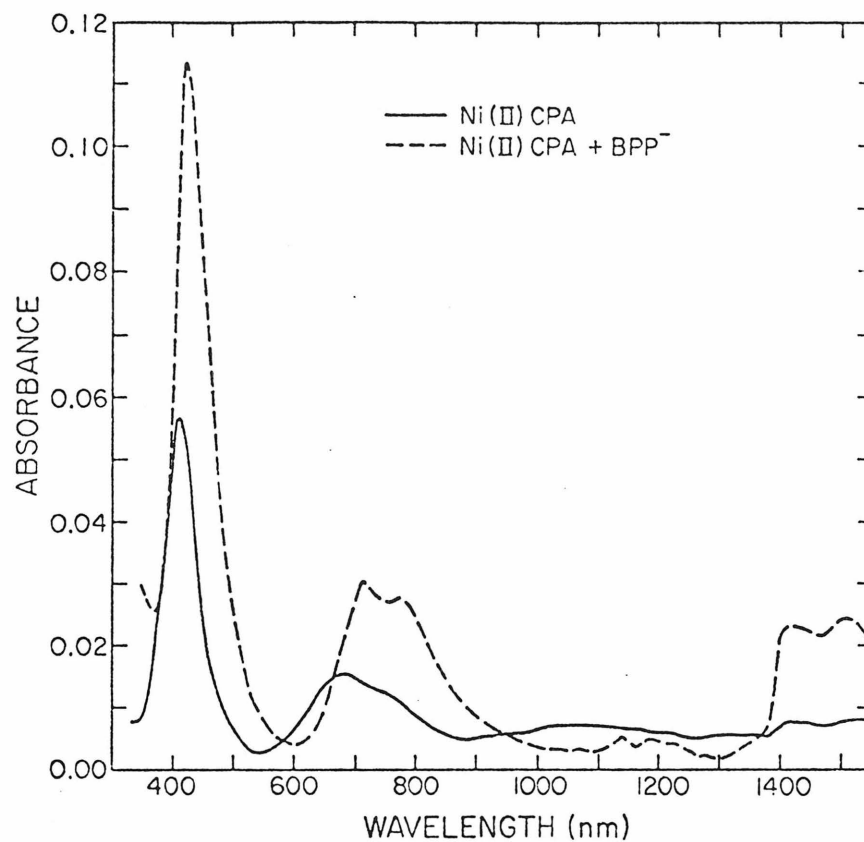


Figure Ni-IX. Absorption spectra of Ni(II)CPA, $[\text{Ni}^{+2}] = 4.71 \times 10^{-4} \text{ M}$; and Ni(II)CPA + Na β PP, $[\text{Ni}^{+2}] = 4.20 \times 10^{-4} \text{ M}$, $[\text{Na}\beta\text{PP}] = 8.48 \times 10^{-3} \text{ M}$ in D_2O buffer.

region are shown in Figure (Ni-X). Values of K_I for each wavelength were calculated from the slope and intercept of the best least squares line through the points. It should be noted that the absolute absorbance differences between the spectra with and without Na β PP are not all that large relative to the uncertainties involved for the region 650 to 800 nm. The results from two determinations involving different but partially overlapping Na β PP concentration ranges agree reasonably well. An average value of $K_I = (3.7 \pm 1.7) \times 10^3 M^{-1}$ was found for the binding constant of β -phenylpropionate to Ni(II)-CPA. The molar extinction coefficient of the Ni(II)-CPA \cdot β PP complex was calculated at each wavelength from the slope and the observed value for Ni(II)-CPA. The absorbance maximum of the Ni(II)-CPA \cdot β PP complex occurs between 425 and 430 nm, with a molar extinction coefficient of roughly 50.

A similar experiment on the effect of Na β PP on the spectrum of Ni(II)-CPA was done in fluoride buffer. The results, as illustrated in Figure (Ni-XI), were quite similar to what was observed in chloride buffer. A significant but not quite so substantial intensity enhancement as well as a slight red shift of the band around 420 nm was observed. Binding constants were determined as in the case of the chloride buffer. An average value of $K_I = (1.6 \pm 0.5) \times 10^{+2} M^{-1}$ was found in fluoride buffer. It is very interesting that the value of the binding constant of β -phenylpropionate is over an order of magnitude smaller in fluoride than in chloride buffer. The calculated spectrum of the Ni(II)-CPA \cdot β PP complex in fluoride buffer has a maximum between

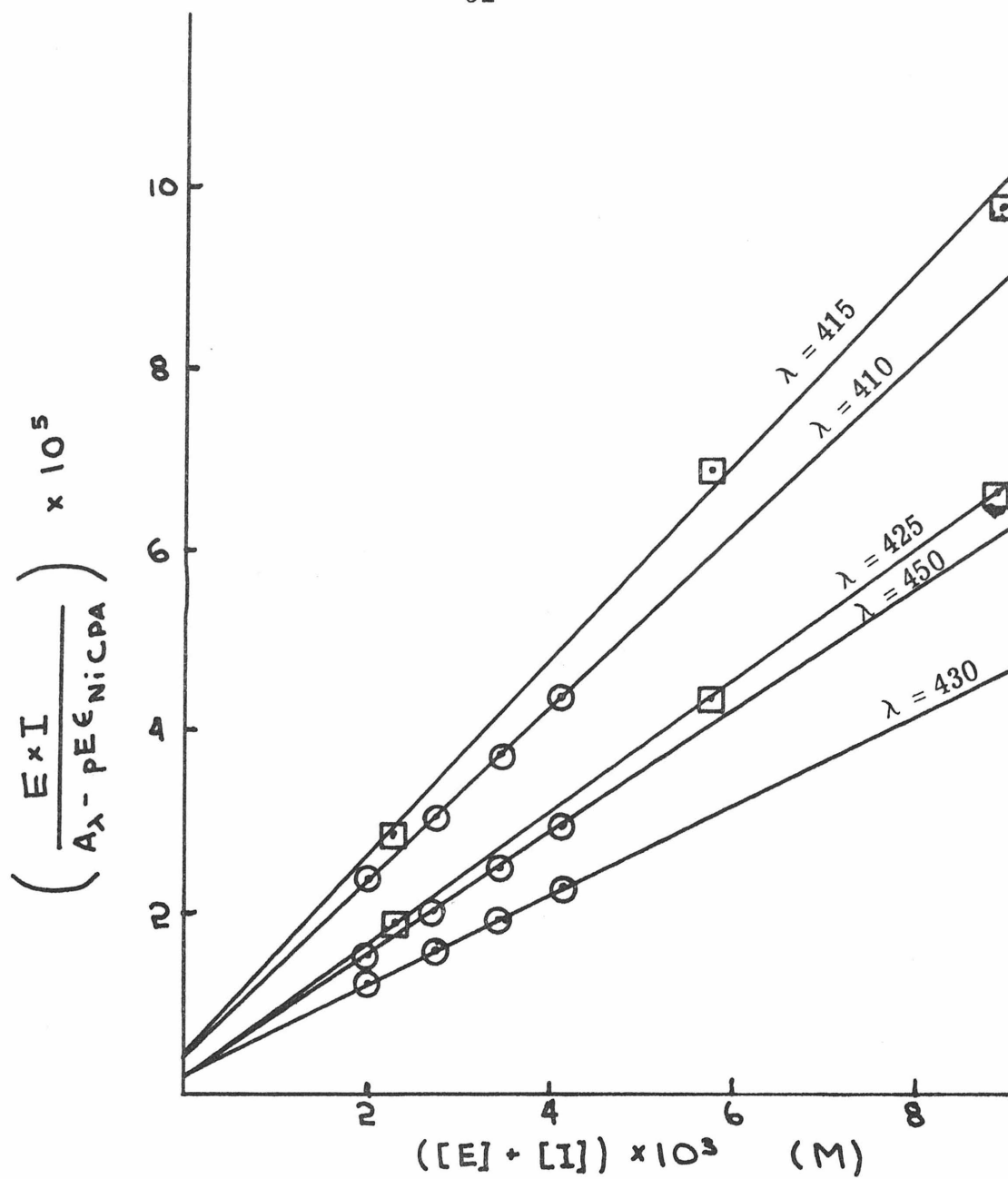


Figure Ni-X. Plots of $\frac{E \times I}{A_{\lambda} - pE\epsilon_{\text{NiCPA}}}$ vs. $E + I$

for the reaction of Ni(II)CPA with Na β PP.

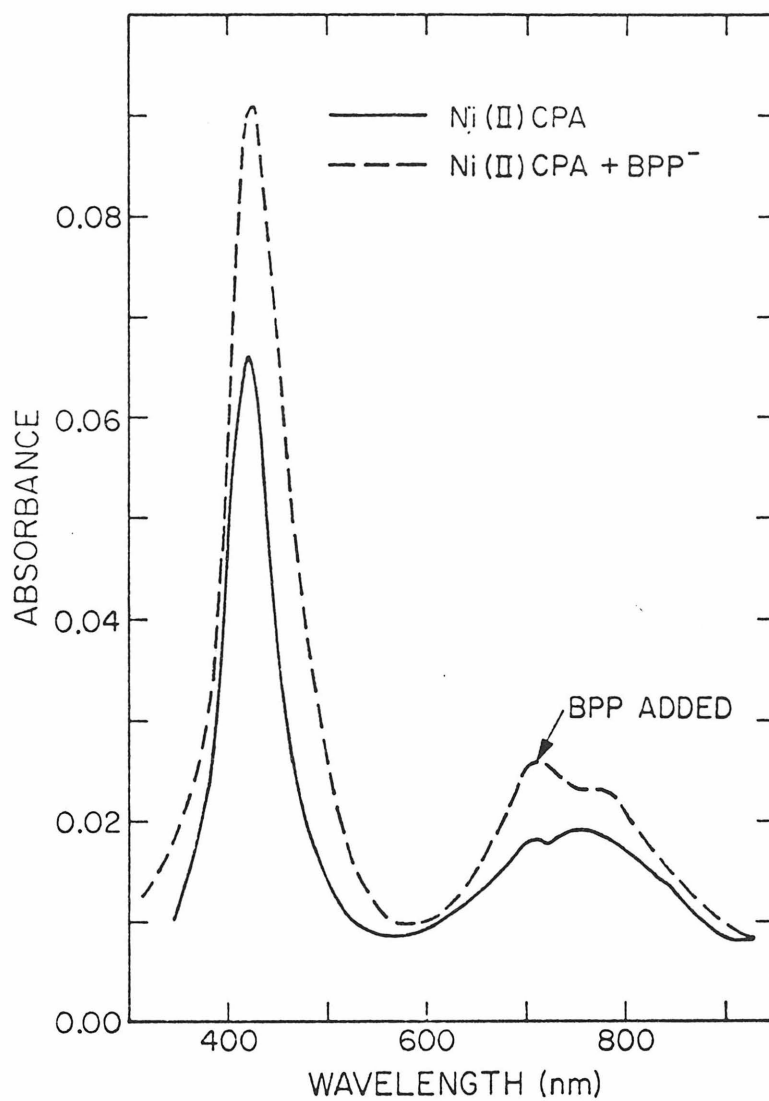


Figure Ni-XI. Absorption spectra of Ni(II)CPA, $[\text{Ni}^{+2}] = 3.35 \times 10^{-4} \text{ M}$; and Ni(II)CPA + Na β PP, $[\text{Ni}^{+2}] = 3.22 \times 10^{-4} \text{ M}$, $[\text{Na}\beta\text{PP}] = 3.87 \times 10^{-3} \text{ M}$ in KF buffer.

430 and 435 nm. Considering the schematic rather than exact nature of the calculated spectrum, it is safe to conclude that the band positions in the enzyme-inhibitor complex are identical in both the fluoride and chloride buffers. This observation is apparent when the rest of the spectrum is considered. The similarity of the curves in Figure (Ni-XII) indicates that fluoride ion is not bound in the Ni(II)-CPA · β PP complex in fluoride buffer.

The difference in the values obtained for the binding constant, K_I , in these two media can be attributed to competition for the nickel site. It should be noted that the method used in calculating the binding constant assumes that there are only two spectrally detectable species in solution. In fact, depending on the magnitude of the binding constant of fluoride ion to Ni(II)-CPA, K_{F^-} , three spectrally detectable species may be present. Under the conditions used in the experiment, $[Ni(II)-CPA]_T \simeq 3.3 \times 10^{-4}$ M, $[F^-] = 0.5$ M, significant amounts of free Ni(II)-CPA will be present if the binding constant (K_{F^-}) is less than or equal to 20. The only reasonable conclusion from this experiment is that the binding of β -phenylpropionate and fluoride are mutually exclusive.

The large change in the spectrum of Ni(II)-CPA when it binds β -phenylpropionate is indicative of a change in coordination number. Considering the increase in molar extinction coefficients, the only reasonable possibilities are five or distorted tetrahedral coordination.

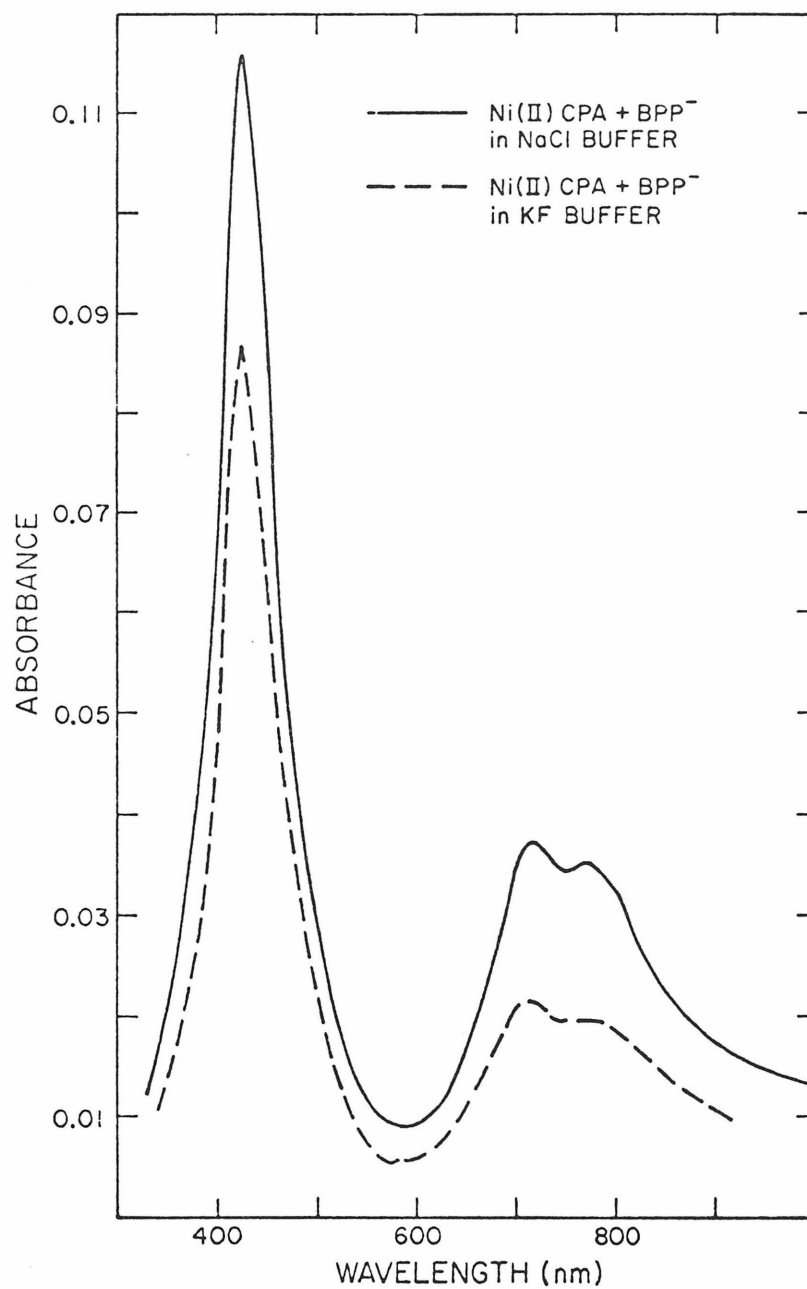


Figure Ni-XII. Absorption spectra of Ni(II)CPA + 12 Na β PP in sodium chloride and sodium fluoride buffers. $[\text{Ni}^{+2}]_{\text{Cl}} = 4.39 \times 10^{-4} \text{ M}$, $[\text{Ni}^{+2}]_{\text{F}^-} = 3.22 \times 10^{-4} \text{ M}$.

Although definitive assignments have not been made, especially of the bands in the near infrared, the spectra of tetrahedral nickel(II) complexes have several unique features with respect to five coordinate nickel(II) complexes. Model distorted tetrahedral nickel(II) complexes with nitrogen or mixed nitrogen and oxygen donors all have at least one absorption band in the 6000 cm^{-1} to $11,000\text{ cm}^{-1}$ region with a molar extinction coefficient of approximately 20. Further, the highest energy ligand field band occurs below roughly $20,000\text{ cm}^{-1}$ for ligands of this type.⁴¹⁻⁴⁸ Stronger field ligands, such as phosphines, are needed in order for bands to occur in the region around $23,000\text{ cm}^{-1}$.⁴⁹

As we have seen, the Ni(II)-CPA · β PP complex has a strong ($\epsilon_m \sim 50$) absorption centered at $23,300\text{ cm}^{-1}$. This band occurs at considerably higher energy than the highest energy ligand field bands in pseudo-tetrahedral nickel(II) complexes which have four strong field nitrogen donors. The near infrared spectrum of the Ni(II)-CPA · β PP complex also does not conform to the characteristics of pseudo-tetrahedral geometry, as there is no significant absorption attributable to a nickel(II) species all across the region.

Five coordinate nickel(II) complexes, on the other hand, have spectra that are quite similar to that of the Ni(II)-CPA · β PP complex. The ligand field spectra of some model five coordinate nickel(II) complexes are summarized in Table (Ni-IV). Several of the models, it should be noted, have their most intense absorption bands at energies comparable to the value observed in the enzyme-inhibitor complex.

Table Ni-IV
Spectra of Some Five Coordinate Nickel(II) Complexes

<u>Complex</u>	<u>Donor Set</u>	<u>Spectra ($\text{cm}^{-1}(\epsilon_{\text{m}})$)</u>
$\text{Ni}(\text{dacoda})(\text{H}_2\text{O})^{\text{a}}$	N_2O_3	12300(21), 13100(25), 15800(28), 26400(86)
$\text{Ni}(\text{Et}_4\text{dien})\text{Cl}_2^{\text{b}}$ (in acetone)	N_3Cl_2	10100(15), 12700(15), 18850(50), 22500(70)
$\text{Ni}(\text{MABenNEt}_2)\text{Cl}_2^{\text{c}}$	N_3Cl_2	8700(13), 13300(40), 19400(?)
$[\text{Ni}(\text{Me}_6\text{tren})\text{Cl}]\text{Cl}^{\text{d}}$	N_4Cl	7100(26), 10500-11600(20), 14900(30), 20000(sh) 23500(1172)
$\text{Ni}(\text{Me}_5\text{dien})\text{Cl}_2^{\text{e}}$	N_3Cl_2	5000, 9600(sh), 11400(sh), 12700(42), 15900(sh) 18700(sh), 21500(165)
$\text{Ni}(\text{Me}_4\text{daeo})\text{Cl}_2^{\text{f}}$	N_2OCl_2	11500(38), 12300(35), 18500(55), 21500(117)

^a Reference 50; dacoda = 1,5-diazacyclooctane-N,N'-diacetate.

^b Reference 51; (Et_4dien) = 1,1,7,7-tetraethyldiethylenetriamine.

^c Reference 52; MABenNEt_2 = N,N-diethyl-N'-10-methylamino-benzylidene)-ethylenediamine.

^d Reference 53; Me_6tren = tris(2-dimethylaminoethyl)amine.

^e Reference 54; Me_5dien = bis(2dimethylaminoethyl)methylamine.

^f Reference 55; Me_4daeo = bis(2-dimethylammoethyl)oxide.

The Ni(dacoda)(H₂O) complex is particularly relevant since it shows roughly the same pattern of bands in the visible as is found for the enzyme-inhibitor complex.

Thus, we conclude that in the Ni(II)-CPA · β PP complex the nickel has a coordination number of five. This decrease in coordination number indicates that there is considerably more crowding about the nickel in the enzyme inhibitor complex than in the free Ni(II) enzyme. Perhaps, the interaction of the phenyl group of the inhibitor with other groups on the enzyme causes a small but significant conformational change which reduces the size of the metal pocket. Some additional interaction, other than acetate coordination to the metal, is clearly involved since the observed binding constant of $K_I = (3.7 \pm 1.7) \times 10^3$ is two orders of magnitude greater than the binding constants of acetate ion to hexaquo nickel(II).⁵⁶

It is worth noting that this evidence of steric crowding around the nickel(II) ion is consistent with the slightly reduced values of the ligand field parameters we found for the resting enzyme.

In conclusion, then, we have established an octahedral-like coordination environment for the nickel(II) ion in Ni(II)-CPA. We have also shown that when the inhibitor β -phenylpropionate is bound the nickel becomes five-coordinate. The general implications of these results will be discussed in Chapter V.

References

1. J. E. Coleman, *Biochem.*, 4, 2644 (1965).
2. D. J. Plocke and B. L. Vallee, *Biochem.*, 1, 1039 (1962).
3. R. D. Kobes, R. T. Simpson, B. L. Vallee, and W. J. Rutter, *Biochem.*, 8, 585 (1969).
4. J. E. Coleman and B. L. Vallee, *J. Biol. Chem.*, 236, 2244 (1961).
5. J. E. Coleman in Bioinorganic Chemistry, G. L. Eichhorn, ed., to be published.
6. J. L. Hall, J. A. Swisher, D. G. Brannon, and T. M. Liden, *Inorg. Chem.*, 1, 409 (1962).
7. W. J. Ray, Jr. and J. S. Multani, *Biochem.*, 11, 2805 (1972).
8. J. Reedijk, P. W. N. M. Van Leeuwen, and W. L. Groeneveld, *Recenil. Trav. Chim.*, 87, 129 (1968).
9. C. J. Ballhausen, Introduction to Ligand Field Theory, McGraw-Hill, New York, 1962.
10. C. K. Jørgensen, *Acta Chem. Scand.*, 9, 1362 (1955).
11. H. B. Gray, private communication.
12. P. J. McCarthy and M. T. Vala, *Mol. Phys.*, 25, 17 (1973).
13. M. D. Sturge, *J. Chem. Phys.*, 51, 1254 (1969).
14. U. Fano, *Phys. Rev.*, 124, 1866 (1961).
15. C. W. Reimann, *J. Res. Nat. Bur. Stand. (USA)*, 72A, 765 (1968).
16. C. K. Jørgensen, *Acta Chem. Scand.*, 10, 887 (1956).
17. B. J. Hathaway and D. G. Holah, *J. Chem. Soc.*, 2400 (1968).

18. R. W. Kiser and T. W. Lapp, *Inorg. Chem.*, 1, 401 (1962).
19. R. S. Drago, D. W. Meek, R. L. Onghi, and M. D. Joesten, *Inorg. Chem.*, 2, 1056 (1963).
20. P. L. Meredith and R. A. Palmer, *Inorg. Chem.*, 10, 1049 (1967).
21. A. B. P. Lever and D. Ogden, *J. Chem. Soc. (A)*, 2041 (1967).
22. G. N. Rao and N. C. Li, *Can. J. Chem.*, 44, 1637 (1966).
23. V. Imhof and R. S. Drago, *Inorg. Chem.*, 4, 427 (1965).
24. C. K. Jørgensen, *Adv. Chem. Phys.*, 5, 33 (1963).
25. R. S. Drago, D. W. Meek, M. D. Joesten, and L. LaRoche, *Inorg. Chem.*, 2, 124 (1963).
26. J. A. Duffy and M. D. Ingram, *J. Chem. Soc. (A)*, 2398 (1969).
27. D. W. Meek, R. S. Drago, and T. S. Piper, *Inorg. Chem.*, 1, 285 (1962).
28. J. A. Duffy, F. P. Glasser, and M. D. Ingram, *J. Chem. Soc. (A)*, 551 (1968).
29. R. G. Shulman, S. Sugano, and K. Knox, *Phys. Rev.*, 130, 512 (1963).
30. D. M. L. Goodgame, M. Goodgame, and M. J. Weeks, *J. Chem. Soc.*, 5194 (1964).
31. R. V. Pisarev, V. V. Druzhinin, S. D. Prochorova, N. N. Nesterova, and G. T. Andreeva, *Phys. Status Solidi*, 35, 145 (1969).
32. J. Hare, private communication.
33. T. Haseda and M. Date, *J. Phys. Soc. Japan*, 13, 175 (1958).

34. B. N. Figgis, Introduction to Ligand Fields, Interscience, New York, 1966, p 266.
35. L. Sacconi, Transition Metal Chem., 4, 199 (1967).
36. W. N. Lipscomb, G. N. Reeke, J. A. Hartsuck, F. A. Quioco, and P. H. Bethye, Phil. Trans. Roy. Soc., B257, 177 (1970).
37. S. A. Latt and B. L. Vallee, Biochem., 10, 4263 (1971).
38. D. S. Auld and B. L. Vallee, Biochem., 9, 602 (1970).
39. R. B. Martin, M. Chamberlin, and J. T. Edsall, J. Amer. Chem. Soc., 82, 495 (1960).
40. S. C. Furman and C. S. Garner, J. Amer. Chem. Soc., 73, 4528 (1951).
41. R. H. Holm, A. Chakravorty, and L. J. Theriot, Inorg. Chem., 5, 625 (1966).
42. L. Sacconi, P. Paoletti, and M. Ciampolini, J. Amer. Chem. Soc., 85, 411 (1963).
43. G. V. Everett, Jr., and R. H. Holm, J. Amer. Chem. Soc., 87, 2117 (1965).
44. L. Sacconi, I. Bertini, F. Mani, Inorg. Chem., 6, 262 (1967).
45. A. L. Lott, II, and P. G. Rasmussen, J. Inorg. Nucl. Chem., 32, 101 (1970).
46. S. G. McGeachin, Can. J. Chem., 46, 1903 (1968).
47. J. E. Fergusson and C. A. Ramsay, J. Chem. Soc., 5223 (1965).
48. J. E. Fergusson and B. O. West, J. Chem. Soc., 1565 (1966).
49. M. C. Browning, R. F. B. Davies, D. J. Morgan, L. E. Sutton, and L. M. Venanzi, J. Chem. Soc., 693 (1962).

50. D. F. Averill, J. I. Legg, and D. L. Smith, *Inorg. Chem.*, 11, 2344 (1972).
51. Z. Dori and H. B. Gray, *J. Amer. Chem. Soc.*, 88, 1394 (1966).
52. L. Sacconi, I. Bertini, and R. Morassi, *Inorg. Chem.*, 6, 1548 (1967).
53. M. Ciampolini and N. Nardi, *Inorg. Chem.*, 5, 41 (1966).
54. M. Ciampolini and G. P. Speroni, *Inorg. Chem.*, 5, 45 (1966).
55. M. Ciampolini and N. Nardi, *Inorg. Chem.*, 6, 445 (1967).
56. L. G. Sillén and A. E. Martell, eds., Stability Constants of Metal-Ion Complexes, Special Pub. No. 17, The Chemical Society, London, 1964.

CHAPTER IV

COPPER(II)CARBOXYPEPTIDASE A

Copper(II) Carboxypeptidase A shows neither peptidase nor esterase activity towards model substrates.¹ Its lack of activity cannot be attributed to an innate substitution inertness at the metal center since Cu(II) complexes are known to undergo rapid ligand substitution reactions.² One possible explanation is that the solvent accessible coordination position on the Cu(II) ion is not oriented properly for productive interaction with bound substrate. Another explanation is that unique features of the CPA-Cu⁺² interaction change the relative positions of other important functional groups in such a way that these groups can no longer act effectively in either binding or attacking bound substrate. Some support for this hypothesis is available in the literature. Low resolution (6Å) X-ray work on the Cu(II) CPA complex with the model substrate Glycyl-L-Tyrosine indicates that the conformational change of Glu 270 associated with substrate binding in the native enzyme does not occur in this case.^{3,4} Of course, many other explanations are also possible.

In order to gain some insight into the coordination number and geometry of the copper in Cu(II)-CPA, certain of its physical properties were investigated. The techniques employed were EPR and NIR-Vis absorption spectroscopy. Measurement of the magnetic moment of Cu(II)-CPA was not attempted. Consideration of the potential accuracy of the data (± 0.1 BM) precluded any meaningful interpretation of the magnetic moment of Cu(II)-CPA since the magnetic moment of copper(II) complexes fall into the relatively narrow range of 1.80-2.00 BM.

Sample Preparation

Apo and Cu(II)-CPA samples were prepared as previously described. NIR and Vis spectral studies were done on a sample of apoCPA to which one equivalent of copper(II) was added. Copper(II) stock solutions were made from CuBr₂ (anhydrous) obtained from Matheson, Coleman, and Bell and used without further purification. The samples used for the EPR measurement had the copper(II) introduced by the usual dialysis procedure. Analytical data for these samples are presented in Table (Cu-I). Both samples gave identical EPR spectra. Room temperature spectra were taken with the enzyme at approximately 4.5×10^{-4} M in 1M NaCl, 0.05M tris pH 7.5 buffer. Low temperature spectra were taken in a 1:1 ethyleneglycol:buffer glass.

The CPA used in the zinc-copper competition experiments described below was fully reconstituted ZnCPA.

Copper-Zinc Competition

In order to demonstrate that the CPA was behaving properly and that copper was binding at the active site and not somewhere else, a competition study was performed. Samples of ZnCPA were dialyzed against buffer solutions containing varying concentrations of cupric ion. Subsequently, the enzyme was crystallized, collected, and redissolved in buffer and metal analysis for zinc and copper as well as activity measurements were made. Prior to crystallization, sample 85-1 was dialyzed against one 500 ml change of 1×10^{-4} M Cu⁺² in buffer, while 85-2 was treated with two 500 ml portions of 1×10^{-3} M Cu⁺² in buffer followed by two 500 ml portions of 1×10^{-4} M Cu⁺² in buffer.

Table Cu-I

<u>Analysis</u>	<u>Sample No.</u>	<u>[CPA]</u>	<u>ppm Metal</u>	<u>Metal/Enz</u>
Cu	93c	4.75×10^{-5}	3.2	1.06
Zn	93s	4.68×10^{-4}	0.48	0.016
Cu	95c	4.38×10^{-5}	2.5	0.90
Zn	95s	4.44×10^{-4}	0.26	0.009

The results of the metal analyses and activity measurements are shown in Table (Cu-II). The data indicate that the system behaves as expected if copper replaces zinc at the active site. Thus, there is a total of one metal atom per CPA molecule and the activity correlates well with the zinc content; i.e., the ratio of zinc contents is equal to the ratio of specific activities of the samples.

EPR of Cu(II)-CPA

The room temperature EPR spectrum of Cu(II)-CPA is not particularly well resolved, especially in the $g_{||}$ region. At low temperature with the enzyme in an ethylene glycol glass extremely good and reproducible spectra were obtained.

Figure (Cu-I) shows the EPR spectrum (1st derivative at liquid nitrogen temperature) of Cu(II) -CPA and the computer simulation based on the parameters which give the best possible fit. Figure (Cu-II) shows the EPR spectrum of $\sim 1 \times 10^{-4} \text{ M Cu}^{+2}$ ion in the ethylene glycol-buffer glass under the same conditions. The large differences between the spectra of Figures I and II indicate conclusively that the cupric ion has not dissociated from the enzyme in the frozen glass. Table (Cu-III) contains the parameters that give the best possible fit with the observed spectrum. For comparative purposes the results from the EPR spectra of Human Copper Carbonic Anhydrase B are also included.⁵

In order to understand the types of information that can or cannot be extracted from frozen glass or powder EPR spectra, some discussion of the theory used in interpreting these spectra is required.

Table Cu-II

<u>Sample</u>	<u>No. Zn/Enz</u>	<u>No. Cu/Enz</u>	<u>Zn + Cu/Enz</u>	<u>No. Units/mg</u>
85-1	0.86	0.11	0.97	111.7
85-2	0.42	0.59	0.99	53.5
	<u>Ratio</u>	<u>Zn/Enz</u>	<u>Units/mg</u>	
	$\frac{85-2}{85-1}$	0.49	0.48	

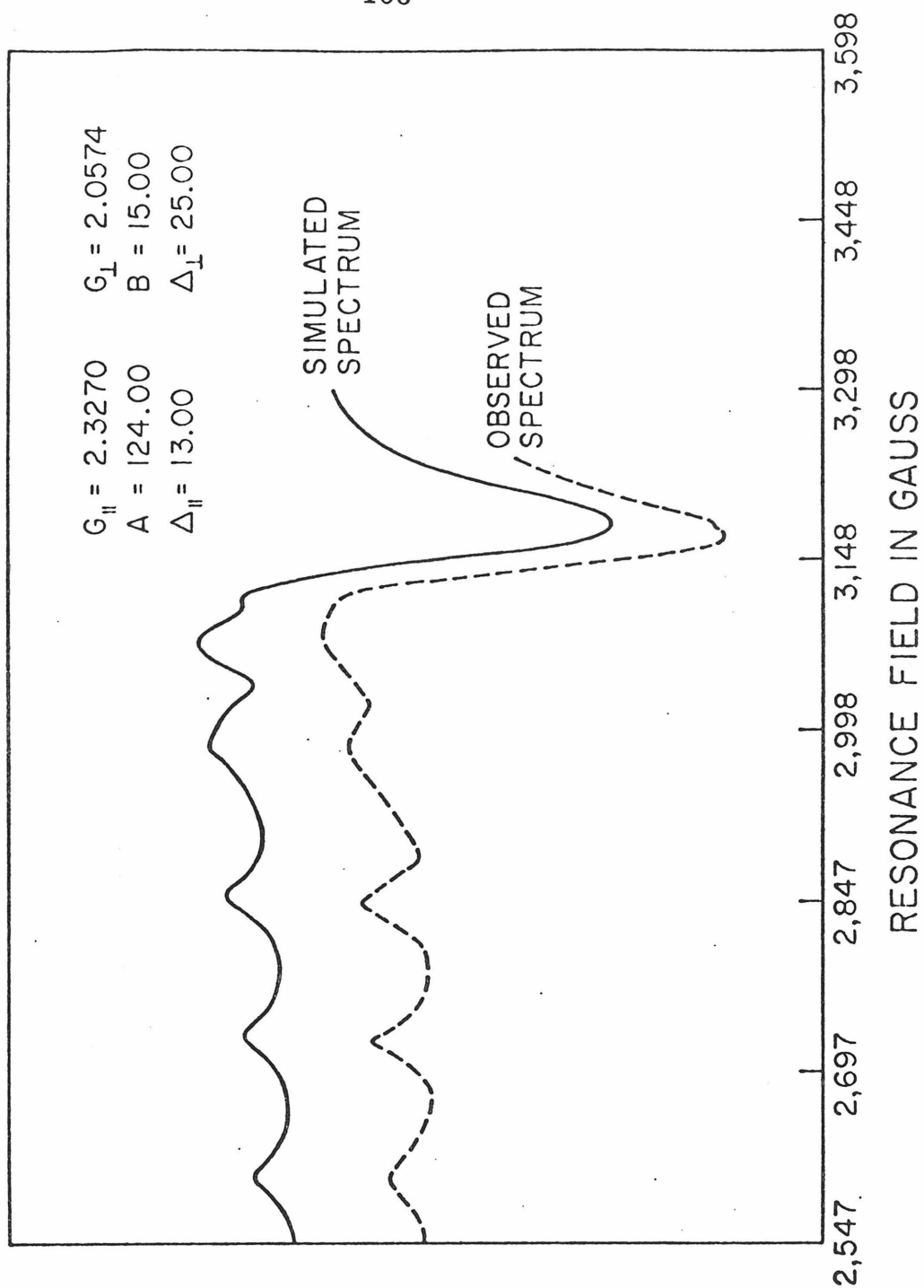


Figure Cu-I. Frozen glass and simulated EPR spectra of Cu(II)CPA.

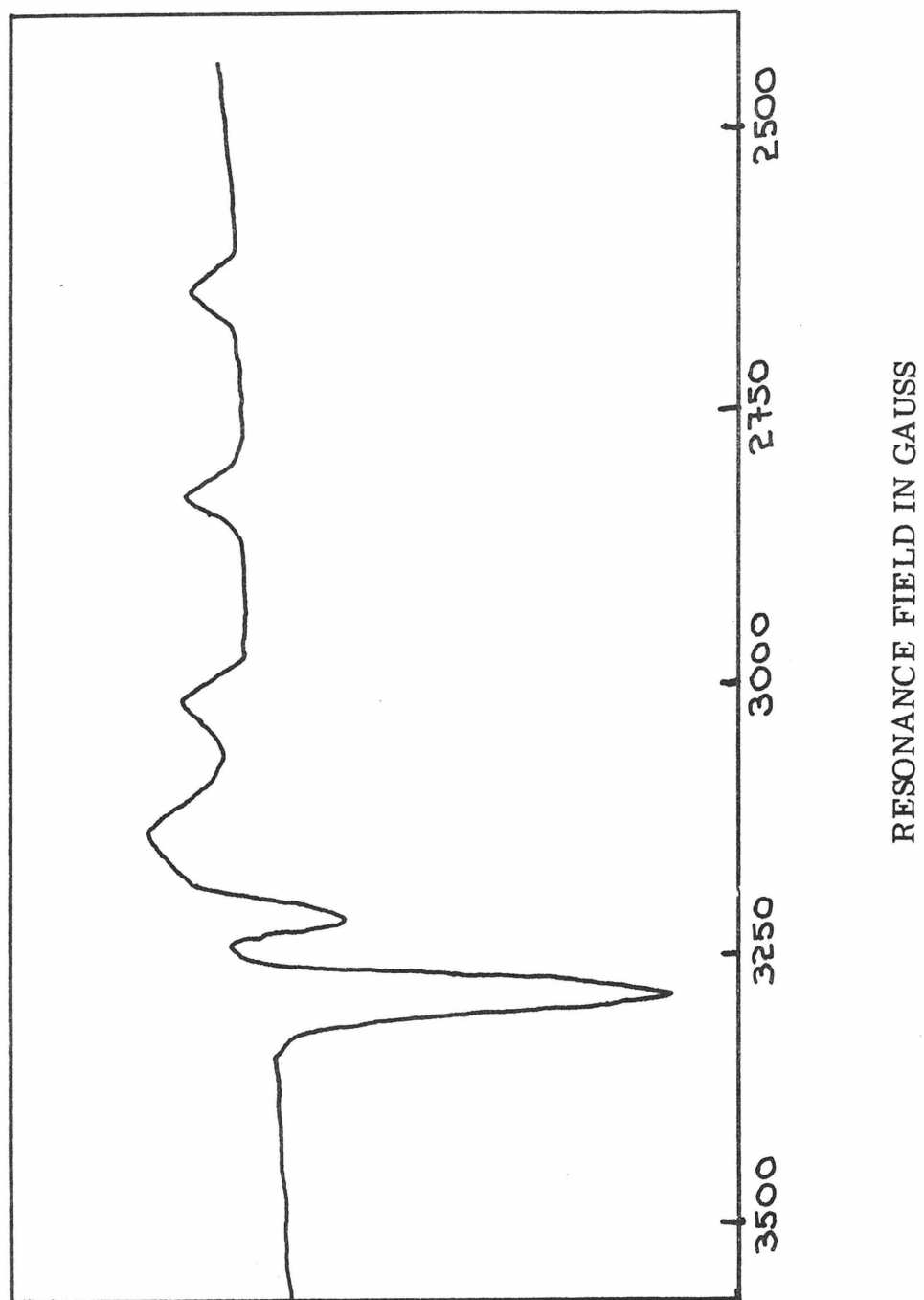


Figure Cu-II. Frozen glass EPR spectrum of Cu^{+2} in Tris buffer.

Table Cu-III

	$g_{ }$	g_{\perp}	$A_{ }$ (gauss)	A_{\perp} (gauss)	(gauss)	
	$\Delta_{ }$	Δ_{\perp}				
CuCPA	2.327	2.057	124.0	15.0	13	25
CuCA (Human) ^a	2.314	2.11	123.0	--	--	--

^aReference 5.

The EPR spectra of transition metal compounds are usually analyzed in terms of the effective spin Hamiltonian for the system. For copper(II), we have⁶

$$\mathcal{H} = \beta \vec{H} \cdot \underline{g} \cdot \hat{S} + A \hat{S} \cdot \hat{I} - g_N \beta_N \vec{H} \cdot \hat{I} \quad (1)$$

where \vec{H} is the applied magnetic field, β and β_N are respectively the Bohr and nuclear magnetons, \hat{S} and \hat{I} are the electron and nuclear spin angular momentum operators with $S = 1/2$ and $I = 3/2$ in this case, A is the nuclear hyperfine coupling constant, g_N is the nuclear g value, and \underline{g} is the g -tensor. For axial symmetry and in the principle axis coordinate system, e.g. the coordinate system for which the \underline{g} tensor is diagonal, it can be shown that

$$\begin{aligned} \mathcal{H} = & g_{||} \beta H_k S_k + g_{\perp} \beta (H_i S_i + H_j S_j) + A_{||} S_k I_k + \\ & + A_{\perp} (S_i I_i + S_j I_j) - g_N \beta_N \vec{H} \cdot \hat{I} \end{aligned} \quad (2)$$

where $g_{||}$ and g_{\perp} are the electron g values parallel and perpendicular to the principal axis, $A_{||}$ and A_{\perp} are the nuclear hyperfine coupling constants parallel and perpendicular to these axes, and i, j , and k refer to the principal axis.

In a powder or frozen glass sample, the molecules are randomly oriented. If θ is the angle between the k axis and the applied magnetic field, it has been shown that the field at which resonance occurs for the allowed transitions ($\Delta M_S = \pm 1$, $\Delta M_I = 0$) is given by⁷:

$$\begin{aligned}
H(\theta, M_I) = H^\circ - \frac{KM_I}{g\beta} - \frac{A_\perp^2 g_\perp^2}{4g^2 \beta^2 H^\circ} \left(\frac{A_\parallel^2 + K^2}{K} \right) [I(I+1) - M_I^2] \\
- (2g^2 \beta^2 H^\circ)^{-1} \left(\frac{A_\parallel^2 - A_\perp^2}{K} \right) \left(\frac{g_\parallel g_\perp}{g} \right)^2 \sin^2 \theta \cos^2 \theta M_I^2
\end{aligned} \quad (3)$$

where $H^\circ = \frac{h\nu^\circ}{g\beta}$, ν° is the microwave frequency employed

$$g^2 = g_\parallel^2 \cos^2 \theta + g_\perp^2 \sin^2 \theta, \quad \text{and} \quad (4)$$

$$K^2 g^2 = A_\parallel^2 g_\parallel^2 \cos^2 \theta + A_\perp^2 g_\perp^2 \sin^2 \theta \quad (5)$$

Since the magnetic field is swept in an EPR experiment, the absorption between H and $H + dH$ should be proportional to the fraction of molecules satisfying the resonance condition. Thus:

$$I = \frac{dN}{dH} = \frac{dN}{d\theta} \times \frac{d\theta}{dH} = \frac{dN}{d\theta} \times \frac{1}{\left(\frac{dH}{d\theta}\right)} \quad (6)$$

Since the number of molecules oriented between θ and $\theta + d\theta$ is proportional to $\frac{N_0}{2} \sin \theta d\theta$, and since

$$\frac{dH}{d\theta} = \frac{\sin \theta \cos \theta}{g^2} [(g_\parallel^2 - g_\perp^2) H^\circ + \frac{M_I}{g\beta} \left(\frac{A_\parallel^2 g_\parallel^2 - A_\perp^2 g_\perp^2}{K} + 2K(g_\perp^2 - g_\parallel^2) \right)] \quad (7)$$

then, as Tsay has shown⁸

$$I = \frac{dN}{dH} = \left(\frac{N_0 g_{\perp}^2}{2 \cos \theta} \right) [(g_{\parallel}^2 - g_{\perp}^2) H^0 + \frac{M_I}{g \beta} \left(\frac{A_{\parallel}^2 g_{\parallel}^2 - A_{\perp}^2 g_{\perp}^2}{K} + 2K(g_{\perp}^2 - g_{\parallel}^2) \right)]^{-1} \quad (8)$$

It can easily be seen from equation (8) that the absorption intensity blows up at $\theta = 90^\circ$ and the value of θ at which the quantity in brackets [] becomes zero. The latter effect is known as the angular anomaly. It should also be noted that $dH/d\theta$ is zero in the g_{\parallel} region ($\theta = 0^\circ$), which indicates that the resonance field does not change too much for molecules that have their principal axis approximately parallel to the applied field. Thus, even though the population factor is small for a given angle θ in this region, significant absorption can develop because $H(\theta, M_I)$ is relatively constant over a range of θ 's. Thus a much weaker absorption is to be expected in the g_{\parallel} region.

The EPR spectrum of Cu(II)-CPA can be understood in terms of the above discussion. The four weak peaks in the g_{\parallel} region arise from the interaction of the unpaired electron with the copper nucleus, nuclear spin $I = 3/2$. For $\theta = 0$, equation (3) reduces to

$$H(0, M_I) = H_{\parallel}^0 - |A_{\parallel}| M_I - \left(\frac{A_{\perp}^2 g_{\perp}^2}{2 H_{\parallel}^0 g_{\parallel}} \right) (I(I+1) - M_I^2) \quad (9)$$

expressed in units of gauss. Since $I = 3/2$ and $M_I = +3/2, +1/2, -1/2, -3/2$, four transitions are to be expected. Because A_{\perp} is approximately an order of magnitude smaller than A_{\parallel} in most monomeric copper(II) complexes, it is possible to neglect the second order contribution to

the spectrum in the parallel region represented by the third term in equation (9). Therefore, we obtain:

$$H(0, M_I) = H_{||}^{\circ} - |A_{||}| M_I \quad M_I = 3/2, 1/2, -1/2, -3/2 \quad (10)$$

The spectrum in the parallel region should have four equally spaced lines centered at $H_{||}^{\circ}$ with a separation $A_{||}$ between adjacent lines.

The perpendicular region is complicated by an angular anomaly which occurs at $\theta = 79^{\circ}$ as determined from the computer simulation. Because there is this additional large absorption so close to $\theta = 90^{\circ}$, it is impossible to obtain accurate values for g_{\perp} and A_{\perp} without doing a computer simulation. Even with a computer simulation, it still may not be possible to detect a small deviation from strict axial symmetry. Thus, even though the EPR spectrum of Cu(II)-CPA was satisfactorily simulated, assuming axial symmetry, a small rhombic symmetry component may still be present.

Another point worth noting regarding the computer simulation is that the A_{\perp} and Δ_{\perp} values are not unique in this case. The spectrum of Cu(II)-CPA can be fitted equally well with a slightly larger splitting A_{\perp} and narrower line width Δ_{\perp} or vice versa. However, the ambiguity in the value of A_{\perp} is not large on the order of 3-5 gauss.

The values found for the principal components of the g and A tensors for Cu(II)-CPA differ significantly from the values found earlier by Malmstrom and Vanngård.⁹ They reported $g_{||} = 2.24$, $g_{\perp} = 2.06$, $A_{||} = 0.019 \text{ cm}^{-1} = 182 \text{ gauss}$. These values, however,

are suspiciously similar to the values obtained here for cupric ion in buffer solution (Figure Cu II) $g_{||} = 2.24$, $A_{||} = 185$ G or 19.4 mK. These investigators measured samples of CuCPA that were freeze dried or were in solution at pH 5.5. It should be noted that freeze drying reduces the specific activity of native CPA by more than 50%. Dialysis of native CPA against buffer at pH 5.0 was one early way of preparing apoCPA.¹⁰ Thus, it is not unreasonable to conclude that Malmstrom and Vanngård observed the EPR signal of cupric ion that was not tightly bound at the active site, but was rather loosely bound elsewhere to the protein or was free in solution.

There is one other report of an EPR study of Cu(II)-CPA in the literature.¹¹ A single crystal study of Cu(II)-CPA₂ revealed three principal g values and superhyperfine interaction from two equivalent nitrogen ligands. Unfortunately, no numerical values for the relevant parameters, g_x, g_y, g_z, A_x, A_y , or A_z were included in this report and none have appeared subsequently.

The similarity in the EPR parameters of Cu(II)-CPA and Cu(II)-CA shown in Table Cu-III is striking, especially in the parallel region where more accurate values can be obtained. The metal environments in the native or zinc enzymes are very similar. The zinc ligands in human carbonic anhydrase are the N(1), N(3), and N(3) imidazole nitrogens of three histidine residues and one water molecule.¹² They form a distorted tetrahedron about the zinc atom. In native bovine CPA as we have seen the zinc ligands are the N(I)'s

of two histidine residues, the carboxyl group of a glutamic acid residue, and one water molecule. Thus, if the coordination number and geometry of the cupric ion are similar, one would expect the physical properties of these two derivatives to be quite similar. We will discuss this point further in the section on the electronic absorption spectra of Cu(II)-CPA.

Considerable structural and EPR data on model cupric complexes are available in the literature. The structural chemistry of the cupric ion (d^9) is dominated by the Jahn-Teller effect. Regular octahedral or tetrahedral structures are all but unknown. For the six coordinate species, a tetragonal distortion is by far the most common. Both axial compression accompanied by equatorial expansion as well as axial elongation with equatorial compression are possible. The latter when extended to complete removal of the axial ligands gives rise to the most common form of four coordination in cupric complexes, square planar. Squashed and pseudo tetrahedral coordination also occurs, especially in the halides and in bis chelates ligands with bulky side chains.¹³ Five coordinate cupric complexes with trigonal bipyramidal, square pyramidal, and intermediate structures are also known.

The g values and other parameters obtained from EPR spectra are usually interpreted in terms of the real spin Hamiltonian for the system. Thus,

$$\mathcal{H}_{\text{Zeeman}} = \beta \vec{H} \cdot (k\vec{L} + g_e \vec{S}) \quad (9)$$

where k is the orbital reduction factor which accounts for the reduction of the spin orbit coupling constant λ below its value in the free ion. Theoretical expressions for the g values have been derived for cupric ion in environments of various symmetries. In order to explain the deviation of the g values from g_e , the value of the free electron, it is necessary to use ground state wave functions that have been corrected for the mixing in of excited states by spin-orbit coupling.

It has been shown,¹⁴ using the above approach, that the g values for cupric ion in tetragonal fields are:

a) axial elongation

$$g_{\perp} = 2 - \frac{2k^2 \lambda}{E(xz, yz \rightarrow x^2 - y^2)} \quad (10)$$

$$g_{||} = 2 - \frac{8k^2 \lambda}{E(xy \rightarrow x^2 - y^2)} \quad (11)$$

b) axial compression = trigonal bipyramidal

$$g_{\perp} = 2 - \frac{6k^2 \lambda}{E(xz, yz \rightarrow z^2)} \quad (12)$$

$$g_{||} = 2.00 \quad (13)$$

In the above expressions, the denominators refer to the energy separation of the ground and various excited states. The above nomenclature assumes that the coordinate axes point directly at the

ligands. It has also been shown that the axial compression case is completely equivalent to trigonal bipyramidal coordination.

Quite clearly the value of $g_{||}$ for axial Cu^{+2} epr spectra is diagnostic of the coordination, at least for the two cases shown above. For trigonal bipyramidal copper(II) complexes values of $g_{||}$ between 2.004 and 2.06 have been found experimentally.¹⁵ Since the $g_{||}$ for Cu(II)-CPA is significantly larger than 2.00 (i.e., 2.33) it can certainly be said that the copper atom is not in an axially compressed tetragonal or trigonal bipyramidal environment. On the basis of the g values alone, only limited conclusions about the structure of the copper site can be made. The data are consistent with a square planar, square pyramidal, or axially elongated octahedral coordination geometry.

The classification of copper in naturally occurring copper proteins is based, in part, on the magnitude of the nuclear hyperfine coupling constant component $A_{||}$. Two types of copper are discernible by this means, as is shown in Figure (Cu-III).¹⁶ Type I copper, as it is commonly called, has rather small values for $A_{||}$, between 3 and 10 mK. Type II copper on the other hand is characterized by much larger values of $A_{||}$, 14-20 mK. Type I copper is also associated with an intense absorption approximately 610 nm in the visible region. All the synthetic copper proteins, i.e. proteins into which copper has been artificially introduced, contain Type II copper, as Figure (Cu-III) illustrates. However, for these proteins, the observed range

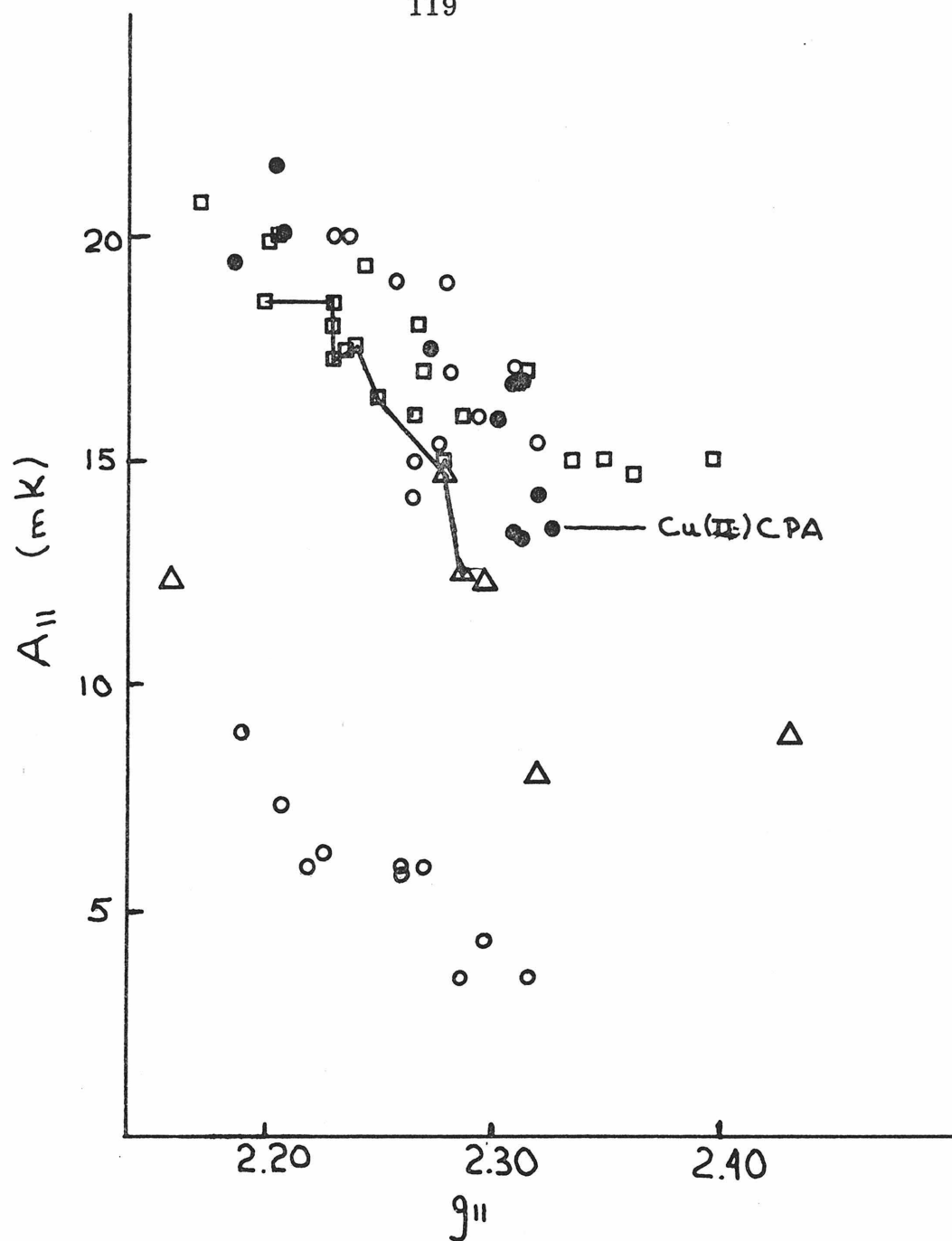


Figure Cu-III. EPR parameters $g_{||}$ and $A_{||}$ for copper(II) systems. \circ , native copper proteins; \bullet , synthetic copper proteins; \square , model tetragonal copper(II) complexes; \triangle , model pseudo-tetrahedral copper(II) complexes. (Adapted from reference 16)

of $A_{||}$'s is somewhat larger than for the native copper proteins. By way of comparison, EPR data for model cupric complexes having both tetragonal (including square planar and distorted octahedral) and pseudo tetrahedral coordination have been included in the figure.

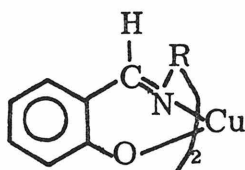
The tetragonally coordinated model complexes have values of $A_{||}$ that fall in the range 15-20 mK, while the pseudo tetrahedral complexes have values of $A_{||}$ that are significantly smaller, 8-15 mK.


The series of bis-N-alkyl(aryl)salicylideneaminatocopper(II) complexes connected by the line in figure (Cu-III) is of particular interest. Complete X-ray structures have been done for a number of compounds in this series. The results indicate that the angle θ between the planes formed by the central metal atom and the nitrogen and oxygen donors of each ligand unit is quite dependent on the nature of the side chain. The values of θ and the parameters $g_{||}$ and $A_{||}$ measured in a frozen glass (1:1 toluene, methylcyclohexane) at 77°K or in doped single crystal of the analogous zinc complex are shown in Table (Cu-IV). Examples of the frozen glass EPR spectra appear in Figure (Cu-IV a,b,c). θ , it should be noted, is equal to 0° for a planar structure and 90° for a tetrahedral one.

The results contained in Table (Cu-IV) indicate that there is a rough correlation between the magnitude of $A_{||}$ and the degree of distortion from planarity, with smaller values of $A_{||}$ corresponding to a more tetrahedral-like structure. An analogous but opposite trend is apparent for the values of $g_{||}$. The absence of an exact correlation

Table Cu-IV

EPR and Structural Results for bis N-substituted Salicylideneaminato-
copper(II) Complexes



<u>R</u>	<u>$g_{ }$</u>	<u>$A_{ }$ (mK)</u>	<u>θ</u>
H(doped in Ni complex)	2.20 ^a	18.5 ^a	0 ^a
n-Pr	2.23	18.6 ± 0.4	0 ^b
n-Bu	2.23	18.3 ± 0.4	0 ^b
Ph	2.23	17.2 ± 0.4	0 ^c
	2.24	17.6 ± 0.4	37 ^d
i-Pr	2.25	16.4 ± 0.4	60 ^e
t-Bu	2.28	14.7 ± 0.4	54 ^f
i-Pr(doped in Zn ⁺² complex)	2.29 ^g	12.5 ^g	> 60 ⁱ
t-Bu(doped in Zn ⁺² complex)	2.29 ^h	12.5 ^h	> 60 ⁱ

^a Reference 17.^d Reference 20.^g Reference 23.^b Reference 18.^e Reference 21.^h Reference 24.^c Reference 19.^f Reference 22.ⁱ Reference 25.

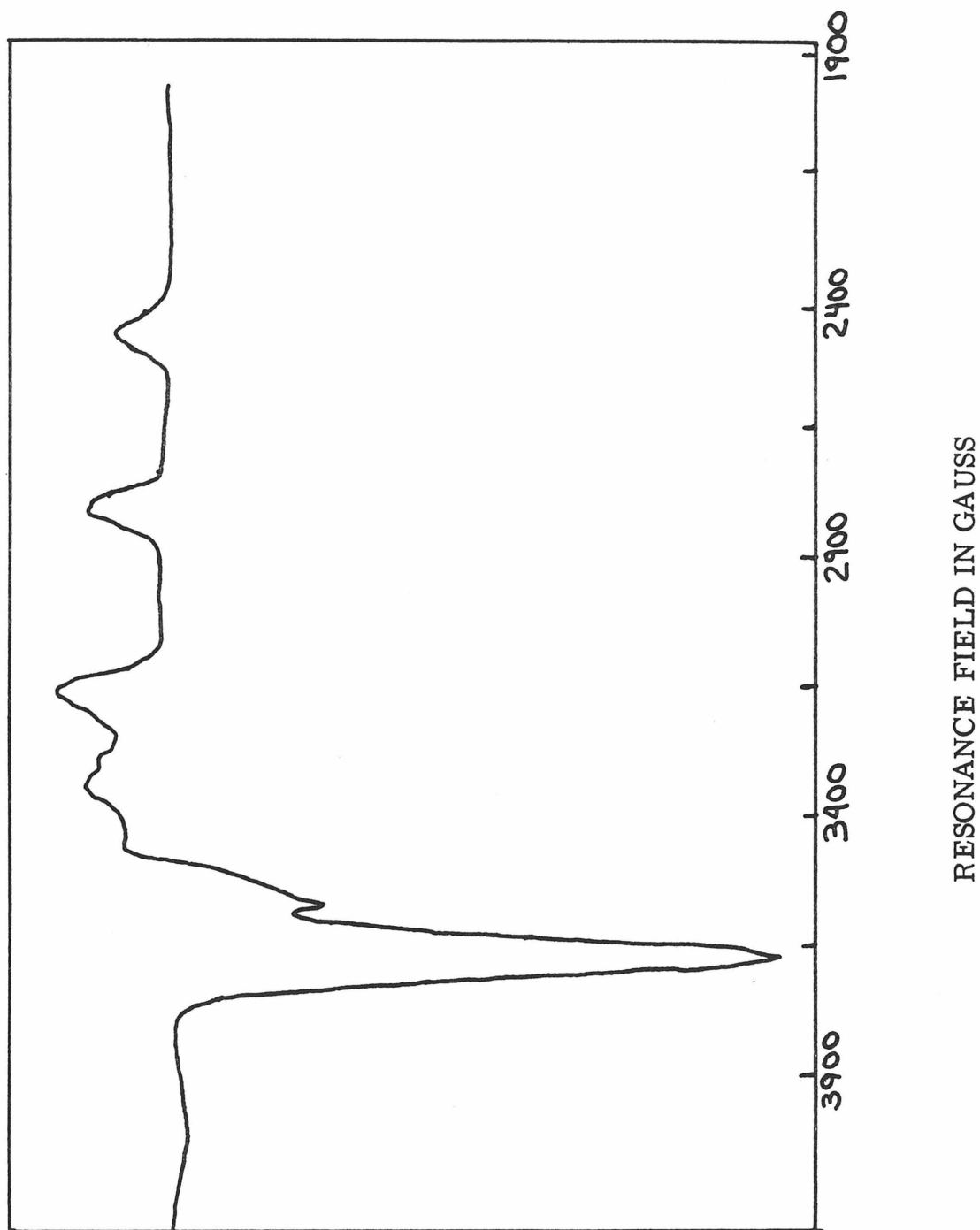


Figure Cu-IVa. Frozen glass EPR spectrum of bis(N-n-propylsalicylideneaminato)copper(II).

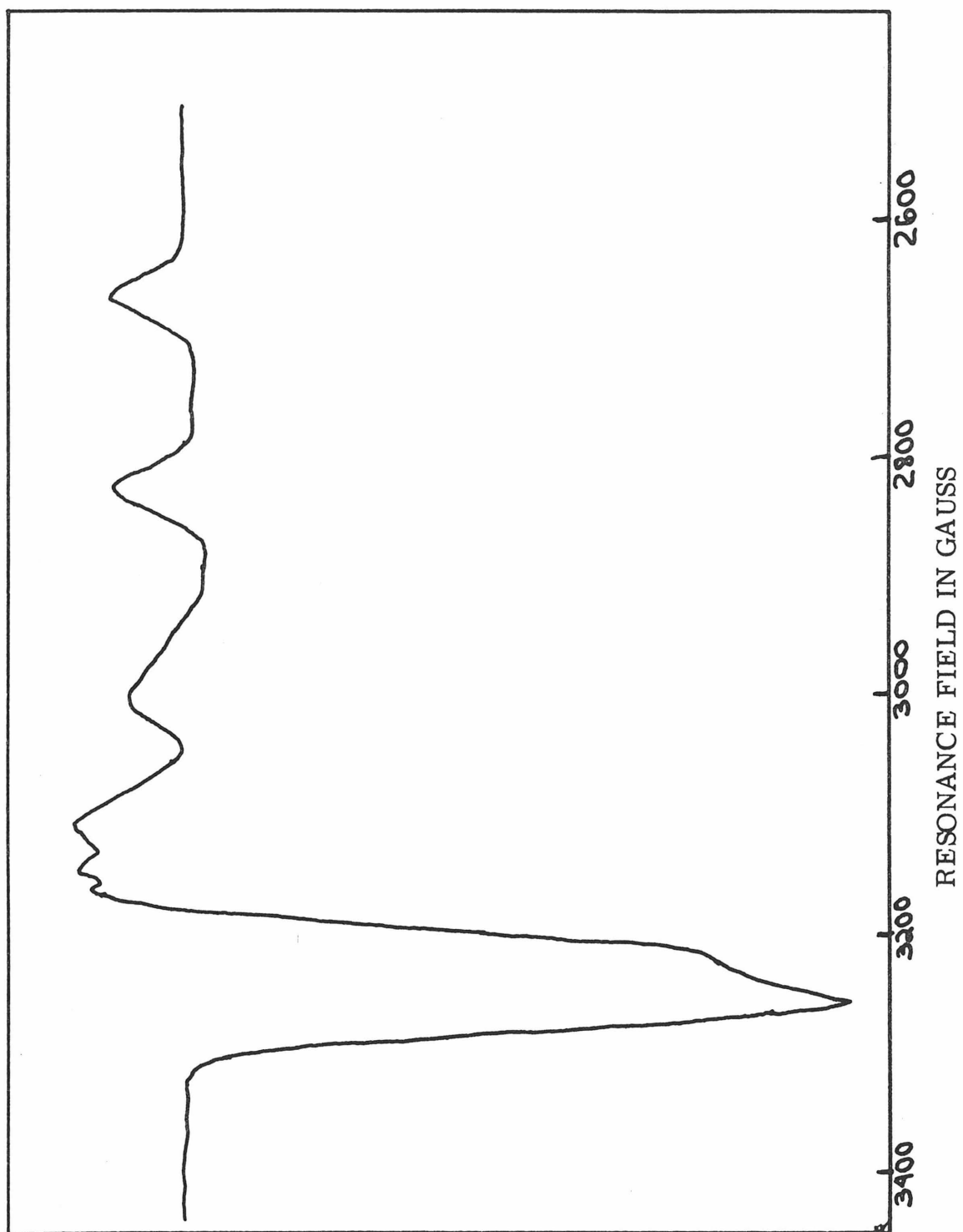


Figure Cu-IVb. Frozen glass EPR spectrum of bis(N-i-propylsalicylideneaminato)copper(II).

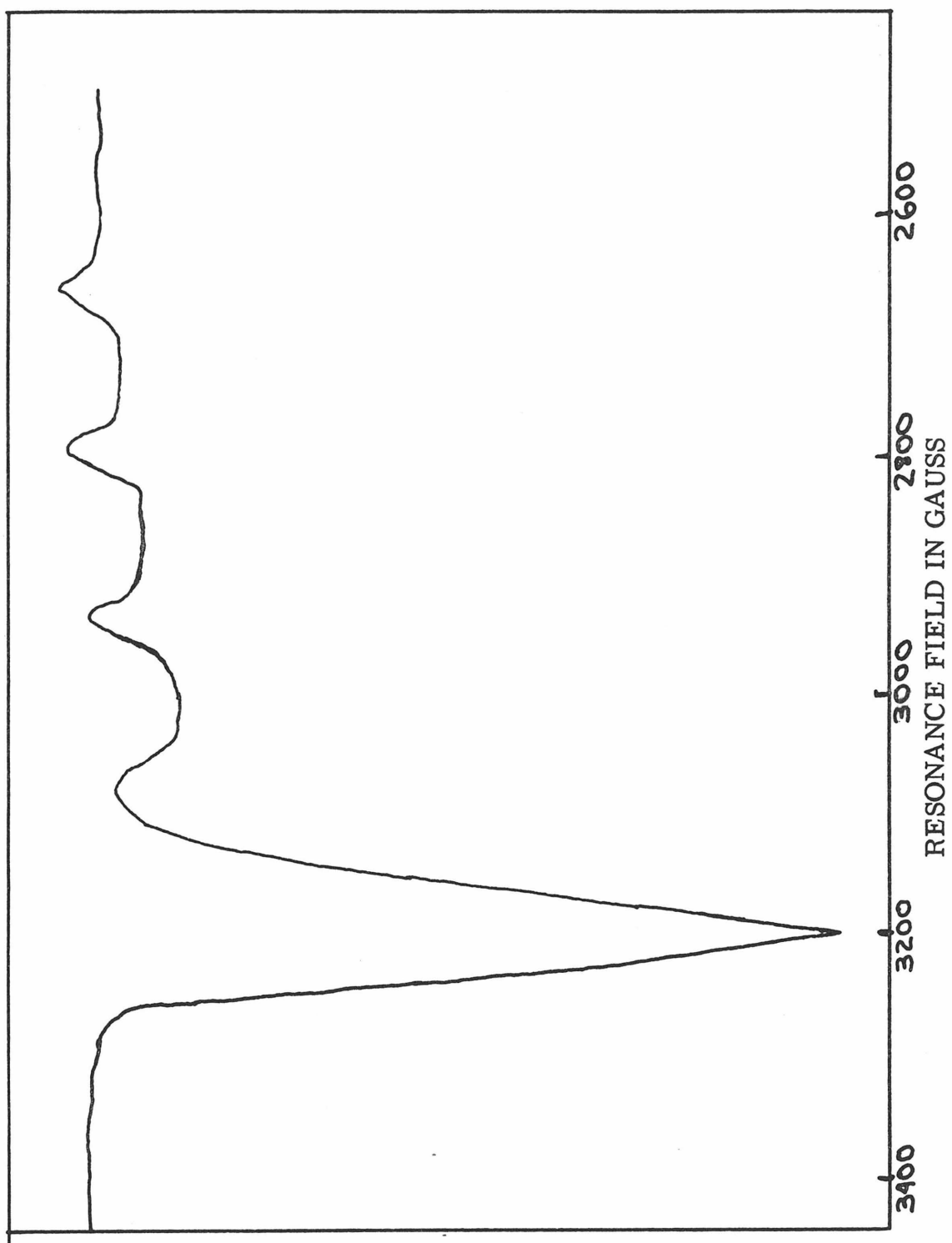


Figure Cu-IVc. Frozen glass EPR spectrum of bis(N-t-butylsalicylideneaminato)copper(II).

between the solid state structure and the EPR results in frozen solution could be explained if some or all of the complexes had slightly different structures in solution. We will discuss this point further in the section on the electronic absorption spectra of the complexes. For now, all we are trying to establish is the range of $g_{||}$ and $A_{||}$ observed in cupric complexes with a pseudo tetrahedral distortion from planar geometry. The structures of N-i-Pr and N-t-Bu complexes doped into single crystals of the respective zinc complexes are undoubtedly best described as only slightly distorted tetrahedral.²⁵ Under the conditions the value of $A_{||}$ is quite low, 12.5 mK; $g_{||} = 2.288$ was also found.^{23, 24}

Another relevant pseudo-tetrahedral model is cupric doped dichloro(1,10,phenanthroline)zinc(II). A value of 79° for θ was found for the host complex. The values $g_{||} = 2.297$, $A_{||} = 12.3(\text{mK})$ have been found in this system.²⁶ The similarity in the $g_{||}$ and $A_{||}$ parameters of this system and the doped salicylideneaminato system is striking. Unfortunately, no other EPR data on copper(II) in related pseudo tetrahedral sites are available in the literature, except for the three other models shown in Figure (Cu-III).

Cu(II)-CPA and Cu(II)-CA have the lowest values of $A_{||}$ (~ 13.5 mK) of all the type II copper proteins, either synthetic or native, shown in Figure (Cu-III). The phosphate complex of Cu(II) Alkaline Phosphatase (AP) has similar properties, although its $A_{||}$ value is slightly larger (14.2 mK). On the basis of these parameters alone,

pseudo tetrahedral geometry must be considered a distinct possibility in these systems. We do not wish to imply, however, that a tetragonal structure such as a planar or near planar array is eliminated as a possibility. Rather, both structures are consistent with the available data.

Extending this argument to some of the other native Cu(II) metalloproteins shown in Figure (Cu-III) pseudo tetrahedral structures are thus possible for porcine benzylamineoxidase, bovine erythrocyte, superoxide dismutase, and one of the type II coppers in human ceruloplasmin.

Copper(II) Spectra

The near infrared and visible "d-d" spectra of copper(II) complexes are remarkably similar. Generally they consist of a broad absorption envelope having a maximum somewhere between $11,000\text{ cm}^{-1}$ and $17,000\text{ cm}^{-1}$ with perhaps a shoulder or two on either or both the high and low energy sides. Upon closer examination, however, one can discern certain trends that can be correlated with changes in coordination number and geometry.

The spectra of Cu(II)-CPA both with and without inhibitor present in D_2O buffer were measured by the apo difference method previously described. The absorbance maximum and overall features are identical with those of spectra taken in H_2O buffer of samples prepared by the dialysis method. One cannot get such fine detail when metal-free tris buffer is used as the reference, since there is significant light scattering all across the visible and into the near IR range (Rayleigh scattering).

The absorption spectra of Cu(II)-CPA alone and in the presence of inhibitor sodium β -phenylpropionate are shown in Figure (Cu-V). Figure (Cu-VI) compares the absorption spectra of Cu(II)-CPA with that of an equimolar solution of cupric ion in tris buffer. Under the conditions employed in the buffer control, 4.66×10^{-4} M CuBr₂ in 1M NaCl, 0.05 M tris pH 7.5, the principal species involving copper have been shown to be $[\text{Cu}(\text{tris})_2(\text{H}_2\text{O})_3]^{+2}$ and $[\text{Cu}(\text{tris})_4(\text{H}_2\text{O})_2]^{+2}$.²⁷

The spectrum of cupric ion in the tris buffer is quite typical of that of aquo tri or tetraamine copper(II) complexes (vide infra), having a maximum at 630 nm ($\sim 15,900 \text{ cm}^{-1}$) and a molar extinction coefficient ϵ_M of about 40 ($\text{M}^{-1}\text{cm}^{-1}$). Copper(II) CPA, on the other hand, has a much more intense absorption at lower energy. Its absorption maximum occurs at 795 nm ($12,580 \text{ cm}^{-1}$) and has a molar extinction coefficient, ϵ_M , of 124. There is also a distinct shoulder on the lower energy side of the absorption envelope in the region of 920 nm ($10,800 \text{ cm}^{-1}$).

When the inhibitor sodium β -phenylpropionate (sodium hydrocinnamate) is present, the band maximum is significantly shifted to lower energy and the molar extinction coefficient increases somewhat. The exact effects of adding increasing amounts of sodium β -phenylpropionate to Cu(II)-CPA are shown in Figure (Cu-VII). The curves shown in the figure represent BPP⁻:Cu(II) ratios of approximately 8:1 and 24:1, respectively. The small but distinct peaks above 1400 nm are undoubtedly due to a small amount of

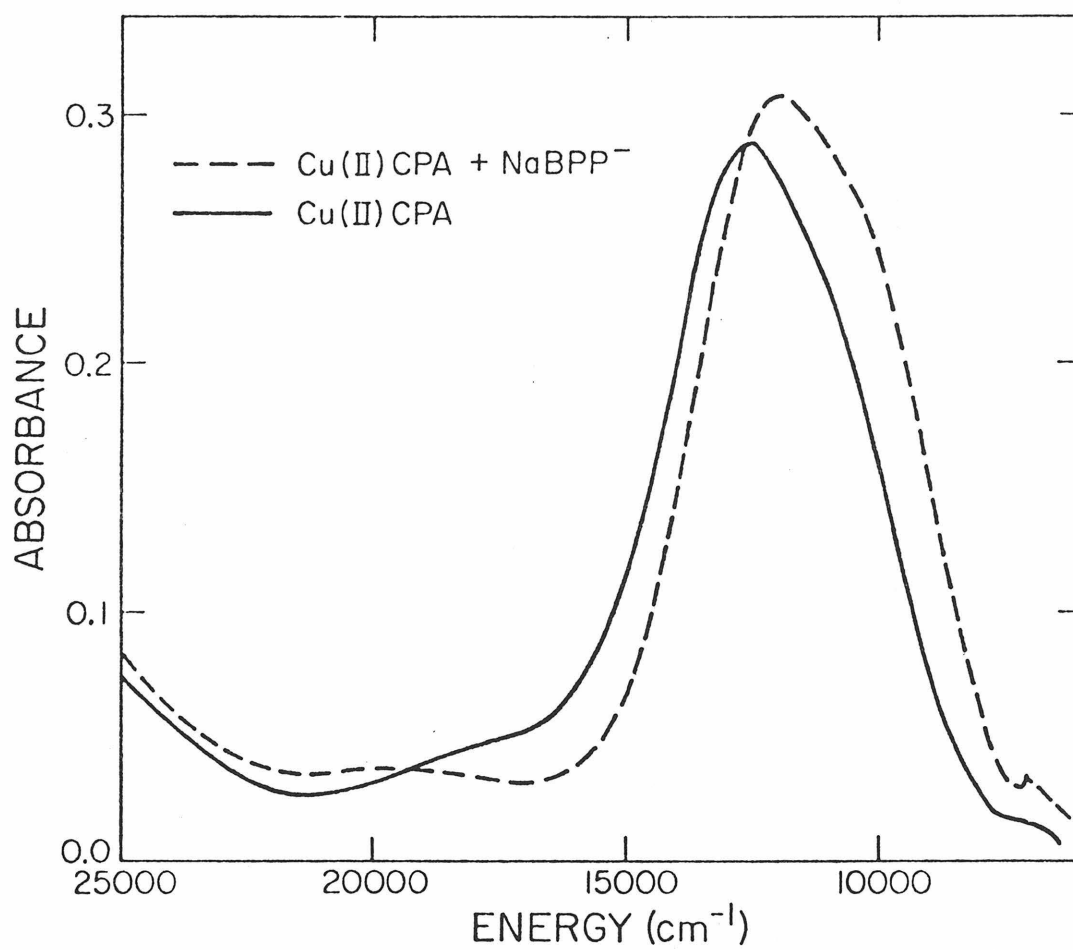


Figure Cu-V. The absorption spectra of Cu(II)CPA, $[\text{Cu}^{+2}] = 4.66 \times 10^{-4} \text{ M}$; and Cu(II)CPA + Na β PP, $[\text{Cu}^{+2}] = 4.25 \times 10^{-4}$, $[\text{Na}\beta\text{PP}] = 6.93 \times 10^{-3} \text{ M}$.

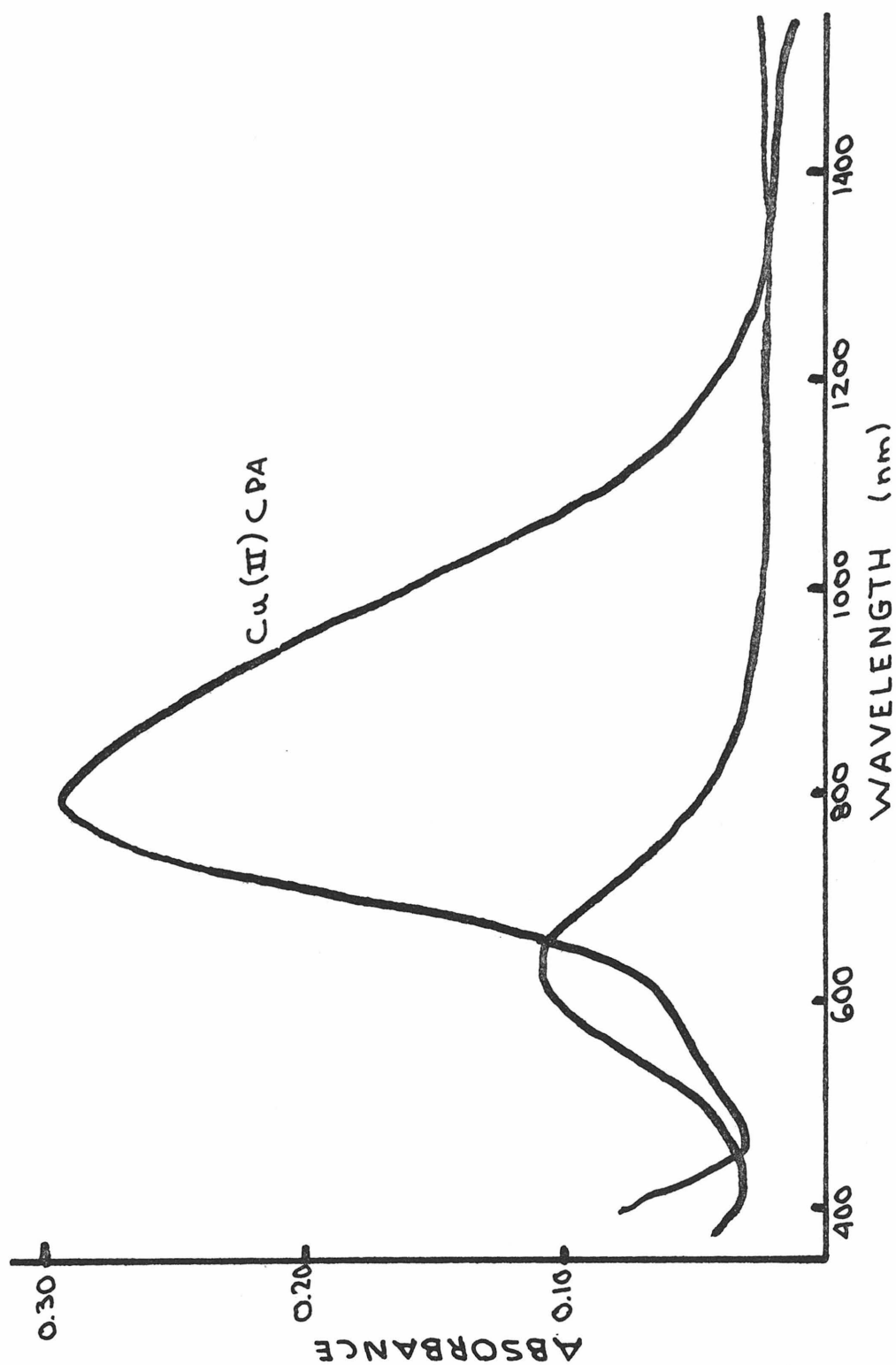


Figure Cu-VI. Absorption spectra of Cu(II)CPA and Cu^{+2} ions in Tris buffer.

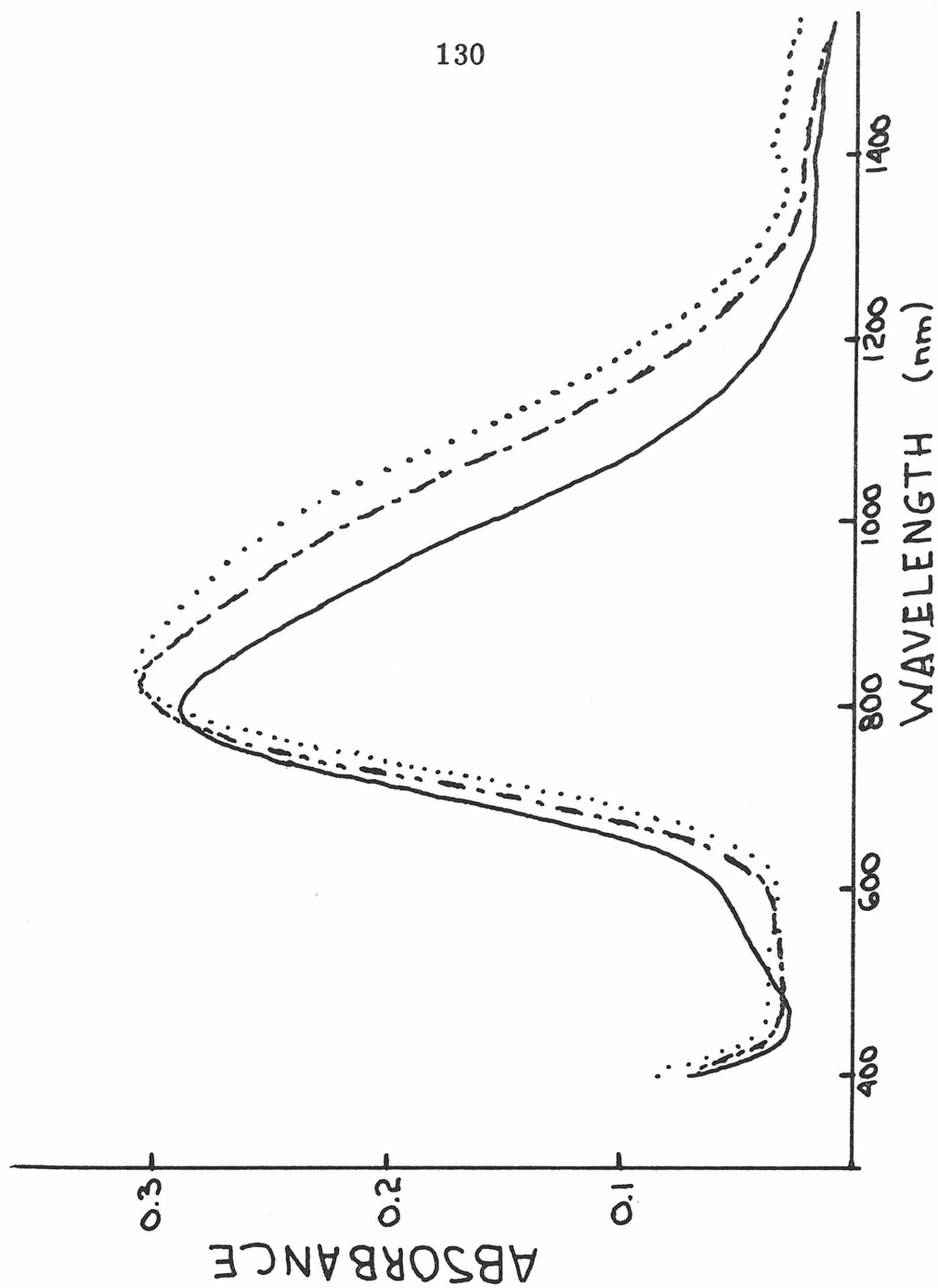


Figure Cu-VII. — Absorption spectrum of Cu(II)CPA; --- absorption spectrum of Cu(II)CPA + 8Naβ PP; absorption spectrum of Cu(II)CPA + 24Naβ PP.

residual water in the sodium β -phenylpropionate solution. A binding constant K_I for the reaction



can be extracted from the spectral data by the procedure of Furman and Garner²⁸ which has already been described. Under the conditions of this experiment approximately 87% of the cupric ion present in the solution is bound to the enzyme, based on the literature value of the binding constant of Cu^{+2} to CPA in the tris buffer ($\log K_B = 5.1$).¹ A correction for the amount of free cupric ion was included in the calculation. Plots of $\text{EI}/A_\lambda - pE\epsilon_{\text{CuCPA}}$ vs $(E + I)$ at several representative wavelengths are shown in Figure (Cu-VIII). The data points are reasonably linear. K_I was determined from the slope and intercept of the best least squares line through the points. The molar extinction coefficients of the $\text{Cu(II)-CPA} \cdot \text{BPP}$ complex were calculated from the slope and the observed values for Cu(II)-CPA . The values of K_I and $\epsilon_{\text{CuCPA} \cdot \text{BPP}}$ determined in this way for each wavelength are shown in Table (Cu-V). It is found that $K_I = 1.40 \times 10^{+2} \text{ M}^{-1}$ with a standard deviation of $0.24 \times 10^{+2}$ (approximately 15%). Such a standard deviation is reasonable for a binding constant determined by this method.

A closer examination of the calculated K_I values in Table (Cu-V) reveals a discontinuity between 750 nm and 770 nm. This discontinuity is most easily seen in Figure (Cu-IX) where $K_I(\text{calc})$ has been plotted

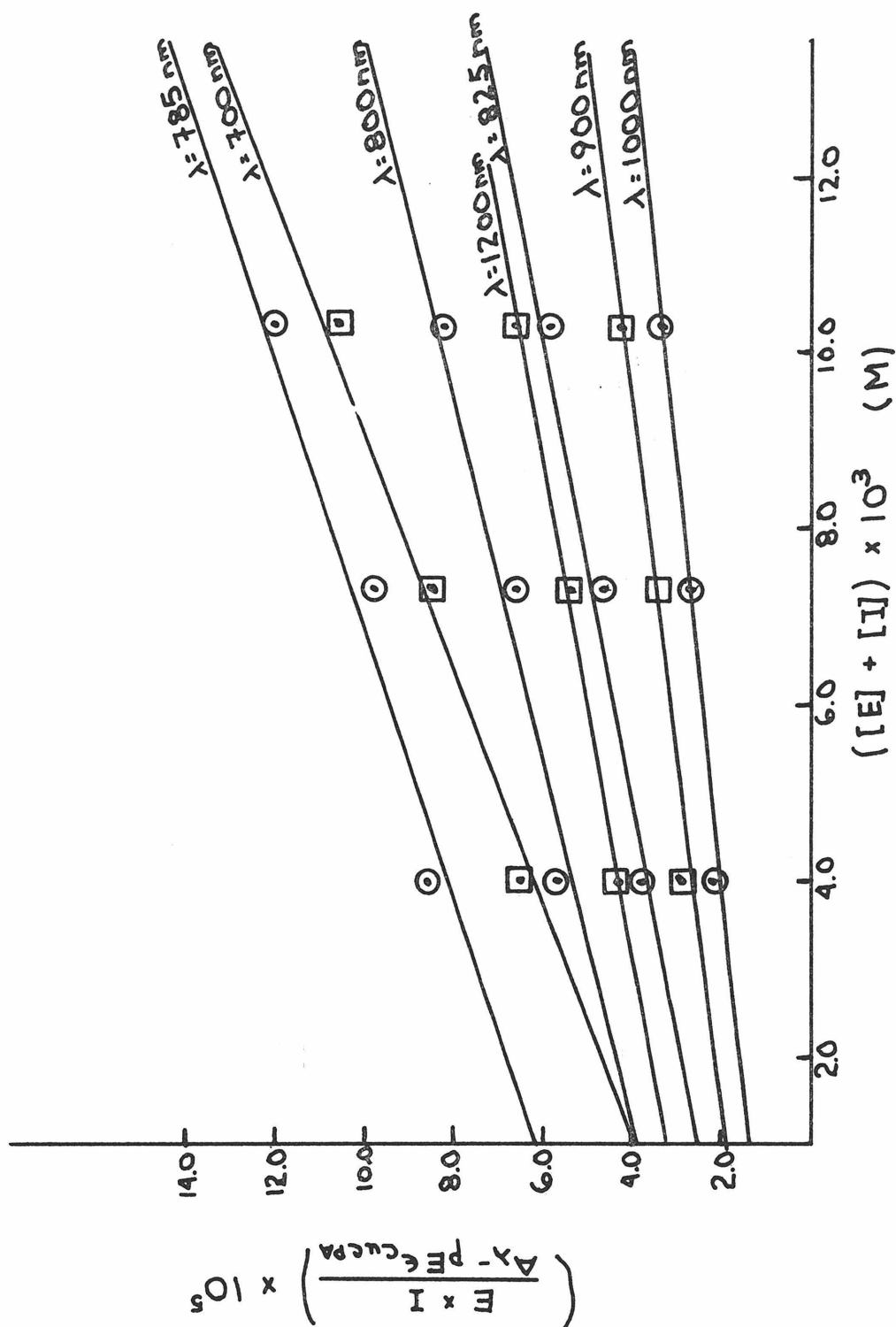


Figure Cu-VIII. Plots of $\frac{E \times I}{A_{\lambda} - pE\epsilon_{\text{Cu(II)CPA}}}$ vs. $E + I$ for the reaction of Cu(II)CPA with $\text{Na}\beta\text{PP}$.

Table Cu-V

λ	$K_I \times 10^{-2} (M^{-1})$	ϵ_M
700	1.71	55
725	2.24	90
740	2.16	113
745	3.11	118
750	5.47	95
770	.61	160
785	.90	178
800	1.08	191
825	1.27	203
850	1.24	209
875	1.19	210
900	1.15	208
925	1.19	203
950	1.23	200
975	1.27	195
1000	1.29	184
1025	1.50	172
1050	1.60	156
1075	1.63	141
1100	1.71	123
1125	1.74	108
1150	1.62	95

Table Cu-V (Continued)

<u>λ</u>	<u>$K_I \times 10^{-2} (M^{-1})$</u>	<u>ϵ_M</u>
1175	1.46	83
1200	1.36	73
1225	1.29	61
1250	1.14	53

$$K_I = (1.40 \pm 0.21) \times 10^2 \text{ M}^{-1}$$

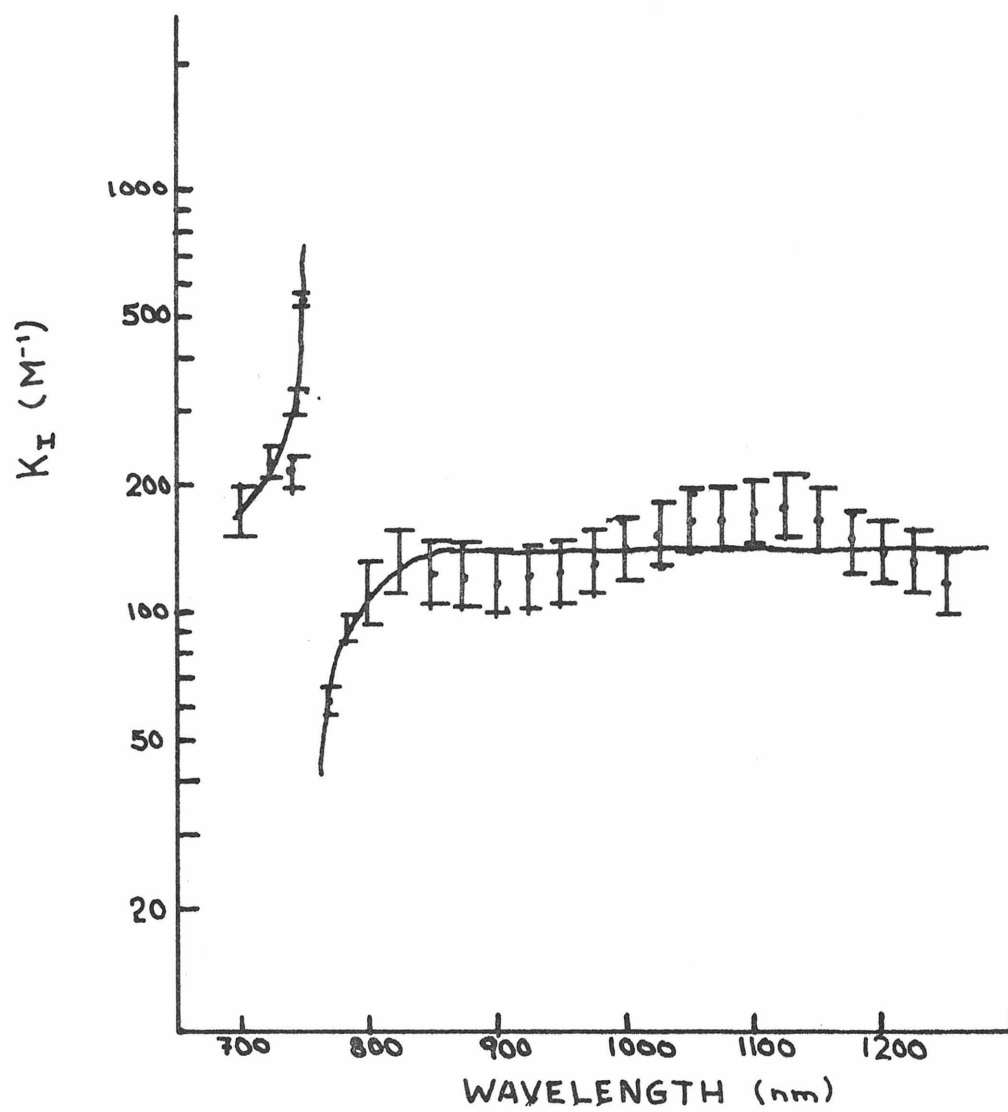


Figure Cu-IX.

as a function of wavelength on a semilog scale. The discontinuity indicates that there is an isobestic point somewhere in the region between 750 nm and 770 nm. The existence of this isobestic point confirms the original assumption that only two spectrally detectable species are involved in the equilibrium, e.g. Cu(II)-CPA and its complex with β -phenylpropionate.

In absolute terms, the K_I for sodium β -phenylpropionate is relatively small for a substance that acts as an inhibitor of other M(II)CPA's. A simple equilibrium calculation reveals that under the particular experimental conditions employed in obtaining the data in Figure (Cu-V) only 59% of the Cu(II)-CPA has BPP bound to it. Thus, it would be nice to have some idea of what the spectrum of the enzyme inhibitor complex looks like in the absence of what might be called contamination by uncomplexed Cu(II)-CPA. The calculated values of the molar extinction coefficients of the Cu(II)-CPA - BPP complex listed in Table (Cu-V) are plotted in Figure (Cu-X) along with the data for Cu(II)-CPA. The spectrum of Cu(II)-CPA \cdot BPP shown in the figure should be considered more schematic than exact and believed only insofar as perceptible trends in the data shown in Figure (Cu-VII) are manifested. It is clear that the band maximum shifts to lower energy, from 795 nm to somewhere in the neighborhood of 860 nm, when BPP binds. In wave numbers, this represents a shift of roughly 1000 cm^{-1} , which is significant. The shoulder on the low energy side of the envelope is also much more pronounced, and the overall intensity of the envelope has noticeably increased in the enzyme-inhibitor complex.

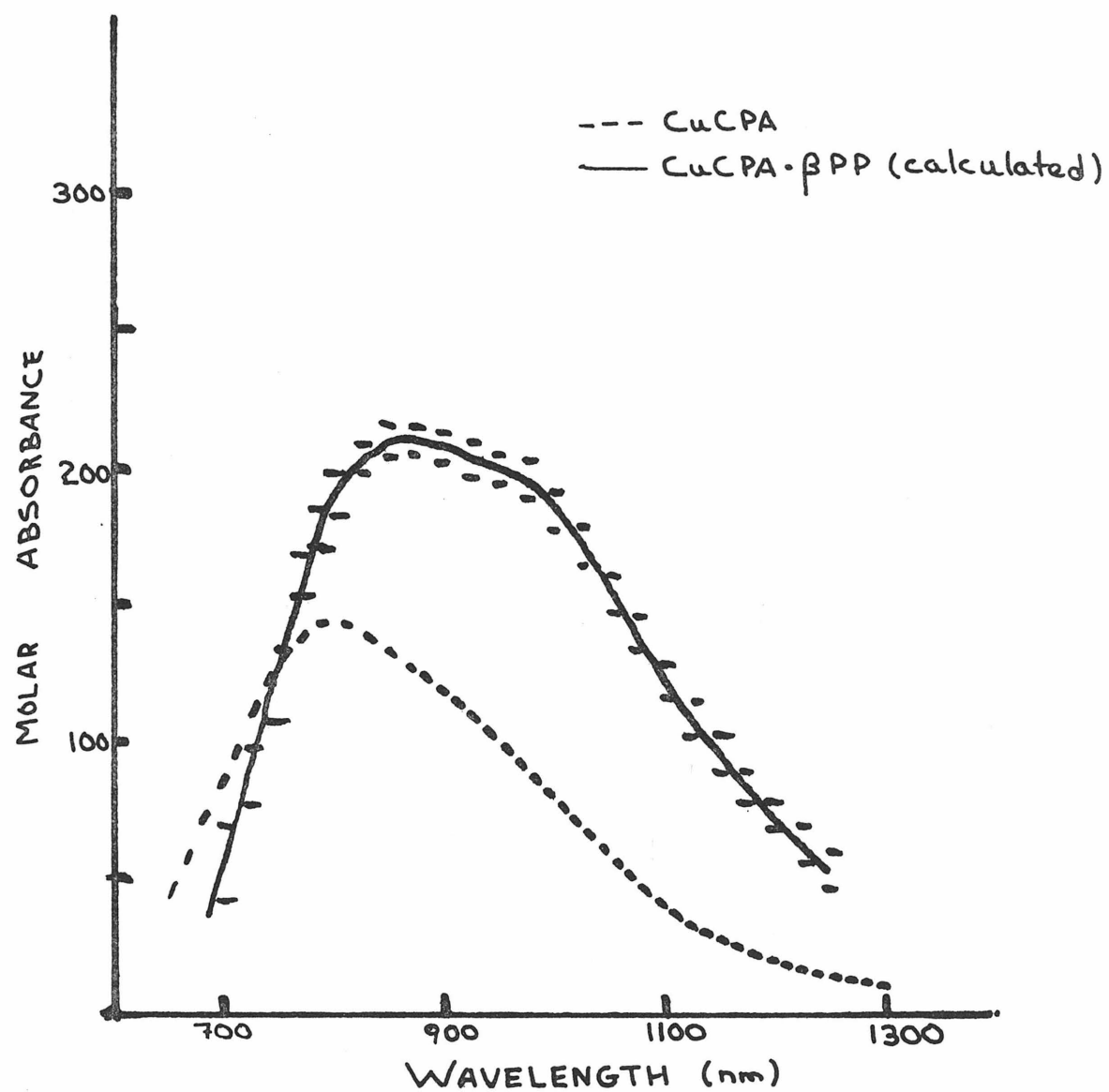


Figure Cu-X. Spectrum of Cu(II)CPA and calculated spectrum of the Cu(II)CPA· β PP complex.

The observed spectrum of Cu(II)-CPA is very similar to that of Cu(II)-CA which in the high pH form has an absorption maximum around $13,900\text{ cm}^{-1}$ with a molar extinction coefficient of at least 110, as well as a prominent low energy shoulder around $11,000\text{ cm}^{-1}$.⁵ Considering the similarities in the observed EPR parameters of these two copper derivatives, this result is not surprising. Assuming that the coordination geometry about the copper atom is similar in both CPA and CA, the blue shift of the spectrum of Cu(II)-CA relative to that of Cu(II)-CPA can be understood in terms of a stronger ligand field environment in the case of CA. As we have seen, the donor set in native CA is roughly N_3O whereas in CPA it is N_2O_2 .

As may well be expected, the position and to some degree the intensities of the absorption bands of copper(II) complexes depend on the nature of the environment created by the ligands. Taking the square planar geometry as a central reference point in our survey, let us see how changes in ligand type as well as geometry affect the spectra of monomeric copper(II) complexes. The relevant geometrical aspects of this approach are shown in Figure (Cu-XI). Complexes with a trigonal bipyramidal structure will be considered separately.

Only complexes having ligands with predominantly nitrogen or oxygen donors are considered in what follows, since only these donors are available in the proteins under consideration. For what we have called the tetragonal branch, the rather extensive series of copper(II) ammonia complexes provides an excellent model system. The

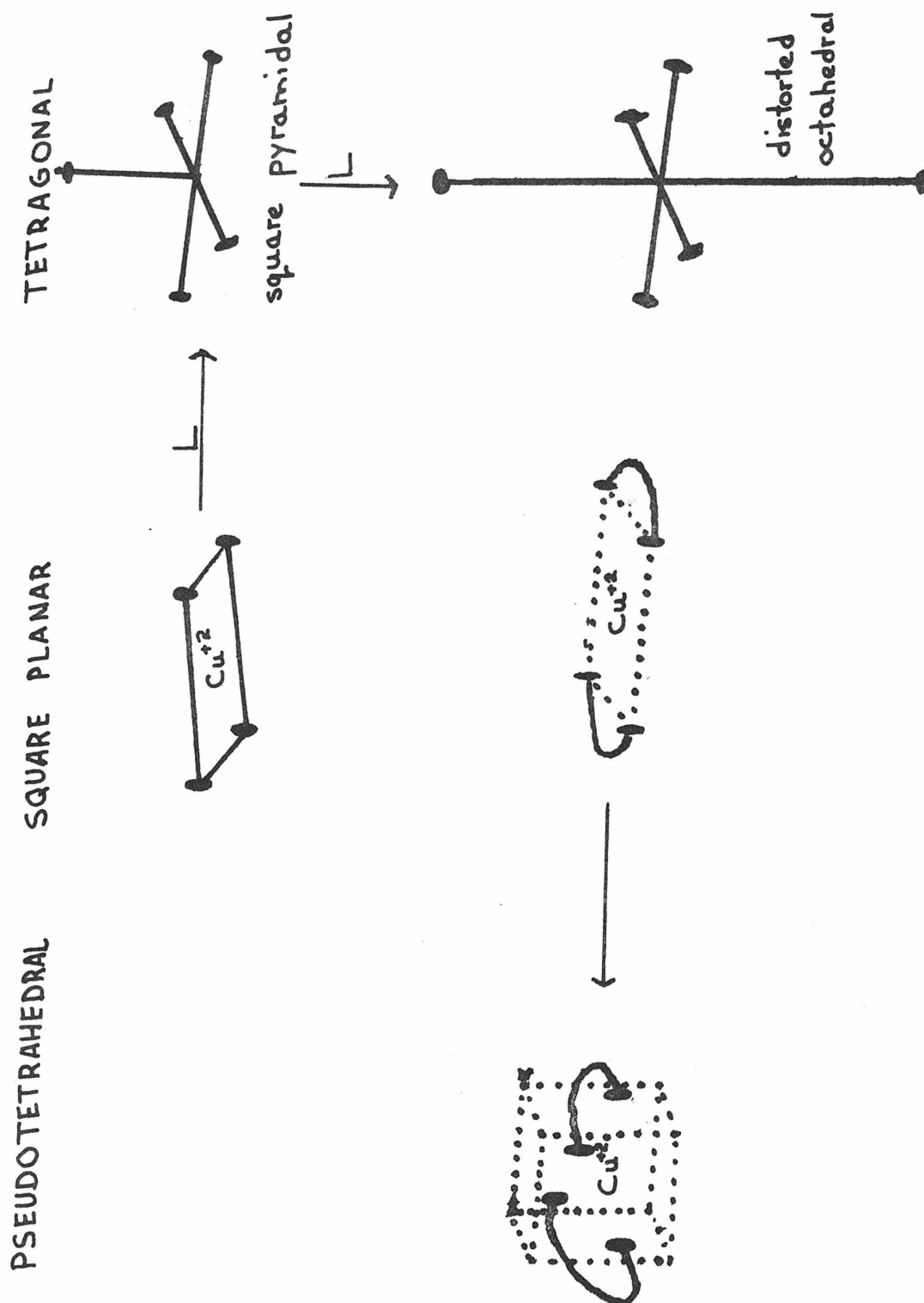


Figure Cu-XI.

properties of these complexes have been recently reviewed by Hathaway and co-workers.^{29, 30} The pseudo-tetrahedral branch is best exemplified by several series of bis chelate complexes that have been reviewed by Holm.¹³

Square planar copper(II) complexes with nitrogen and/or oxygen donor ligands have their absorption maxima in the region 14,000-20,000 cm^{-1} . Examples from the various series we will be discussing are shown in Table (Cu-VI). The relative energy of the absorption maximum correlates well with the position of the donor set in the spectrochemical series. The complexes with nitrogen ligands absorb at higher energy than the complexes with oxygen ligands.

As additional ligands are added axially, giving first a square pyramidal and then a tetragonally elongated octahedral structure, the observed band maxima move to lower energy. In the cupric ammine series, for example, $\text{Na}_4\text{Cu}(\text{NH}_3)_4[\text{Cu}(\text{S}_2\text{O}_3)_2]_2 \cdot \text{H}_2\text{O}$, which is believed to contain essentially isolated $\text{Cu}(\text{NH}_3)_4$ units, has its absorption maxima at 19,200 cm^{-1} .³¹ The mono ammine adduct $\text{Na}_4\text{Cu}(\text{NH}_3)_4-[\text{Cu}(\text{S}_2\text{O}_3)_2]_2 \cdot \text{NH}_3$, which contains the $\text{Cu}(\text{NH}_3)_5^{+2}$ (square pyramidal) unit, has its absorption maximum shifted to 17,700 cm^{-1} . Concurrently, a low energy shoulder near 13,200 cm^{-1} appears. There also is an overall increase in the intensity of the absorption envelope upon coordination of an additional ammonia. This shift to lower energy and concomitant increase in intensity has been called the "pentaamine effect." The pentaammine effect was first observed in aqueous solution

Table Cu-VI

Complex	Donor Set	Absorption Max	ϵ_M	Ref.
$\text{Na}_4\text{Cu}(\text{NH}_3)_4\{\text{Cu}(\text{S}_2\text{O}_3)_2\}_2\text{H}_2\text{O}$	N_4	19,200	--	a
$[\text{Cu}(\text{en})_2](\text{BF}_4)_2$	N_4	19,400	--	b
$\text{Cu}(\text{H-pa})_2$	$(\text{NN})_2$	19,600	~ 75	c
$\text{Cu}(\text{N-nPrSal})_2$	$(\text{NO})_2$	16,600	~ 30	d
$\text{Cu}(\text{H-PhHMe})_2$	$(\text{NO})_2$	17,500	74	e
$[\text{n-C}_3\text{H}_7)_4\text{N}]_2\text{Cu}(\text{Cat})_2$	$(\text{OO})_2$	$\sim 15,000$	--	f
$\text{Cu}(\text{facfac})_2$	$(\text{OO})_2$	13,500	40	g

^a Reference 31.

^b Reference 32.

^c Reference 33, pa = pyrrolle-2-aldimino

^d N-n-PrSal = N-n-propyl-salicylideneaminato

^e Reference 34, H-PhHMe = $\text{C}_6\text{H}_5-\overset{\text{O}}{\parallel}\text{C}-\text{CH}-\overset{\text{NH}}{\parallel}\text{C}-\text{CH}_3$ (β -ketimino)

^f Reference 35, cat = pyrocatecholate.

^g References 36 and 37, facfac = $\text{CF}_3-\overset{\text{O}}{\parallel}\text{C}-\text{CH}-\overset{\text{O}}{\parallel}\text{C}-\text{CF}_3$ (β -diketone)

on addition of ammonia to solutions containing $\text{Cu}(\text{NH}_3)_4(\text{H}_2\text{O})_2^{+2}$.³⁸ A molar extinction coefficient of about $80 \text{ (M}^{-1}\text{cm}^{-1})$ was found for the 'pentaammine species in this case. Another example is the copper(II) bis ethylenediamine system.^{32, 39} Whereas $[\text{Cu}(\text{en})_2](\text{BF}_4)_2$ has a maximum at $19,400 \text{ cm}^{-1}$, in $[\text{Cu}(\text{en})_2\text{NH}_3](\text{BF}_4)_2$ the maximum has been shifted to $17,400 \text{ cm}^{-1}$ and there is a strong shoulder at $\sim 11,000 \text{ cm}^{-1}$. Also, the intensity increases by roughly 30-40%.

A similar but somewhat smaller effect is also observed with some of the bis chelate systems listed in Table (Cu-VI). In strongly donating solvents such as pyridine, red shifts and some intensity enhancement have been found for the acetylacetone system.⁴⁰ The differences in the spectrum of $\text{Cu}(\text{N-n-PrSal})_2$ in chloroform and pyridine are illustrated in Figure (Cu-XII). In pyridine, the absorption maximum is shifted slightly to the red, from $16,600 \text{ cm}^{-1}$ to $16,000 \text{ cm}^{-1}$ and there is a noticeable low-energy shoulder. The intensity is also somewhat enhanced in pyridine solution although this effect is obscured by the tail of a charge transfer band that runs through the region of interest.

The band shifts of the pentaammine effect on these systems have been interpreted in terms of a decreased tetragonal distortion along the z axis as additional ligands are introduced. This approach is illustrated in the energy level diagrams in Figure (Cu-XIII).

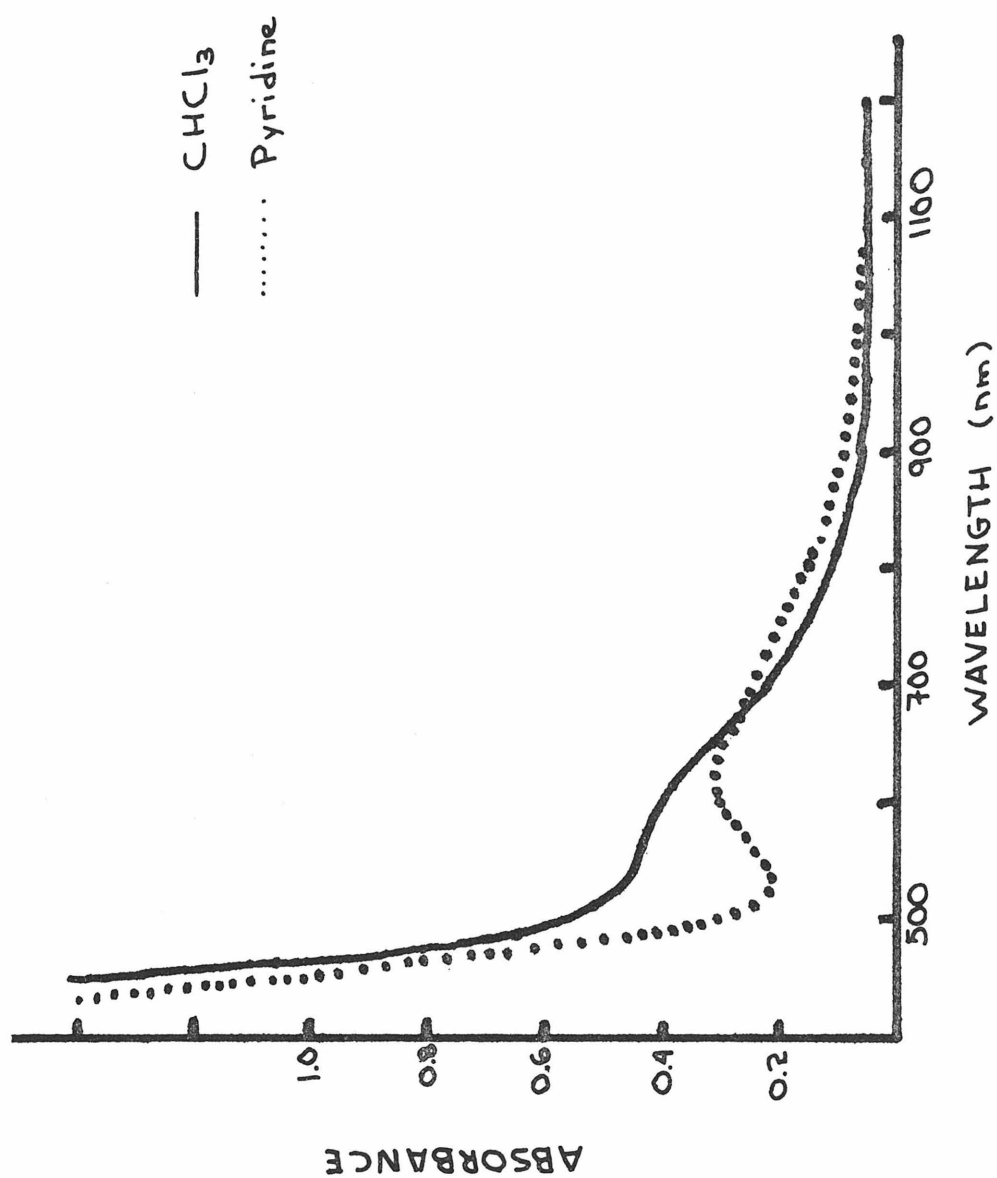


Figure Cu-XII. Absorption spectrum of bis(N-n-propylsalicylideneaminato)copper(II) in CHCl_3 and pyridine.

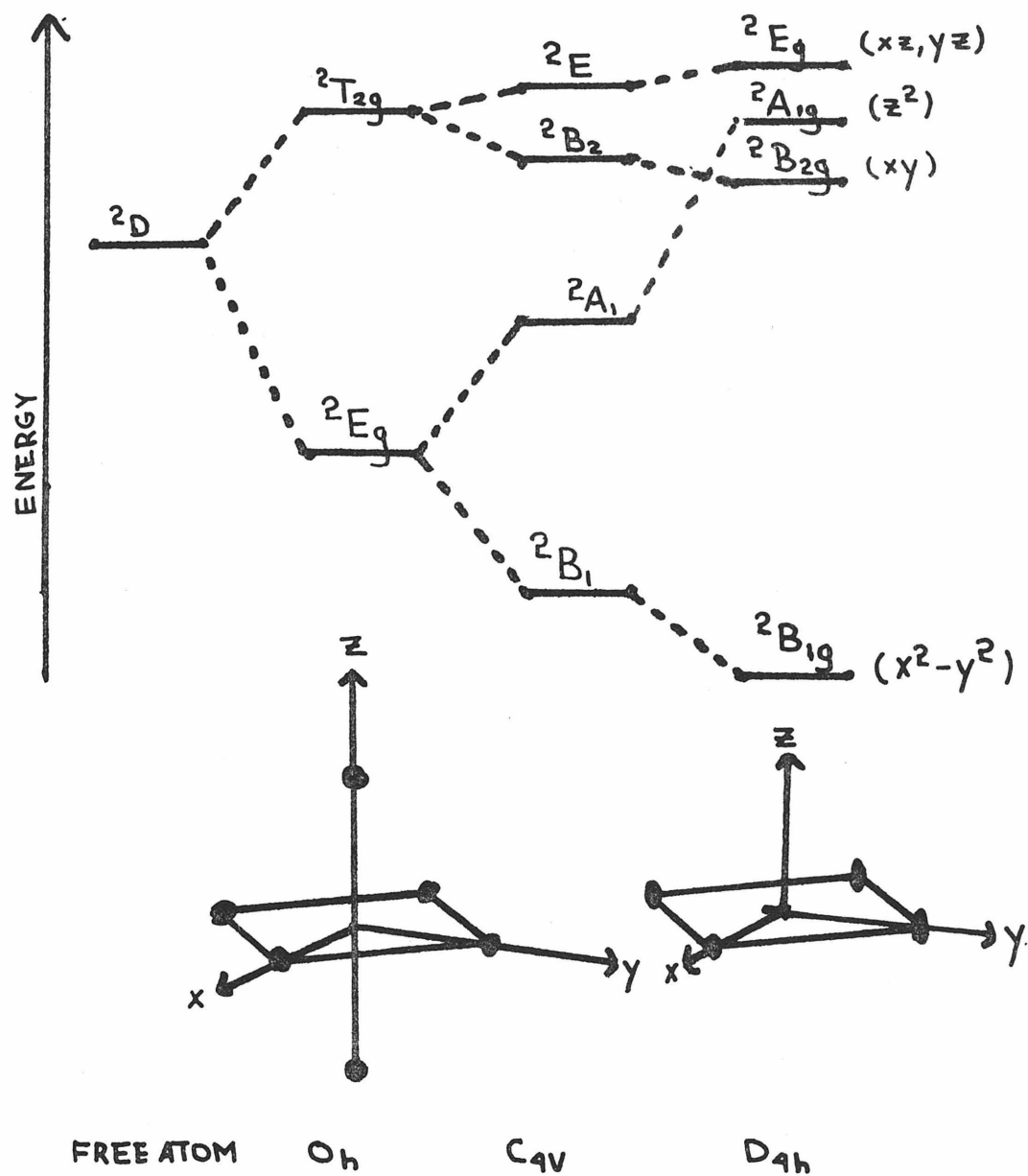
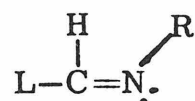


Figure Cu-XIII. Energy level diagram for copper(II) in octahedral (O_h), square pyramidal (C_{4v}), and square planar (D_{4h}) ligand fields.

When a fifth ligand is added along the axis (z) perpendicular to the plane of the original four ligands in a square planar complex, the energy of the ${}^2A_{1g}$ state is significantly lowered. Because of the center of gravity rule, the absolute energy of the ground state (${}^2B_{1g}$) will be accordingly raised, since both of these states are derived from the 2E_g state in octahedral symmetry. To a first approximation, the energies of the other states will not be changed. The net result is a decrease in the energy separation between the ground and excited states and thus a red shift in the observed spectra. If a sixth ligand is then added, a further red shift in the absorption envelope is expected by the same line of reasoning. In general, then, one should expect a red shift in the observed spectrum when a weakly bound axial ligand is replaced by another ligand that is higher up in the spectrochemical series.

A reduction in symmetry, particularly the loss of an inversion center, is frequently invoked in order to explain the enhanced intensity associated with the pentammine effect. This same explanation is also used to explain the intensity enhancement observed in what might be called the pseudo-tetrahedral effect, which we will now discuss.

The chelating ligands containing nitrogen or mixed nitrogen and oxygen donors cited in Table (Cu-VI) are basically substituted imines of the form



where L represents the other nitrogen or oxygen containing part and R is an aliphatic or aromatic hydrocarbon. As the imine nitrogen substituent R is varied over a range of normal, iso, and tertiary alkanes, changes in the structure and spectral properties of these complexes have been found. The available structural and spectral data are shown in Table (Cu-VII). θ is the dihedral angle between the planes formed by the copper atom and the donor atoms of each chelating ligand in these bis complexes. As we mentioned earlier in the section on EPR, for a square planar structure $\theta = 0^\circ$ while for a tetrahedral or squashed tetrahedral (D_{2d} symmetry) $\theta = 90^\circ$. The data indicate that the degree of distortion from planarity is determined by steric factors, e.g., the bulkiness of the imine substituent. In each case there is a red shift of $3000\text{--}4000\text{ cm}^{-1}$ as θ varies from 0° to approximately 60° . A slight but noticeable increase in band intensity is correlated with the red shift of the absorption envelope. An energy level diagram illustrating the origin of the observed red shifts is shown in Figure (Cu-XIV).

These changes in the bis salicylideneaminato series are illustrated in Figure (Cu-XV). The molar extinction coefficients of this series are particularly hard to evaluate since the band in question is superimposed on the tail of a relatively strong charge transfer absorption which obscures its high energy side. It should also be noted that there is some inconsistency between the solution and solid state results in this system. The trends in both the band positions and dipole moments measured in solution as well as the EPR results in frozen

Table Cu-VII

Absorption Spectra of Pseudo Tetrahedral Cu(II) Chelates

<u>Complex</u>	<u>Donors</u>	<u>ν_{\max}</u>	<u>ϵ</u>	<u>μ_D</u>	<u>θ</u>	<u>Ref.</u>
Cu(H-pa) ₂	(NN) ₂	19,600	~ 75		0	a
Cu(n-Bupa) ₂		18,940	~ 110		-	b
Cu(i-Pr-pa) ₂		18,600	~ 110		-	b
Cu(t-Bupa) ₂		15,000	~ 160		~ 60	b, c
Cu(H-PhHMe) ₂	(NO) ₂	17,500	~ 75		0	d
Cu(CH ₃ -PhHMe) ₂		16,000	~ 95		-	d
Cu(iPr-PhHMe) ₂		13,800	~ 110		-	d
Cu(N-nPrSal) ₂	(NO) ₂	16,600 ⁱ	~ 30 ⁱ	1.77	0	e, m
Cu(N-nBuSal) ₂		15,750 ⁱ	~ 25 ⁱ	1.86	0	e
Cu(salN- ϕ - ϕ -N-Sal)		14,900 ⁱ	~ 110 ⁱ	--	37	f
Cu(N-i-PrSal) ₂		14,700 ⁱ	~ 40 ⁱ	2.72	60	e, g
Cu(N-PhSal) ₂		14,100 ⁱ	~ 45 ⁱ	2.77	0	h
Cu(N-t-BuSal) ₂		12,900 ⁱ	~ 90 ⁱ	3.38	54	e, j
Cu(DPM) ₂	(NN) ₂	11,700	325		68	k
		10,300	210			
Cu(o-phen)Cl ₂	N ₂ Cl ₂	13,800	--		79	l
		11,630	--			

^a Reference 33.^b Reference 41.^c Reference 13.^d Reference 34.^e References 42 and 18.^f Reference 20.^g Reference 21.^h Reference 19.

Table Cu-VII (Continued)

ⁱ This work.

^j Reference 22.

^k References 43 and 44, DPM = Dipyrromethene.

^l Reference 26.

^m Reference 18.

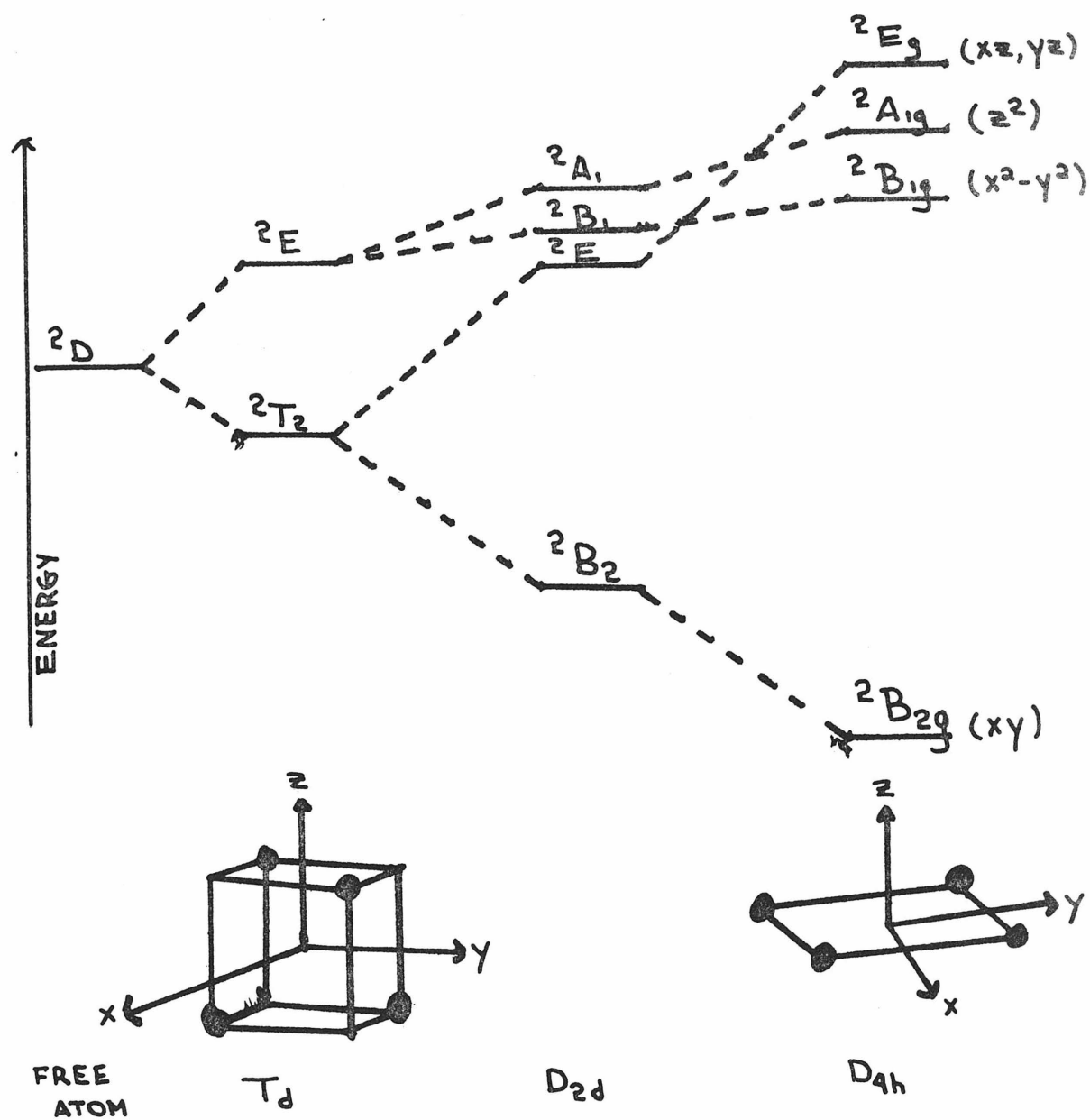


Figure Cu-XIV. Energy level diagram for copper(II) in tetrahedral (T_d), pseudo-tetrahedral (D_{2d}), and square planar (D_{4h}) ligand fields.

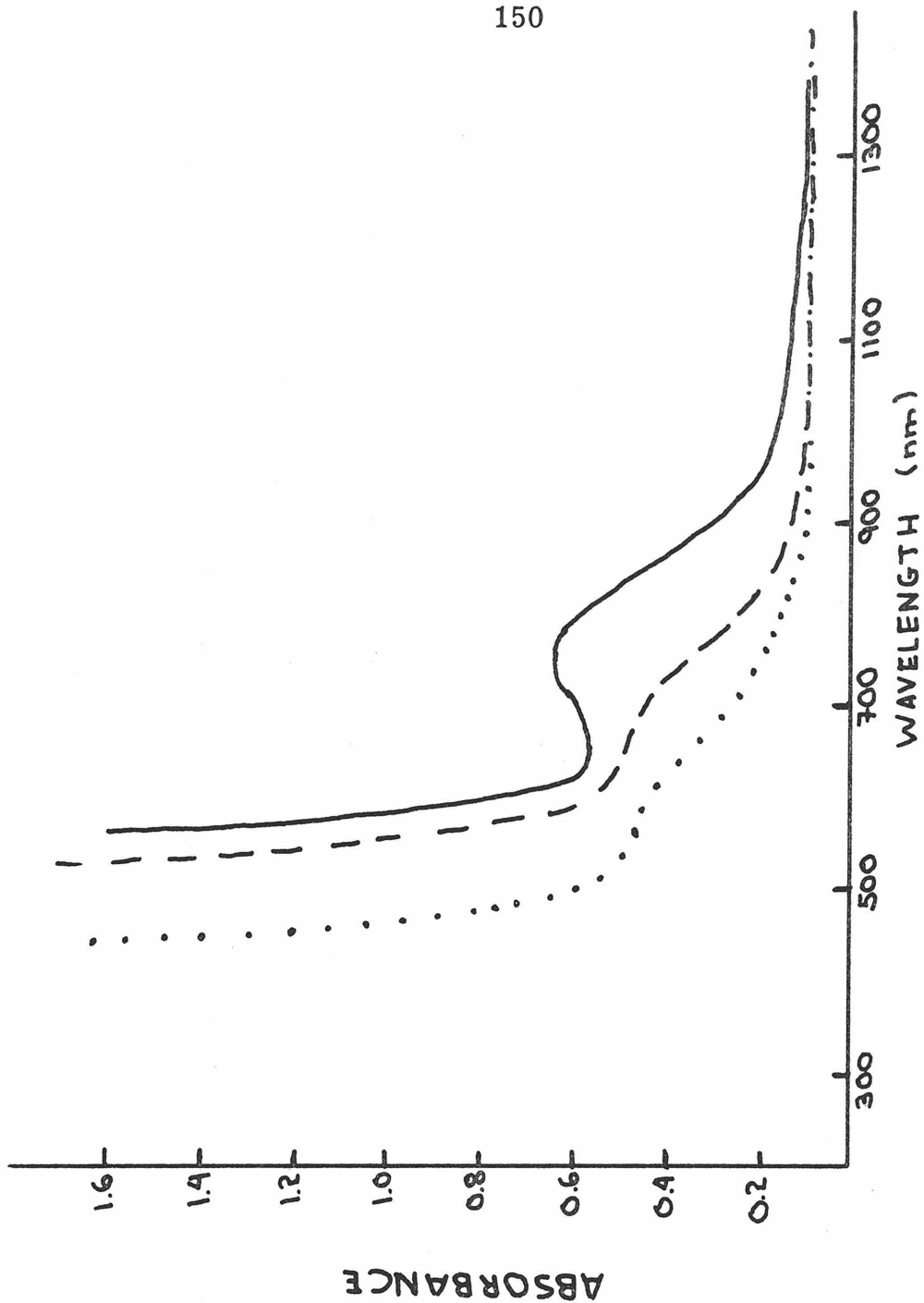


Figure Cu-XV. Absorption spectra in CHCl_3 of
 bis(N-t-butyl-salicylideneaminato)copper(II), — ;
 bis(N-i-propylsalicylideneaminato)copper(II) and
 bis(N-phenylsalicylideneaminato)copper(II), - - - ;
 and bis(N-n-propylsalicylideneaminato)copper(II),

solution indicate the order of the effect is $n\text{-Br} \sim n\text{-Bu} < \text{biPh} < i\text{-Pr} \lesssim \text{Ph} < t\text{-Bu}$. Of these compounds the bi-phenyl derivative has an anomalously high extinction coefficient, which may occur because it alone of the members of the series derives from a cis-planar structure. All the others can be viewed as having structures distorted from a trans-planar array. The single crystal X-ray work gives $n\text{-Pr} \sim n\text{-Bu} \sim \text{Ph} < \text{bi-Ph} < t\text{-Bu} \lesssim i\text{Pr}$ as the order of increasing distortion from planarity. It should be noted that even the complexes with $\theta = 0^\circ$ are not strictly planar. Rather they have a stepped planar structure in which the salicylaldimine ligands lie in parallel planes. The solid state reflectance spectra of these complexes, shown in Figure (Cu-XVI), are consistent with the trends found in the X-ray work. The planar compounds all have similar spectra, as do the $i\text{-Pr}$ and $t\text{-Bu}$ derivatives. The bi-Phenyl derivative has a spectrum that is roughly intermediate, showing the broad band in the near IR but not the much more intense band at around 500 nm. That appears in the spectra of both the $N\text{-}i\text{-Pr}$ and $N\text{-}t\text{-Bu}$ derivatives. In solution the spectra of the $N\text{-}i\text{-Pr}$ and $N\text{-}t\text{-Bu}$ derivatives are not very similar, which is not what one would have expected on the basis of their solid state properties. The spectrum of the $N\text{-}t\text{-Bu}$ is essentially unchanged from what it is in the solid state. The prominent band at around 480 nm in the $N\text{-}t\text{-Bu}$ complex is reduced to a very weak shoulder in the $N\text{-}i\text{-Pr}$ substituted species. Further, as the data in Table (Cu-IV) show, the $N\text{-}i\text{-Pr}$ complex most closely resembles the $N\text{-Ph}$ complex in solution. But, as we have seen, the $N\text{-Ph}$ complex is planar in the solid state and its solution and solid state spectra are very similar.

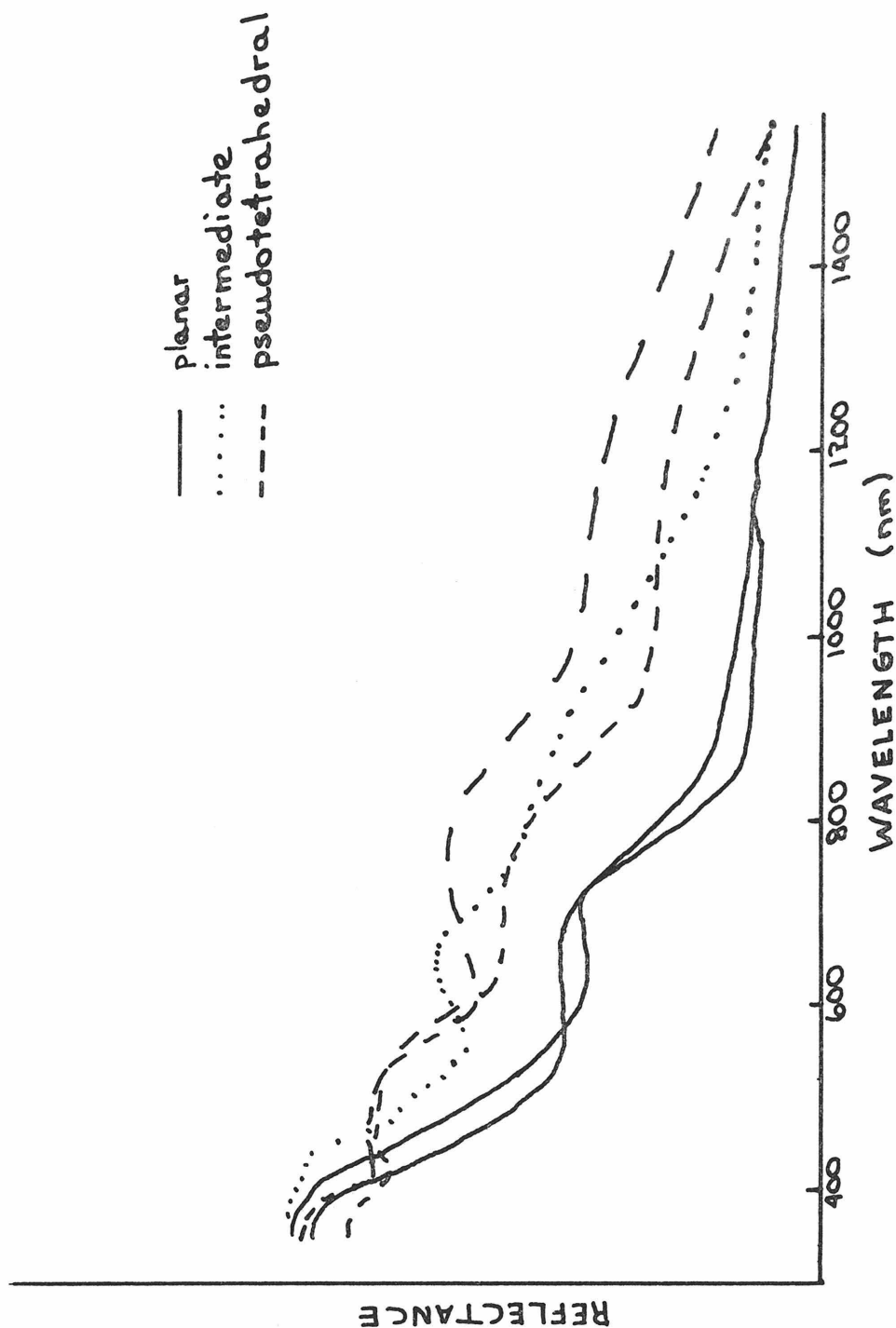


Figure Cu-XVI. Solid state reflectance spectra of bis(N-R-salicylideneaminato)copper(II) complexes.

R = n-propyl, phenyl, —; R = biphenyl,;

R = i-propyl, t-butyl, ----.

Two explanations of the discrepancies between the solid and solution state properties of some of these complexes have been postulated. The Russian group has argued that there is a planar \rightleftharpoons tetrahedral equilibrium and that the solution properties, particularly the dipole moment, reflect the position of the equilibrium in each case.¹³ The other explanation, favored by Sacconi and co-workers,⁴² is that only one species is present in solution in each case. The frozen glass EPR spectra support the latter explanation since they are relatively sharp and contain only four lines in the g_{\parallel} region. If two species having considerably different values of g_{\parallel} and especially A_{\parallel} were present, a much broader and less distinct spectrum would be expected in this region.

Although the details of the bis-salicylideneaminato Cu(II) series are somewhat unclear, especially the anomalous solution dipole moment and spectra of the N-phenyl derivative, the overall trend towards a lower energy, more intense absorption maximum with increasing pseudo-tetrahedral distortion from planarity is clear especially if only the N-n-pr, N-n-Bu, and N-t-Bu complexes are considered. The N-t-Bu derivative, in particular, is an excellent model for both the spectral and EPR properties of Cu(II)-CPA.

The above trend in the spectra is particularly clear in the cupric dipyrromethene complex in which the absorption maxima are shifted quite far out into the near infrared, even though the system involves four nitrogen donors. A prominent low energy side shoulder is also observed.⁴⁴ A similar pattern is observed for Cu(o-phen)Cl₂ doped into a single crystal of Zn(o-phen)Cl₂.²⁶

There is little detailed data in the literature on the spectra of copper(II) in a trigonal bipyramidal environment. The available data are summarized in Table (Cu-VIII). The absorption maxima in trigonal bipyramidal complexes occur at rather low energies, roughly between 12-13 kK. The most noticeable and distinguishing feature of these spectra, however, is the large molar extinction coefficients of the envelopes, usually of the order of several hundred.

Discussion

In the EPR section we tentatively concluded that trigonal bipyramidal coordination was not consistent with the value of $g_{||}$ observed for Cu(II)-CPA. The optical spectrum of Cu-CPA is also quite different than those observed for model copper(II) complexes having that coordination geometry. Although the band positions are roughly comparable, the molar extinction coefficients observed in model trigonal bipyramidal cupric complexes are substantially higher than the value we found for Cu(II)-CPA and the known value for Cu(II)-CA. The concurrence of the EPR and optical spectral findings, therefore, permits us to eliminate trigonal bipyramidal coordination as a possibility in these systems.

The next possibility we shall consider is square planar coordination. The g values and nuclear hyperfine coupling constants found for Cu(II)-CPA and Cu(II)-CA occur at the interface between values observable for copper(II) in tetragonal and pseudo-tetrahedral environments, as is shown in Figure (Cu-III). The spectra of the square planar models, summarized in Table (Cu-VI), have absorption

Table Cu-VIIISpectral Data for Trigonal Bipyramidal Copper(II) Complexes

<u>Complex</u>	<u>Donor Set</u>	<u>Spectra</u>	<u>Ref.</u>
$\text{Cu}(\text{NH}_3)_2\text{Ag}(\text{CN})_3$	N_5	12,800 (~ 500) 14,500 (sh)	a
$[\text{Cu}(\text{tren})\text{NCS}]\text{SCN}$	N_5	11,900 (~ 700) 14,700 (sh)	a
$[\text{Cu}(\text{bipy})_2\text{I}]\text{I}$	N_4I	12,500 (~900)	b
$\text{Cu}(\text{Et}_4\text{dien})(\text{N}_3)_2$	N_5	13,170 (308)	c
$\text{Cu}(\text{Me}_5\text{dien})(\text{Cl})_2$	N_3Cl_2	13,100 (260)	d

^a Reference 46.

^b Reference 47.

^c Reference 48.

^d Reference 49.

maxima at much higher energies than are observed in either Cu(II)-CPA or Cu(II)-CA. Even the complexes having only oxygen donors have their maxima at higher energies, which is significant. All of the donor ligands in CPA (two imidazole nitrogens, carboxylate, and water) are higher in the spectrochemical series than either facfac(hexafluoroacetylacetonate) or catecholate. Thus, if the cupric ion is in a square planar site, we would expect its absorption maxima to fall somewhere around $16,000\text{ cm}^{-1}$, but certainly well above $14,500\text{ cm}^{-1}$, on the basis of the model system data. The fact that the absorption maxima for both Cu(II)-CPA and Cu(II)-CA occur at considerably lower energy allows us to rule out square planar geometry as well.

We are left then with three possible coordination geometries for the cupric ion: pseudotetrahedral, square pyramidal, and distorted octahedral. All are consistent with the observed band position and intensity. The EPR results lead us to a preference for a pseudotetrahedral environment. Based on the model bis chelate systems data we may conclude that the extent of the distortion from planarity is significant. In terms of the angle θ , a value in the range of 30° - 50° might be reasonable. Of course, this parameter probably has no real significance in a system that is perhaps better described as involving four monodentate ligands.

Finally, let us consider spectrum of the Cu(II)-CPA · BPP complex. The substantial increase in intensity over that of uncomplexed Cu(II)-CPA cannot be explained by a ligand exchange alone (e.g., carboxylate for water). Only the red shift can be explained by such a mechanism since carboxylate is below water in the spectrochemical

series. In order to explain the increase in intensity, we must invoke a structural change of some sort. The red shift in the spectrum coupled with an increase in band intensity are extremely reminiscent of the "pentaammine effect." One possibility, then, is coordination expansion to a distorted square pyramidal structure about the copper atom. Another is that the interaction of the inhibitor with groups in the active site region induces a more pseudo-tetrahedral like arrangement of the other ligands. In other words, ligand substitution is accompanied by a small structural distortion. Perhaps an EPR study of the Cu(II)-CPA β PP complex could resolve this uncertainty.

APPENDIX

Preparation of N-alkyl(aryl)salicylideneaminato copper(II) complexes: The following complexes were prepared by the literature method.⁴² They were recrystallized from chloroform-ethanol solution and air dried.

$\text{Cu}(\text{N-nPrSal})_2$	mp 126 °C	literature value 127-128 °C
$\text{Cu}(\text{N-nBuSal})_2$	mp 79.5-80 °C	
$\text{Cu}(\text{N-iPrSal})_2$	mp 141.5-142 °C	literature value 143 °C
$\text{Cu}(\text{N-tBuSal})_2$	mp 184.5-185 °C	literature value 185 °C
$\text{Cu}(\text{N-PhSal})_2$	mp 233.5-235 °C	

2, 2' -bis(salicylideneaminato)diphenyl Cu(II) was prepared by the literature method.⁵⁰ 2, 2' -diaminodiphenyl was obtained from Aldrich Chemical Company and used without further purification.

EPR Measurements:

The x-band EPR spectra of the substituted salicylidene-aminatocopper(II) complexes were measured on a Varian V-4502 EPR spectrometer equipped with a 12 inch Varian electromagnet with a Varian Mark II Fielddial field sweep control unit. 100 KHz modulation was used. A Varian V 4532 rectangular cavity fitted with a quartz liquid nitrogen dewar was used. The magnetic field was calibrated with a solid sample of DPPH (diphenyldipicrylhydrozyl). The microwave frequency was measured by a wave meter attached to the microwave bridge. Spectra at liquid nitrogen temperature were obtained by immersing the sample tube in liquid nitrogen.

A one-to-one mixture of toluene, methylcyclohexane, which forms a nice glass at 77°K was used as the solvent.

The x-band EPR spectrum of Cu(II)-CPA was measured by Dr. Paula K. Bernstein on a Varian V4502 spectrometer with a 9 inch Varian electromagnet with Fielddial, using 100 KHz modulation. The system has a V-4502 dual sample cavity fitted with a quartz dewar. The magnetic field was calibrated in every experiment with a sample of solid DPPH placed in the rear compartment of the dual cavity. The DPPH signal was detected using a low frequency (20-400 Hz) modulation and detection system. The microwave frequency was measured by a wave meter attached to the microwave bridge. Low temperature experiments were done by passing a stream of nitrogen gas through a liquid nitrogen heat exchanger and then through the quartz dewar containing the sample. A Varian V-4540 temperature controller was used to monitor the rate of gas flow.

REFERENCES

1. J. E. Coleman and B. L. Vallee, *J. Biol. Chem.*, 236, 2244 (1961).
2. F. Basolo and R. G. Pearson, Mechanisms of Inorganic Reactions, 2nd ed., J. Wiley and Sons, New York, 1967.
3. T. A. Steitz, M. L. Ludwig, F. A. Quiocho, and W. N. Lipscomb, *J. Biol. Chem.*, 242, 4662 (1967).
4. F. A. Quiocho and W. N. Lipscomb, *Adv. Protein Chem.*, 25, 1 (1971).
5. S. Lindskog and P. O. Nyman, *Biochem. and Biophys. Acta*, 85, 462 (1964).
6. A. Abragam and M. H. L. Pryce, *Proc. Roy. Soc. London*, A205, 135 (1951).
7. B. Bleaney, *Phil. Mag.*, 42, 441 (1951).
8. F.-D. Tsay, H. B. Gray, and J. Danon, *J. Chem. Phys.*, 54, 3760 (1971).
9. B. G. Malmstrom and T. Vanngård, *J. Mol. Biol.* 2, 118 (1960).
10. B. L. Vallee, J. A. Rupley, T. A. Coombs, and H. Neurath, *J. Amer. Chem. Soc.*, 80, 4750 (1958).
11. A. S. Brill, P. R. Kirkpatrick, C. P. Scholes, and J. H. Venable, in Probes of Structure and Function of Macromolecules and Membranes, Vol. I, B. Chance, C. Lee, J. K. Blasic, eds., Academic Press, New York, 1971.
12. S. Lindskog, L. E. Henderson, K. K. Kannan, A. Liljas, P. O. Nyman, and B. Strandberg in "The Enzymes," Vol. 5, P. D. Boyer, Ed., Academic Press, New York, 1971, p. 587.

13. R. H. Holm and M. J. O'Connor, *Prog. Inorg. Chem.*, 14, 325 (1971).
14. B. R. McGarvey, *Transition Metal Chem.*, 3, 90 (1960), and references therein.
15. R. C. Slade, A. A. G. Tomlinson, B. J. Hathaway, and D. E. Billing, *J. Chem. Soc. (A)*, 1968, 61.
16. Data in part from T. Vanngård in Biological Applications of Electron Spin Resonance, H. M. Swartz, J. R. Bolton, and D. C. Borg, eds., J. Wiley and Sons, Inc., 1972.
17. A. H. Maki, B. R. McGarvey, *J. Phys. Chem.*, 29, 35 (1958).
18. G. Bombieri, C. Panattoni, E. Fursellini, and R. Graziani, *Acta Cryst.*, B25, 1208 (1969).
19. L. Wei, R. M. Stogsdill, and E. C. Lingafelter, *Acta Cryst.*, 17, 1058 (1964).
20. T. P. Cheesman, D. Hall, and T. N. Waters, *Proc. Chem. Soc.*, 1963, 379.
21. P. L. Orioli and L. Sacconi, *J. Amer. Chem. Soc.*, 88, 277 (1966).
22. T. P. Cheesman, D. Hall, and T. N. Waters, *J. Chem. Soc. A*, 1966, 685.
23. H. P. Fritz, B. M. Golla, and H. J. Keller, *Z. Naturforsch.*, 21b, 1015 (1960).
24. *Ibid.*, 23b, 876 (1968).
25. E. Frasson and C. Panattoni, *Z. Krist.*, 116, 154 (1961).
26. G. F. Kokoszka, C. W. Reimann, and H. C. Allen, Jr., *J. Phys. Chem.*, 71, 121 (1967).

27. J. L. Hall, J. A. Swisher, D. G. Brannon, and T. M. Liden, *Inorg. Chem.*, 1, 409 (1962).
28. S. C. Furman and C. S. Garner, *J. Amer. Chem. Soc.*, 73, 4528 (1951).
29. B. J. Hathaway and A. A. G. Tomlinson, *Coord. Chem. Rev.*, 5, 1 (1970).
30. B. J. Hathaway and D. E. Billing, *ibid.*, 5, 143 (1970).
31. B. J. Hathaway and F. Stephens, *J. Chem. Soc. A*, 1970, 884.
32. I. M. Procter, B. J. Hathaway, and P. Nicholls, *J. Chem. Soc. A*, 1968, 1678.
33. A. Chakravorty and T. S. Kannan, *J. Inorg. and Nucl. Chem.*, 29, 1691 (1967).
34. D. H. Gerlach and R. H. Holm, *Inorg. Chem.*, 9, 589 (1970).
35. F. Röhrscheid, A. L. Balch, and R. H. Holm, *Inorg. Chem.*, 5, 1545 (1966).
36. J. P. Fackler, Jr., F. A. Cotton, and D. W. Barnum, *Inorg. Chem.*, 2, 97 (1963).
37. J. A. Bertrand and R. I. Kaplan, *Inorg. Chem.*, 5, 489 (1966).
38. J. Bjerrum, C. J. Ballhausen, and C. K. Jørgensen, *Acta Chem. Scand.*, 8, 1275 (1954).
39. A. A. G. Tomlinson and B. J. Hathaway, *J. Chem. Soc. (A)*, 1968, 1685.
40. R. L. Belford, M. J. Calvin, and G. Belford, *J. Chem. Phys.*, 26, 1165 (1957).

41. R. H. Holm, A. Chakravorty, and L. J. Theroit, *Inorg. Chem.*, 5, 625 (1966).
42. L. Sacconi and M. Ciampolini, *J. Chem. Soc.*, 1964, 276.
43. M. Elder and R. B. Penfold, *J. Chem. Soc. A*, 1969, 2556.
44. J. E. Fergusson and C. A. Ramsey, *J. Chem. Soc.*, 1965, 1565.
45. V. A. Kogan, O. A. Osipov, S. N. Shcherbak, T. A. Zhuchenko, *J. Gne. Chem. USSR*, 38, 1556 (1968).
46. R. C. Slade, A. A. G. Tomlinson, B. J. Hathaway, and D. E. Billing, *J. Chem. Soc. A*, 1968, 61.
47. H. E. Elliott, B. J. Hathaway, and R. C. Slade, *J. Chem. Soc. A*, 1966, 1443.
48. R. Shelby, R. F. Ziolo, and H. B. Gray, in preparation.
49. M. Ciampolini and G. P. Speroni, *Inorg. Chem.*, 5, 45 (1966).
50. F. Lions and K. V. Martin, *J. Amer. Chem. Soc.*, 79, 1273 (1957).

CHAPTER V

CONCLUSIONS

We have established the coordination number and geometry involved in three first row transition metal derivatives of CPA. On the basis of its magnetic susceptibility and absorption spectrum, the cobalt(II) ion in Co(II)-CPA was shown to be five coordinate. The same techniques revealed that the nickel(II) ion in Ni(II)-CPA is in a six coordinate, octahedral or very nearly octahedral environment. When the inhibitor β -phenylpropionate is bound to this derivative, however, the environment of the nickel(II) becomes five coordinate. The absorption and EPR spectra of Cu(II)-CPA showed that the cupric ion is in a four coordinate, pseudo-tetrahedral environment that is significantly distorted from a planar structure.

Considering the above results, it is worth noting that these structures are all ordinary in the sense that numerous model complexes having these properties are known. It is also interesting to note that the metal site in CPA can accommodate metal ions with coordination numbers ranging from four to six, while the enzyme remains fully active. Coordination numbers of at least five also occur in Mn(II)-CPA and in VO^{+2} -CPA although these systems have somewhat reduced activity.^{1,2}

A coordination number of six is achieved only with some sacrifice. The values of the ligand field parameters Dq and B indicate that an optimal octahedral nickel(II) ligand geometry or interaction

cannot occur, perhaps because of either steric crowding or restraints imposed by the protein configuration.

We have shown that formation of the enzyme-inhibitor complex with β -phenylpropionate has an effect that is far greater than a simple ligand exchange should produce. In fact, changes in either coordination number or coordination geometry are involved. For the nickel(II) system it is clear that an inhibitor induced conformational change, however small, causes increased crowding about the metal, forcing extrusion of an additional ligand, water, from the first coordination sphere.

The binding constants of β -phenylpropionate to the various derivatives provide a convenient standard for comparing the effects of different metals on the protein conformation, at least as regards the inhibitor binding site. The available data are summarized in Table (V-I). It is very interesting that the active derivatives have K_I values that are quite similar. It is unfortunate that the error involved in the measurement on the nickel(II) system is large enough to obscure whether the K_I could be correlated further with enzymatic activity. It is significant, however, that the inactive cupric derivative has a value for K_I that is well over an order of magnitude smaller than the binding constants observed for the active derivatives. Clearly the presence of cupric ion in the metal site significantly disrupts the inhibitor binding site. It is tempting to extend the argument and conclude that either substrate binding or mechanistically important groups have also been shifted from their optimal positions.

Table V-I

Binding Constants of β -Phenylpropionate to M(II)-CPA

<u>M(II)-CPA</u>	<u>$K_I \times 10^4 (\text{M}^{-1})$</u>
Mn(II) ^a	0.28
Co(II) ^b	> 0.5
Ni(II)	0.37 ± 0.17
Cu(II)	0.014
Zn(II) ^c	0.53

^a Reference 1.^b Reference 3.^c Reference 4.

A metal induced conformational change of either type could explain the inactivity of Cu(II)-CPA. This conclusion is at least partially substantiated by the low resolution X-ray work on the gly-L-tyr complex with both Cu(II)-CPA and apoCPA.^{5,6} In these cases, the conformational change of Glu-270 associated with substrate binding in the native enzyme is not observed.

Of all the structural results, the finding of octahedral coordination in Ni(II)-CPA is by far the most significant. This result on a fully active derivative severely discredits the entatic state hypothesis of the role of the metal in metalloenzymes, at least as it applies to so called "Acid-Base Catalysts."⁷ This theory postulates that a significant part of the enzymatic activity is due to the existence of a locally energized region in the enzyme that more closely resembles the transition state of one or more of the catalytic steps. As applied to metalloenzymes such as CPA in which the metal functions as a binding site for and activator of substrate, this theory predicts a coordinatively unsaturated metal center with unusual physical properties that is open to attack by substrate, presumably by an associative process. For nickel(II), however, octahedral coordination is the quintessence of coordinative saturation and regularity. Ligand substitution in such systems is known to be rapid and to proceed by dissociative not associative processes.^{8,9}

Thus, it would appear that all that is required of the metal ion in CPA is that it have a properly oriented, substitution labile ligand site that can accommodate the carbonyl oxygen of the substrate.

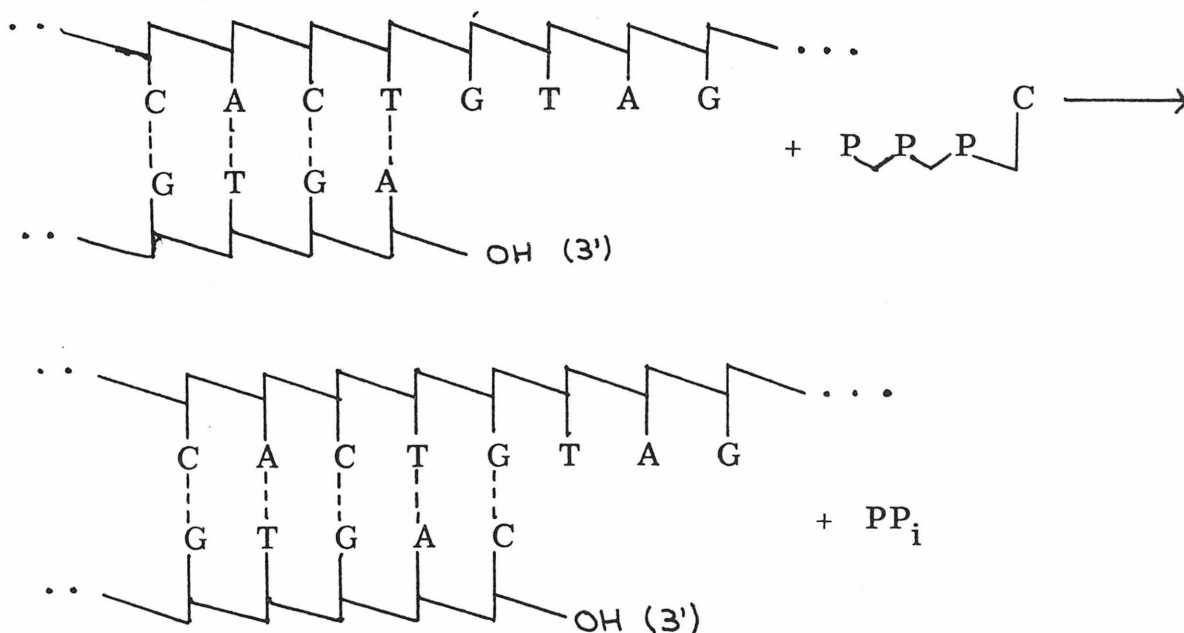
As long as these criteria are met, the coordination number and geometry of the metal are not particularly important.

References

1. G. Navon, R. G. Shulman, B. J. Wyluda, and T. Yamane, J. Mol. Biol., 51, 15 (1970).
2. N. D. Chasteen, private communication.
3. J. E. Coleman and B. L. Vallee, Biochem., 3, 1874 (1964).
4. D. S. Auld and B. L. Vallee, Biochem., 9, 602 (1970).
5. T. A. Steitz, M. L. Ludwig, F. A. Quiocho, and W. N. Lipscomb, J. Biol. Chem., 242, 4662 (1967).
6. F. A. Quiocho and W. N. Lipscomb, Adv. Prot. Chem., 25, 1 (1971).
7. R. J. P. Williams, Inorg. Chim. Acta Rev., 5, 137 (1971).
8. K. Kustin and J. Swinehart, Prog. Inorg. Chem., 13, 107 (1970).
9. R. G. Wilkins and M. Eigen, Adv. Chem. Ser., 49, 55 (1965).

PROPOSITION I

It has recently been shown that E. coli DNA polymerase I contains two zinc ions per molecule.¹ The enzyme also requires a divalent cation such as magnesium or manganese as a cofactor for activity.² The zinc has been implicated in the binding of the DNA template to the enzyme,^{1,3,4} while the manganese ion is apparently involved in the binding of the deoxynucleoside triphosphate substrate.⁵ The enzyme has a molecular weight of approximately 109,000 and contains roughly 970 amino acid residues in one continuous polypeptide chain.⁶ Although the exact in vivo function of DNA polymerase I has not been completely established, it appears that it functions best as an endopolymerase working from the 3'-hydroxyl end of the primer strand. It catalyzes reactions of the type



It is proposed that other divalent, first row transition metal ions, such as Ni^{+2} , Cu^{+2} and particularly Co^{+2} , be substituted for Zn^{+2} in DNA polymerase I. Since the enzyme is inhibited by chelating agents such as o-phenanthroline,^{1,3} it should be possible to prepare a metal-free enzyme by dialysis of the native enzyme against an o-phenanthroline solution. A titration of metal-free enzyme with added zinc ions should be made to see if activity can be restored by reconstitution. Since E. coli DNA polymerase I contains two gram-atoms of zinc per molecule, it will be interesting to see at what point in the reconstitution activity is restored. The possible activities and requirements of the other proposed derivatives should also be evaluated in this way. The assay procedure involves the incorporation of either ^{14}C or $\alpha\text{-}^{32}\text{P}$ -labeled deoxynucleotides into an acid insoluble product.^{7,8}

It would also be interesting to study activity as a function of pH for any active derivatives. Depending on the buffer system, the pH for optimal activity varies over the range 7.5 to 9.2 in the native enzyme. Binding constants for the various metals could be determined by equilibrium dialysis techniques. Competition studies could be employed to determine whether the metals bind at the same site(s) on the enzyme.

Once the various derivatives have been characterized in this manner, it would be very interesting to examine their spectral properties in order to get some idea of the coordination numbers and geometries that are involved in the binding site(s). As we found in the

case of Co(II)CPA, measurement of the magnetic moment of Co(II)DNA polymerase could be extremely useful. The absorption spectrum of the nickel(II) derivative could provide some information about the type of ligands involved in metal binding. Finally the absorption and frozen glass EPR spectra of the cupric derivative should be studied.

It would be very interesting to see if the binding of either nucleoside triphosphates or template DNA effects the spectral properties of any of the derivatives. For the cupric derivative it might be interesting to see if addition of manganese(II) has any effect on the observed EPR spectra, since it has been suggested that the zinc and manganese sites are extremely close.⁵

References

1. J. P. Slater, A. S. Mildvan, and L. A. Loeb, Biochem. and Biophys. Res. Comm., 44, 37 (1971).
2. M. J. Bressman, I. R. Lehman, E. S. Simms, and A. Kornberg, J. Biol. Chem., 233, 177 (1958).
3. L. M. S. Chang and F. J. Bollum, Proc. Natl. Acad. Sci. U.S., 65, 1041 (1970).
4. P. T. Englund, R. B. Kelly, and A. Kornberg, J. Biochem., 244, 3045 (1969).
5. J. P. Slater, I. Tamir, L. A. Loeb, and A. S. Mildvan, J. Biol. Chem., 247, 6784 (1972).
6. N. N. Jovin, P. T. Englund, and L. L. Bertsch, J. Biol. Chem., 244, 2996 (1969).
7. C. C. Richardson, C. L. Schildkraut, H. V. Aposhian, and A. Kornberg, J. Biol. Chem., 239, 222 (1964).
8. L. A. Loeb, J. Biol. Chem., 244, 1672 (1969).

PROPOSITION II

To date no reasonable models of the "blue copper" site in copper proteins have been prepared. The properties of the "blue copper" are somewhat unique. The name derives from an unusually intense absorption band with a maximum between 600 and 625 nm ($16,000$ – $16,670\text{ cm}^{-1}$) and a molar extinction coefficient of from 3500 to 6000 that gives these proteins their characteristic blue color.¹ The EPR spectra of these proteins are also unusual. They all show axial spectra with small values of the parallel nuclear hyperfine coupling constant, $A_{||}$: 0.003 to 0.008 cm^{-1} .² Normal cupric complexes, as we have seen, have values that range from 0.010 to 0.022 cm^{-1} .³ Finally the reduction-oxidation potentials of these proteins are anomalously high. Reduction potential values greater than $+0.3$ volts are common, while for the $\text{Cu}^{+2}/\text{Cu}^{+1}$ couple in dilute acid $E'_0 = +0.15\text{ V}$.¹

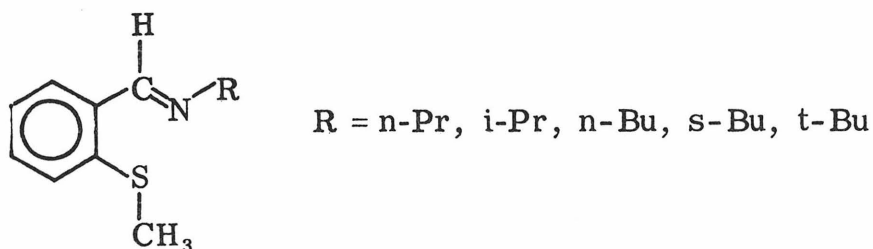
One possible model that has received some experimental support and considerable speculation is a pseudo-tetrahedral site involving one or more sulfhydryl ligands.^{4,5} The bis(N-alkylsalicylideneaminato) - copper(II) complexes which were extensively discussed in the chapter on Cu(II)CPA provide an excellent starting point.

The more pseudo-tetrahedral members of this series, such as bis(N-t-Bu-salicylideneaminato)copper(II) have an absorption band around 480 nm ($\epsilon_m \sim 1500$) that is not present in the complexes with a planar structure. This absorption is undoubtedly a charge transfer band. The fact that it is at such a low energy in the pseudo-tetrahedral

complexes suggests the possible usefulness of these complexes as models for the blue copper site. Substitution of sulfur for oxygen in the donor set should cause this charge transfer band to move to even lower energy.

By replacing the hydroxyl group in the salicylideneaminato system with a thio ether moiety, a series of copper(II) complexes having (NS)₂ coordination could be synthesized. By varying the amine used in forming this Schiff base ligand from n-propyl, n-butyl, i-propyl, s-butyl, to t-butyl, bis-copper(II) complexes having both planar and pseudo-tetrahedral structures could be expected by analogy to the bis-salicylideneaminatocopper(II) series.

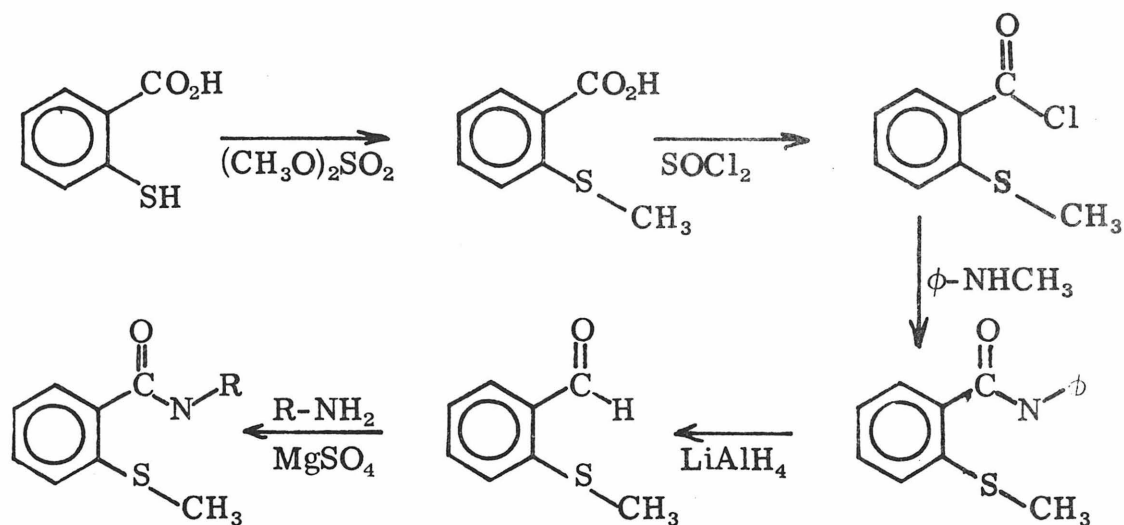
The ligand we are proposing has the following structure



For convenience, we shall abbreviate this ligand as N-R-MSB. Metal complexes of the $R = \text{CH}_2\text{-CH}_2\text{N}(\text{C}_2\text{H}_5)_2$ derivative (MSBenNEt₂) have been synthesized and characterized.⁶ The complexes Ni(MSBenNEt₂)X₂, X = Cl, Br, and I, all are five coordinate in the solid state, indicating that the sulfur is capable of coordinating to a metal. In solution, however, there is evidence for some dissociation of the sulfur donor to give a four coordinate species. It is reasonable

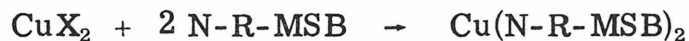
to expect that N-R-MSB will act as a bidentate ligand with cupric ion.

The ligand N-R-MSB can be synthesized as follows⁷:



N-R-MSB

The complexes of interest $(\text{N-R-MSB})_2\text{Cu}$ can be prepared by refluxing stoichiometric amounts of an appropriate cupric salt with the ligand in a suitable solvent such as anhydrous alcohol.



Once prepared, the physical properties of these complexes will be extensively studied both in the solid state and in solution. In particular, the absorption spectra, frozen glass EPR spectra, and reduction-oxidation potentials will be examined. As an aid in establishing the structures of the various derivatives, measurement of the dipole moment of the complexes in solution might also prove useful.

References

1. R. Malkin and B. G. Malmström, *Adv. in Enzyme*, 33, 177 (1970).
2. T. Vanngard in Biological Application of EPR, H. M. Swarz, J. R. Bolton, and D. C. Bord, Eds., Wiley-Interscience, New York, 1972.
3. This work, Chapter IV.
4. L. Morpurgo, A. Finazzi-Agrò, G. Rotilio, and B. Mondovi, *Biochem. and Biophys. Acta*, 27, 292 (1972).
5. R. J. P. Williams, *Inorg. Chim. Acta Revs.*, 5, 137 (1971).
6. L. Sacconi and G. P. Speroni, *Inorg. Chem.*, 7, 295 (1968).
7. B. Eistert, W. Schade, and H. Selzer, *Chem. Ber.*, 97, 1470 (1964).

PROPOSITION III

Ceruloplasmin (Cp) is a copper containing glycoprotein that accounts for over 90% of the copper found in normal human plasma.¹ Functionally, it is one of four oxidases capable of reducing molecular oxygen directly to water. The identity of the in vivo substrate(s) of ceruloplasmin, however, has not been definitively established. Two distinct types of compounds have been shown to be capable of reducing ceruloplasmin in vitro. They are ferrous ion (Fe^{+2}) and a large group of aromatic polyphenols and polyamines including such biochemically active amines as serotonin, dopamine, norepinephrine, and L-epinephrine.^{2,3} The ferro-oxidase activity of ceruloplasmin has led Frieden and others^{4,5} to postulate that ceruloplasmin is the link between the cellular storage and the serum mobilization of iron by transferrin, the body's iron transport protein.

Ryden⁶ has recently established a molecular weight of 132,000 for human ceruloplasmin in solution, in excellent agreement with the molecular weight determined crystallographically.⁷ Ten per cent by weight of the ceruloplasmin molecule is carbohydrate and the rest is a single polypeptide chain of approximately 1050 amino acid residues. Ceruloplasmin, prepared from fraction IV-1 of human plasma by successive ion exchange chromatography on DEAE Sephadix followed by crystallization, contains seven copper atoms per molecule. Treatment of ceruloplasmin with Chelex-100 reduces the number of coppers per molecule to six, without any loss in oxidase activity.⁸

There are three different types of copper in oxidized ceruloplasmin.⁹ Type I is the so-called "blue copper." It is characterized by an intense visible absorption band at 610 nm and EPR signal having $g_{\parallel} = 2.21$, $g_{\perp} = 2.05$ and an unusually small hyperfine coupling constant $A_{\parallel} = 0.0083 \text{ cm}^{-1}$. Type II copper is known as the EPR detectable copper. Its signal is characterized by $g_{\parallel} = 2.28$, $g_{\perp} = 2.04$ and a larger hyperfine coupling constant of $A_{\parallel} = 0.0136 \text{ cm}^{-1}$. There is apparently no observable visible absorption band associated with the Type II copper. Type III copper is the so-called "diamagnetic copper." It is not detectable by EPR or magnetic susceptibility measurements, and is thought to represent either Cu(I) or an anti-ferromagnetically coupled pair(s) of Cu(II) atoms. It is characterized by a strong absorption at 330-340 nm.

The relative numbers of Type I, Type II, and Type III copper in oxidized ceruloplasmin has not been definitively established. Integration of the EPR spectrum of ceruloplasmin shows approximately equal amounts of Type I and Type II copper. Reyden⁶ has suggested that there are two Type I coppers in ceruloplasmin since the observed molar extinction coefficient of the 610 nm band is approximately double that found in blue copper proteins that contain only one copper per molecule. If this conclusion is true, there would be two Type I, two Type II, and two Type III copper atoms per molecule in ceruloplasmin.

Carrico¹⁰ has shown that under equilibrium conditions oxidized ceruloplasmin can accept one electron per copper. Thus,

titration of ceruloplasmin with an appropriate reductant abolishes the characteristic absorption and EPR spectra of the Type I, II, and III coppers. It is thus apparent that all the copper in ceruloplasmin, even the "diamagnetic" copper, can participate in the electron transfer process.

The spectral bands associated with the Type I and Type III copper can be used to study the kinetics of the reduction process in this system. In particular, I propose to study the anaerobic reduction of human ceruloplasmin by ferrous ion by following the reaction at both 610 and 340 nm in a stopped flow kinetic apparatus. Some work on this problem has already been done. Osaki and Walaas¹¹ studied the ferrous ion reduction of ceruloplasmin at 610 nm (blue copper) in acetate buffer at pH 5.9. They found a second order rate constant $k_1 = 1.2 \times 10^6 \text{ M}^{-1}\text{sec}^{-1}$ for the reaction



However, they used conditions that did not allow the reaction to go to completion, e.g., a slight excess of Cp with respect to Fe(II). Carrico¹² has shown that both the 610 nm and the 340 nm chromophors participate in the electron transfer reaction. Unfortunately, no kinetic parameters were extracted from this work since ferrous ion, present in only trace amounts was used as an electron shuttle between ascorbic acid and ceruloplasmin.

It would seem logical to extend the work of Osaki and Walaas by studying the reduction of ceruloplasmin by ferrous ion at both 610 and 340 nm under pseudo first order conditions. The dependence of

the observed rate on substrate (ferrous ion) concentration and temperature will be studied.

It will be very interesting to see whether reduction of both the 610 nm and the 340 nm chromophors involve the **same** rate determining step. The magnitude of the activation parameters obtained may illuminate whether a large conformational change is involved in the reduction process and if so at what point it occurs.

One problem that will be encountered in following the rate of reduction at 340 nm will be interference from ferric ion produced in the reaction. Ferric ion has a significant absorbance across the ultraviolet; but its absorbance is relatively flat in the region around 290 nm. Of course ceruloplasmin itself has a strong absorbance at 280 nm, but this should remain constant during the course of any kinetic run. By following the reaction at 290 nm and by knowing the molar extinction coefficient of ferric ion in the reaction mixture at both 290 nm and 340 nm, it should be possible to subtract out any changes in absorbance at 340 nm due to the production of ferric ion. In this way the true reduction rate of ceruloplasmin at 340 nm can be obtained.

Although ferrous ion, or more accurately a ferrous acetate complex of undetermined stoichiometry, can facilely reduce ceruloplasmin, $\text{Fe}(\text{EDTA})^{2-}$ (EDTA = ethylenediaminetetracetate) and $\text{Fe}(\text{CN})_6^{4-}$ apparently cannot, even though their oxidation potentials are favorable.^{13,2} Perhaps one or more water molecules in the inner

coordination sphere of the ferrous ion reductant are required before fast electron transfer to ceruloplasmin can occur. In order to test this hypothesis complexes of the type $[\text{Fe}(\text{HEDTA})(\text{H}_2\text{O})]^{-1}$ or $[\text{Fe}(\text{EDDA})(\text{H}_2\text{O})_2]$ will be evaluated as substrates for ceruloplasmin. It may also prove useful to investigate the effect of deuterium on the ferrous ion reduction of ceruloplasmin.

An investigation of one of the second class of ceruloplasmin substrates will also be undertaken. Young and Curzon³ have recently shown that hydroquinone is in fact a true substrate of ceruloplasmin. It should be very interesting to investigate the kinetics of the reduction of ceruloplasmin by hydroquinone at 340 nm and 610 nm and to compare the results to those obtained in the ferrous system. This system is complicated by the fact that both hydroquinone and semiquinone are potential substrates for the enzyme. However, since the equilibrium constant of the rapid disproportionation of semiquinone to hydroquinone and quinone is known, it will be possible to avoid complications by working under conditions that are pseudo-first-order in semiquinone, *i.e.*, a large excess of both hydroquinone and quinone. The rate of reduction can then be measured as a function of changes in both the initial hydroquinone or quinone concentrations. Rate constants for both the semiquinone and hydroquinone reduction of ceruloplasmin will be obtained from the slope and the intercept, respectively of a plot of k_{obs} vs. $(\text{hydroquinone})^{\frac{1}{2}} \times (\text{quinone})^{\frac{1}{2}}$. By studying the reaction at several different temperatures activation parameters will be obtained for reduction of both chromophores.

Finally, the effect of various added anions such as N_3^- and F^- on the rates of reduction of the Type I and Type III coppers will be investigated, with either or both ferrous ion or hydroquinone as substrate. Curzon and co-workers^{14,15} have shown that both N_3^- and F^- inhibit the reduction of oxygen by ceruloplasmin. Andreasson has shown by EPR measurements that both N_3^- and F^- bind to the Type II copper.¹⁶ Thus it will be very interesting to see what effect these anions have on the rates of reduction of the 610 nm and 340 nm chromophores.

References

1. A. White, P. Handler, and E. L. Smith, Principles of Biochemistry, 3rd. Ed., McGraw-Hill, New York, 1959.
2. J. A. McDermott, T. C. Hunter, S. O. Saki, and E. Frieden, *Biochim. Biophys. Acta*, 151, 541 (1968).
3. S. N. Young and G. Curzon, *Biochem. J.*, 129, 273 (1972).
4. S. Osaki, D. A. Johnson, and E. Frieden, *J. Biol. Chem.*, 246, 3018 (1971).
5. H. B. Roeser, G. R. Lee, S. Nacht, G. E. Cartwright, *J. Clin. Invest.*, 49 (12), 2408 (1970).
6. L. Rydén, *Eur. J. Biochem.*, 26, 380 (1972).
7. B. Magdoff-Fairchild, F. M. Lovell, and B. W. Low, *J. Biol. Chem.*, 244, 3497 (1969).
8. T. C. Huber and E. Frieden, *J. Biol. Chem.*, 245, 3973 (1970).
9. R. Mulkin and B. G. Malmström, *Adv. Enzym.*, 33, 177 (1970).
10. R. J. Carrico, B. G. Malmström, and T. Vanngard, *Eur. J. Biochem.*, 20, 518 (1971).
11. S. Osaki and O. Walaas, *J. Biol. Chem.*, 242, 2653 (1967).
12. R. J. Carrico, G. B. Malmström, and T. Vanngard, *Eur. J. Biochem.*, 22, 127 (1971).
13. G. Curzon and S. N. Young, *Biochim. Biophys. Acta*, 268, 41 (1972).
14. G. Curzon, *Biochem. J.*, 100, 295 (1967).
15. G. Curzon and B. E. Speyer, *Biochem. J.*, 109, 25 (1968).
16. L. E. Andréasson and T. Vanngard, *Biochim. Biophys. Acta*, 200, 247 (1970).

PROPOSITION IV

Considerable study has been devoted to elucidating the mechanism of ligand substitution reactions in square planar and octahedral metal complexes.¹ Different mechanisms have been found in each case. Square planar complexes have been found to follow a two term rate law of the form

$$r = k_1[\text{ML}_3\text{X}] + k_2[\text{Y}][\text{ML}_3\text{X}] \quad (1)$$

for the reaction

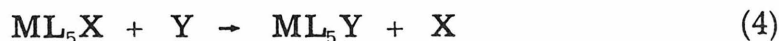


This rate law is indicative of two associative pathways, one involving solvent, and one the reactant Y as the nucleophiles. For a given complex ML_3X , k_1 is independent of the nature of Y.

Octahedral complexes, on the other hand, have been found to follow a rate law that is independent of the concentration of the reactant Y, except when $\text{Y} = \text{OH}^-$.

$$r = k_1[\text{ML}_5\text{X}] \quad (3)$$

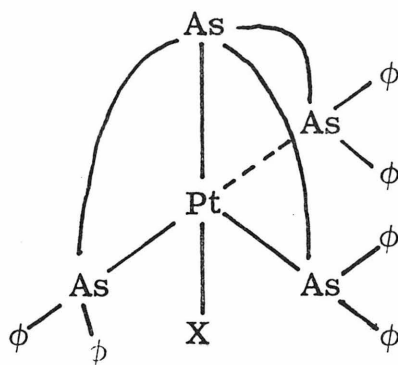
for the reaction



The observed rate law is explained in terms of a dissociative mechanism.

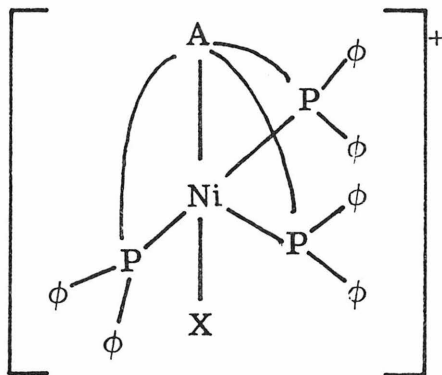
Stereochemically five coordinate complexes lie between square planar and octahedral species. However, the mechanism of

substitution reactions in five coordinate systems has received scant attention. A little work has been done on the mechanism of substitution in trigonal bipyramidal iron and manganese carbonyl complexes. Dissociative and associative mechanisms were found, respectively.^{2,3} This process was also studied in a trigonal bipyramidal platinum(II) system of the form⁴:

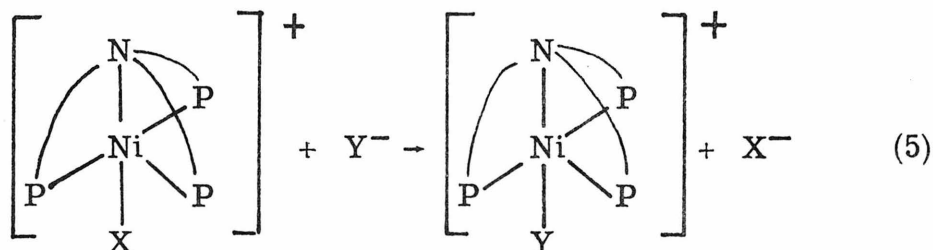


In methanol the kinetics were complicated by ion pair formation not related to the substitution reaction. The results indicate that an associative mechanism was involved.

Low spin, trigonal bipyramidal nickel(II) complexes of the form:



are known with $X = \text{Br}^-$, I^- , and $A = \text{N}$, and P .^{5,6} It is proposed that the mechanism of substitution for X be studied in this system.

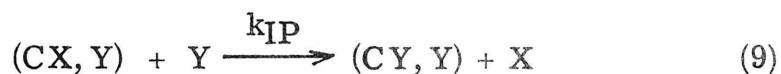
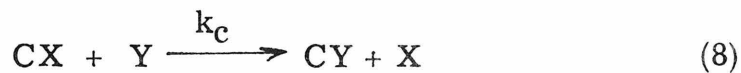
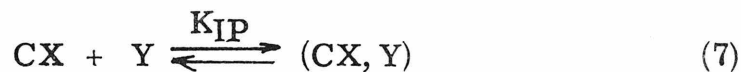


In particular the system where $A = \text{Nitrogen}$ would be used since the rates of substitution should be slower than in those with a phosphorus trans to the leaving group X . In planar complexes the relative reactivities of Ni^{+2} , Pd^{+2} , and Pt^{+2} are roughly $5 \times 10^6 : 10^5 : 1$, respectively.¹ In the platinum arsine system observed rate constants of the order of 10^{-1} to 10^{-3} sec^{-1} were found depending on the nature of Y . Arsine and phosphine ligands both have a very large trans labilizing effect while amines do not. Thus we might expect a decrease of over 10^3 on switching from $A = \text{phosphorus}$ to $A = \text{nitrogen}$. Using this number and the relative reactivity found in the square planar systems we should see observed rate constants of the order of:

$$k_{\text{obs}} \cong 10^{-1} \times 5 \times 10^6 \times 10^{-3} = 5 \times 10^2 \quad (6)$$

which are well within the range of a stopped flow kinetic apparatus.

In nonaqueous solvents like DMF, in which we propose to study the reaction, ion pairing should be significant. For an associative mechanism, including the effects of ion pairing, and with a large excess of Y , we have:



The observed rate constant is given by

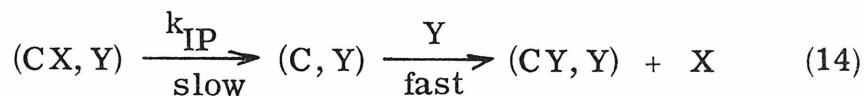
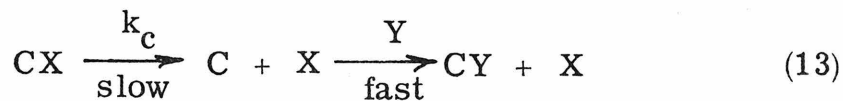
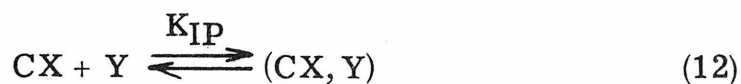
$$k_{\text{obs}} = \frac{k_{\text{c}}[\text{Y}] + k_{\text{IP}}K_{\text{IP}}[\text{Y}]^2}{1 + K_{\text{IP}}[\text{Y}]} \quad (10)$$

For conditions where $K_{\text{IP}}[\text{Y}] \gg 1$ equation 10 reduces to:

$$k_{\text{obs}} = \frac{k_{\text{c}}}{K_{\text{IP}}} + k_{\text{IP}}[\text{Y}] \quad (11)$$

It should be noted that $k_{\text{c}}/K_{\text{IP}}$ will vary with the reagent Y.

For a dissociative mechanism under the same constraints we have:



The observed rate constant is given by:

$$k_{\text{obs}} = \frac{k_{\text{c}} + k_{\text{IP}}K_{\text{IP}}[\text{Y}]}{1 + K_{\text{IP}}[\text{Y}]} \quad (15)$$

For $K_{IP}[Y] \gg 1$ equation 15 reduces to:

$$k_{obs} = \frac{k_c}{K_{IP}[Y]} + k_{IP} \quad (16)$$

These two cases are clearly distinguishable by the behavior at very high incoming ligand concentrations.

The reaction of nucleophiles such as Cl^- , NO_2^- , N_3^- , I^- , SCN^- , and CN^- with $X = Br^-$ complex will be evaluated. If an associative mechanism is involved the order in which the nucleophiles are listed would be the expected order of increasing reactivity by analogy to the square planar platinum(II) results. In either case, examination of the effect of changes in the leaving group, X, on the rate could provide insight as to the degree of bond breaking involved in the transition state. Steric effects could also be investigated by changing the bulkiness of the groups attached to the equatorial phosphine ligands. Depending on whether an associative or a dissociative mechanism is found for the phenyl case, more or less bulky groups could be introduced.

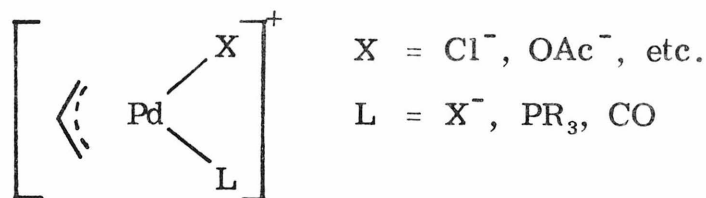
References

1. F. Basolo and R. G. Pearson, Mechanisms of Inorganic Reactions, 2nd Ed., J. Wiley and Sons, New York, 1967.
2. E. E. Siefert and R. S. Angelici, J. Organometal. Chem., 8, 374 (1967).
3. H. Hawersik and F. Basolo, J. Amer. Chem. Soc., 89, 4626 (1967).
4. R. G. Pearson, M. M. Muir, and L. M. Venanzi, J. Chem. Soc., 5521 (1965).
5. L. Sacconi and I. Bertini, J. Amer. Chem. Soc., 90, 5443 (1968).
6. G. Dyer, J. G. Hartley, and L. M. Venanzi, J. Chem. Soc., 1293 (1965).

PROPOSITION V

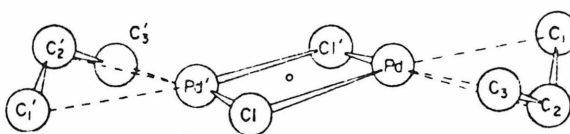
π -Allyl metal complexes are thought to be important intermediates in olefin polymerizations catalyzed by transition metals.¹

In fact, π -allyl complexes of the form

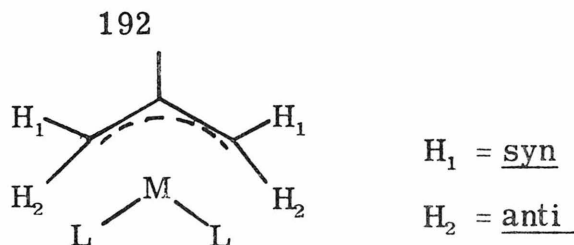


are themselves catalysts. The nature of L often determines the stereochemical course of a particular reaction. Complexes with $\text{X} = \text{L} = \text{PR}_3$, however, are catalytically inactive.

Structural work on the bis(π -allylpalladium chloride) dimer indicates that the whole allyl group is planar, hydrogens included, and tilted at an angle of $\sim 129^\circ$ to the plane formed by the palladiums and the two bridging chloride ions.²



Many π -allyl metal complexes have been shown to be fluxional.³ This fluxional behavior often takes the form of syn-anti proton exchange.



One commonly invoked mechanism for this type of exchange involves dissociation of one of the metal π -allyl bonds to give an intermediate that has a metal to carbon σ bond, in which rotation about either the metal to carbon or the adjacent carbon-carbon σ bond can occur followed by reformation of the π -allyl bonds.

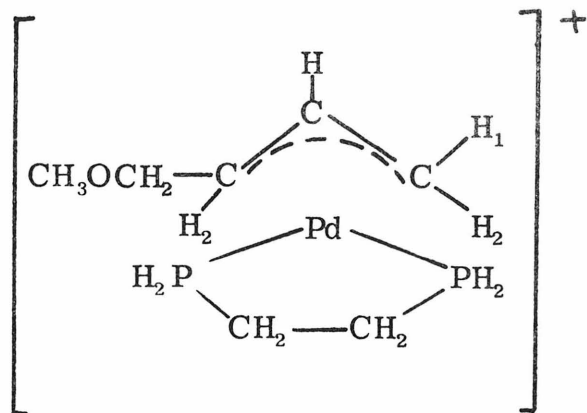
Tibbetts and Brown⁴ have shown by nmr techniques that in the absence of added base the complex $[(\pi\text{-2-methylallyl})(\text{diphos})\text{Pd}](\text{PF}_6)$ is non-fluxional. It is interesting to note that this species with $\text{L}_1 = \text{L}_2 = \text{P}$ should be catalytically inactive, as outlined above. If one of the terminal hydrogens is replaced by a substituent, the existence of syn-anti isomers is possible. It has been shown, however, that only the substituent = syn is formed synthetically.⁵

Natarajan and Adamson⁶ have shown that aquation of ethylene from Zeise's salt $\text{Pt}(\text{C}_2\text{H}_4)\text{Cl}_3^-$ is the dominant photoreaction on irradiation of the d-d bands of this system and that this photoaquation can be sensitized by acetone and acetophenone.

On this basis it is proposed that the potential syn-anti photoisomerization in a substituted $[\pi\text{-allyldiphosPd}]^+$ type system be studied. $[\pi\text{-allyldiphosPd}][\text{PF}_6]$ complexes are simply prepared by the addition of diphos to a solution of the appropriate π -allyl-palladiumchloride dimer in dichloromethane.⁴ It might also be

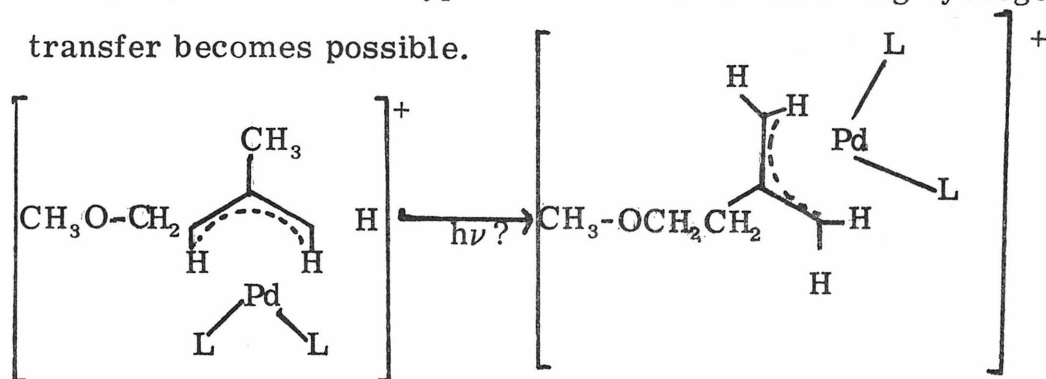
interesting to try to make and study the behavior of $[(\pi\text{-allyl}(\text{en})\text{Pd})][\text{PF}_6]$ complexes.

In particular, the complex π -4-methoxybut-2-enyl(diphos)-palladium(II)hexafluorophosphate



provides an excellent system for this study. The H_1 and H_2 resonances occur at 5.5 and 6.7 σ (ppm) with respect to TMS, respectively by analogy to the unsubstituted system.⁴ For the syn isomer, which is the starting material, the intensity ratio should be $\text{syn/anti} = 0.5$, whereas for the anti-isomer the intensity ratio $\text{syn/anti} = 2.0$. The u.v. absorption spectra of the $[\pi\text{-allyldiphosPd}]^+$ system has not been measured. Because of the strong field nature of both ligands it would be reasonable to expect significant absorption only below 300 nm. It would, of course, be informative to study the isomerization at the wavelengths where the complex absorbs. It might also be interesting to see if the reaction can be sensitized by high energy sensitizers such as acetone or acetophenone.

If a methyl group is introduced into the central carbon of the π -allyl system another type of isomerization involving hydrogen ion transfer becomes possible.



This type of isomerization would produce a product in which syn/anti = 1.0.

Finally, it might be interesting to see if olefin polymerization can be photoinduced in this system.

References

1. W. Kein in Transition Metals in Homogeneous Catalysis,
G. N. Schrauzer, ed., Marcel Drucker, Inc., New York, 1971,
pp 59-91.
2. W. E. O. Berhansli and L. F. Dahl, J. Organometallic Chem., 3,
43 (1965).
3. K. Vrieze, H. C. Volger, and P. W. N. M. van Leeuwen,
Inorg. Chim. Acta Revs., 3, 109 (1969).
4. D. L. Tibbetts and T. L. Brown, J. Amer. Chem. Soc., 92,
3031 (1970).
5. S. D. Robinson and B. L. Shaw, J. Chem. Soc., 4806 (1963).
6. P. Natarajan and A. W. Adamson, J. Amer. Chem. Soc., 93,
5599 (1971).